

Department of Precision and Microsystems Engineering

Identification of damping in joints using dynamic substructuring techniques

Name: M. Bakker B.Sc.

Report no: EM 11.041
Coach TU Delft: dr. ir. D. de Klerk
Coach Techno Fysica: ing. M. van der Heijde
Professor: prof. dr. ir. D.J. Rixen
Specialisation: Engineering Mechanics
Type of report: Masters Thesis
Date: Delft, December 7, 2011



Acknowledgements

During the last 11 months, Techno Fysica gave me the opportunity to perform my Master's research project at their company. I have been busy with testing, modelling and validating results. I learned a lot about modal testing, dynamic substructuring and data analysis. Several people helped me during the period. I would like to mention these people here.

Many thanks to Marcel van der Heijde who coached me at Techno Fysica. His practical knowledge about modal testing and knowledge about dynamics in general were very helpful to me. Also thanks to the other colleagues at Techno Fysica for their cooperation and pleasant working atmosphere.

I would like to express my gratitude to Dennis de Klerk, who supervised my the last one and a half year of my study period including this Master's thesis project. He was always available for discussing several topics and spent a lot of time to help me.

Thanks also to prof. Dr. Ir. D. Rixen for his advices during the project, for his amazingly quick replies, availability and helpfulness.

Additionally I would like to thank the other students working concurrently on their Master's thesis. Many discussions were very helpful in the process of making this thesis.

Finally I would also like to thank my friends and family and especially my wife Mieke for their support during my study time.

Gouda, December 2011

Matthijs Bakker

Abstract

Predicting and characterizing damping in joints and connections is a bottleneck in many design processes. New analysis techniques can be used to advance the engineering practice. These techniques would for example be useful to make a better estimation of the coupled dynamics of an engine-generator set (gen-set) on a ship. Large ships are commonly equipped with a gen-set to provide power to the vessels and to the electrical consumers on board. In some cases the engine vibration levels are too high to satisfy vibration guideline limits. In order to get insight in the system dynamics and to propose useful structural modifications an accurate system description of the total system is needed. In the Msc. project, research has been done on the identification of the dynamic behaviour of joints. Joints can significantly influence the dynamics of the entire system. The identification will be done by using Dynamic Substructuring (DS) techniques. The joint will be modelled and treated as a subsystem and the properties will be iteratively obtained. An often encountered problem in practice is the absence of crucial response measurements on the interface due to tight packaging of the system. A method is proposed to describe the unmeasured interface Degrees of Freedom (DoF), which are needed for compatibility of motions on the interface, in terms of measured DoF. Measurements are done on a base-upright test structure which is tested in different support conditions. It is shown that DS techniques can be used to identify properties of joints. The proposed method for describing unmeasured DoF has been validated with simulated experiments. Further investigation is needed to use this method with measured data.

Contents

I	Theory	1
1	Mechanical systems with damping	3
1.1	Viscously damped systems	3
1.1.1	State space description	4
1.1.2	First order perturbation method	5
1.1.3	Proportional damping	6
1.2	Non-viscously damped systems	7
1.2.1	Hysteretic damping	7
1.2.2	General non-viscous damping	7
1.3	Damping matrices	8
2	Modal parameter identification	11
2.1	Mode indicator functions	12
2.1.1	Summation function	12
2.1.2	Complex mode indicator function	12
2.1.3	Stability diagram	13
2.2	SDoF Circle fit method	13
2.2.1	Theory	14
2.2.2	Fit Procedure	15
2.3	MDoF modal analysis methods	17
2.3.1	Rational fraction polynomial method	18
2.3.2	Complex exponential method	19
3	Dynamic substructuring	21
3.1	Introduction	21
3.2	Coupling in the frequency domain	21
3.2.1	Primal formulation	22
3.2.2	Dual formulation	22
3.3	Appending non-measured DoF to a set of measured DoF	23
II	Measurements, Modelling and Validation	27
4	Measurement	29
4.1	Introduction	29
4.2	Test object	29
4.3	FEM Analysis	30
4.4	Test set up	30
4.4.1	Suspension	31
4.4.2	Data acquisition	31

4.4.3	Sensor and sensor positions	31
4.4.4	Input force and input positions	31
4.5	Modal analysis	32
4.5.1	ME'scope	32
4.5.2	Circle fit method	33
4.6	Damping sources	37
4.7	Conclusions	38
5	Results	41
5.1	Damped base rigid motions	41
5.2	Eigenfrequencies	41
5.3	Modeshapes	42
5.4	Damping	44
5.5	Discussion	47
6	Modelling	49
6.1	Modal Model	49
6.2	Response model	49
6.2.1	Rigid Body modes	50
6.2.2	Higher Residual modes	51
6.3	Discussion	52
III	Identification of damping in joints	53
7	Coupling two plates in the frequency domain	55
7.1	Description of a rigid substructure	55
7.2	Assembling two plates based on partial measurement	56
7.3	Weakening of interface compatibility	58
8	Validation of methods	61
8.1	Rigid membrane behaviour	63
8.1.1	Construction of system matrices	63
8.1.2	Construction of Boolean matrices	64
8.1.3	Results	65
8.2	Describing rotational DoF on the interface with modes.	66
8.2.1	Rigid body modes	66
8.2.2	Flexible modes	67
9	Coupling measured plates	69
9.1	Rigid body modes	69
9.2	Flexible modes	70
10	Identification of damping in rubber mountings	73
10.1	Rubber mounting properties	73
10.2	Model descriptions	74
10.3	Coupling procedure	74
10.4	Identification of damping and stiffness	75
11	Conclusions and Recommendations	81
11.1	Summary	81
11.2	Conclusions	81

11.2.1 Identification of rubber mounting properties	81
11.2.2 Identification of bolted joint properties	82
11.3 Recommendations	83
Nomenclature	85
A Fundamentals of Plates	89
A.1 Homogeneous equations	89
A.2 Analytical solutions	90
B Data sheets	91
C Mode Shapes	97

Introduction

Research context

My masters research has been done at Techno Fysica, a company located in Barendrecht which main business is to solve problems concerning mechanical equipment and installations in marine, industrial and offshore branches. One problem they regularly face is that the noise and vibration level in (cruise) ships is too high due to engine vibrations.

Large ships are commonly equipped with a generator set (genset) to provide power to the vessel(s) and to the electrical consumers on board. This genset is a combination of a combustion engine which delivers mechanical power and a generator which converts the mechanical power into electrical power. A typical setup of a genset can be seen in Figure 1.

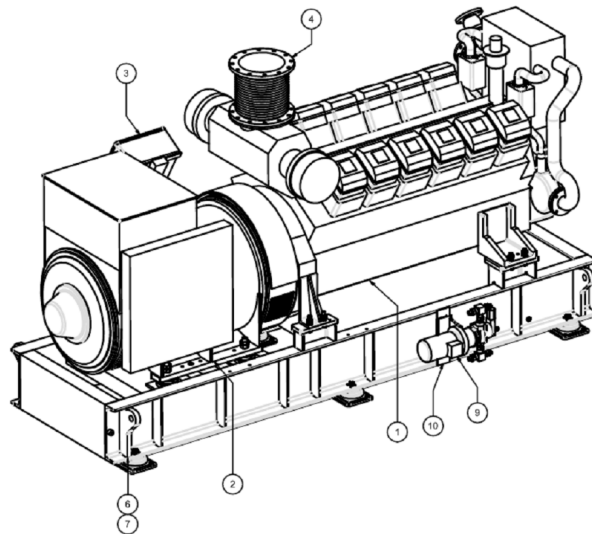


Figure 1: Typical setup of a genset

The vibrations of the engine and generator are assumed to be damped out by the rubber mountings underneath the base frame. However, in some cases the vibration level remains too high to satisfy vibration guideline limits. In such a case Techno Fysica is asked to modify the assembly in order to lower the vibration levels. To know how to modify the assembly, the dynamic behaviour of the assembly after modification needs to be predicted in order to suggest useful modifications. To predict the dynamic response after modification, a good understanding of the coupled dynamics of structures is needed. The coupled dynamics are heavily dependent on the damping in the joints between the different substructures of the genset and the rubber mountings of the genset to the ship. This research will focus on the identification of damping in joints. In the next section the thesis assignment will be worked out.

Thesis Assignment

In the previous section the context of this research was introduced. The goal of this research is to obtain a method to be able to identify the damping in the joints between the substructures. To be able to identify these joints, they will be approached as a substructure. As a test structure, a base upright will be used in two different configurations. Steel plates and beams are common components in machines and engineering structures, and are therefore representative for a lot of practical cases.

One topic of this research is the identification of joints when all the important interface DoF are known (measured). For this part the base plate will be used as a test structure, which will be supported by rubbers on the floor. This setup is mainly one dimensional, and interface can be described also as one dimensional. The properties of this rubber joint will be identified.

The other topic of the research is the identification of damping in joints, for an interface that is partially measured. For this part a base upright test structure will be used. The base and upright will be measured separately and will be modelled. These models will be coupled dynamically. The coupled model will be compared to a validation measurement. The damping in the joint will be identified by comparing the modal damping of the validation measurement and the coupled substructures. The coupling procedure of the base and upright is not straight forward because the interface DoF are partially measured.

Partially measured joints are common in engineering practise because of tight packaged machine assemblies. For this reason it is of great importance to be able to identify joints when the interface cannot completely be measured.

An overview of the identification method can be seen in Figure 2.

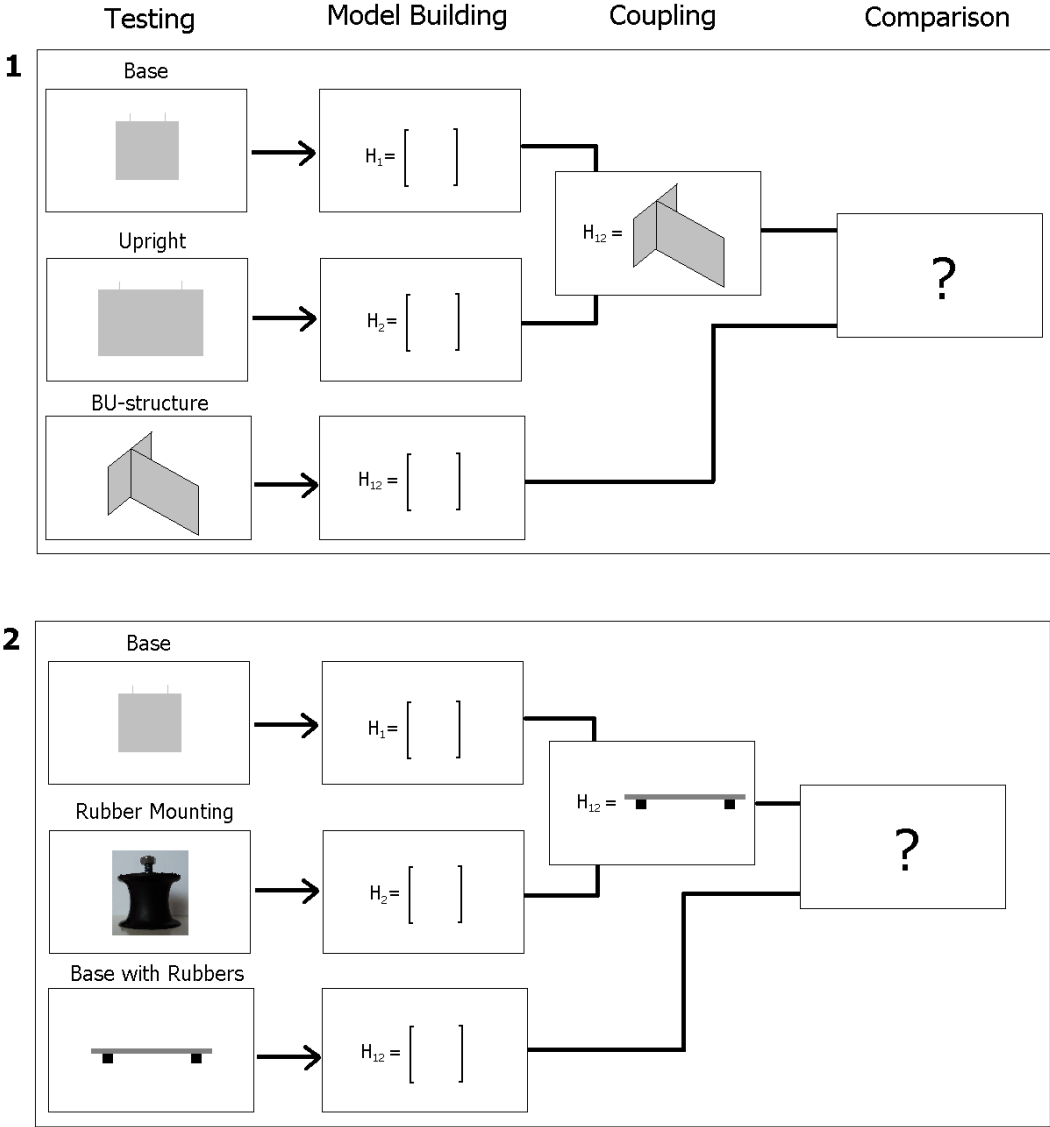


Figure 2: Overview of research

Thesis outline

The research of this thesis is divided into three main parts. Part I presents the theory of damped systems, modal identification techniques and dynamic substructuring and the fundamentals of plates. In part II the measurement and results will be discussed. Based on these results models will be made and validated. In part III the models will be coupled and compared with validation measurements to identify the damping in the joints. More specifically, the parts consist of the following chapters

Part I: Theory

- Chapter 1 is about damping in dynamic systems. Both viscous and non-viscous damping will be discussed. Also the construction of damping matrices will be addressed. This chapter is adapted from my literature survey [7].
- Chapter 2 is about the different modal identification techniques. The circle fit method will be discussed more extensively, for especially this method will be used for the identification of damping in this research. This chapter is partially adapted from my literature survey [7].
- Chapter 3 is about dynamic substructuring techniques. These techniques will be used for the plate coupling procedures.

Part II: Measurements, Modal analysis and Modelling

- In Chapter 4 the measurement set up will be discussed. Also processing of the data will be addressed. The influence of the measurement set up on the identified damping in the structures will be analysed.
- In Chapter 5 the identified eigenproperties will be presented. Eigenfrequencies and modeshapes will be compared and validated with the FEM model. The accuracy of the measured damping and the orthogonality of the modeshapes will be discussed.
- In Chapter 6 a response model will be built of the base and the upright.

Part III: Identification of damping in joints

- In Chapter 7 is explained how dynamic substructuring techniques can be used to couple to partially measured plates
- In Chapter 8 the methods to couple two plates based on partial measurements will be validated.
- In Chapter 9 the plate models that are built will be coupled using the method that is validated.
- In Chapter 10 the results of the identification of the rubber mountings will be presented.
- In Chapter 11 the conclusions and recommendations will be presented.

Part I

Theory

Chapter 1

Mechanical systems with damping

All real-world mechanical systems possess damping. There are a lot of different sources of damping. Damping can be caused by external dissipation of energy, but it is also inherent to materials due to friction at molecular scale. A lot of different models exist for damping. These are for example described by Bert [9] and Lazan [17], and more recently by Woodhouse [30]. Despite a wide variety in damping models, the viscous damping model is the only damping model which is common in engineering practice. In this chapter an overview is given of dynamic systems with linear damping, and it is explained how they can be solved. The first section is about viscously damped systems, and the second section is about non-viscously damped systems.

1.1 Viscously damped systems

A damping force due to viscous damping can be described as follows

$$f_d = c\dot{q}. \quad (1.1)$$

This is a linear model in which the damping force solely depends on the instantaneous generalized velocities \dot{q} , and on no other state variables. c is the viscous damping constant. Such a damping force appears in the case of solids moving at a relatively low speed in viscous fluids. Rayleigh introduced this model via his famous dissipation function [23]. This viscous damping model is widely used because a dynamic analysis of a given system becomes easy, and it is appropriate as an approximate and local description of more complex systems [22]. However, there is no physical reason why a general mechanical system behaves like this.

The linearized dynamic damped system can be written as

$$\mathbf{M}\ddot{\mathbf{q}}(t) + \mathbf{C}\dot{\mathbf{q}}(t) + \mathbf{K}\mathbf{q}(t) = \mathbf{f}(t), \quad (1.2)$$

where \mathbf{M} is the mass matrix, \mathbf{C} is the damping matrix and \mathbf{K} is the stiffness matrix. \mathbf{f} is the external force vector and \mathbf{q} is the vector of generalized coordinates. This system of equations can in general not be written in terms of uncoupled equations by means of modal expansion. This is due to the fact that the eigenmodes are orthogonal with respect to the \mathbf{M} and \mathbf{K} matrix but are in general not orthogonal to the \mathbf{C} matrix, unless the \mathbf{C} matrix is partially composed of the \mathbf{M} and \mathbf{K} matrix. In that special case, the system can be solved as an undamped system in terms of real modes.

When the C matrix is not diagonalizable, the system of equations has complex eigensolutions. Practically, this means that the eigenvalue consists of a real value representing the damping, and an imaginary value representing the frequency.

When a system has complex eigensolutions, there are different ways to solve this problem. One way is to formulate the system as a state space description, and solve it completely. Another way is to assume that the system is low damped and has no closely spaced modes. The system can then be solved using the perturbation theory.

Thus, there are three different ways to solve the problem:

- General solution in state space
- Perturbation theory, assuming the normal equations to be uncoupled
- Assuming proportional damping, the system can be solved as the undamped system.
- Applying mode superposition with coupled normal equations by the damping matrix.

The first three solution methods will be further explained in the next sections.

1.1.1 State space description

In general, the damping matrix is not diagonalizable with K and M . The assumption of low damping and no closely spaced modes is also not valid in general. Therefore in general the eigenmodes and eigenvalues need to be considered as complex, and if one wants to apply classical eigensolvers to compute the eigensolutions, it is necessary to recast Equation (1.2) in state space form [12], [11], since eigensolvers can not solve the general eigenvalue problem $(\lambda^2 m + \lambda c + k)x = 0$

$$A\dot{\mathbf{z}} + B\mathbf{z} = \mathbf{u}, \quad (1.3)$$

where

$$\mathbf{z} = \begin{bmatrix} \mathbf{q} \\ \dot{\mathbf{q}} \end{bmatrix}, \quad \mathbf{u} = \begin{bmatrix} \mathbf{0} \\ \mathbf{f} \end{bmatrix}, \quad (1.4)$$

and A and B are both symmetric

$$A = \begin{bmatrix} C & M \\ M & 0 \end{bmatrix}, \quad B = \begin{bmatrix} K & \mathbf{0} \\ \mathbf{0} & -M \end{bmatrix}. \quad (1.5)$$

It can be seen that the upper equation is the system equation, and the lower one is a trivial equation that causes the matrices to be symmetric. If \mathbf{x} is assumed to be $\mathbf{x}e^{\lambda t}$ the eigenvalue problem for the free system becomes

$$(\lambda A + B)\mathbf{z} = \mathbf{0}, \quad (1.6)$$

where $\mathbf{z} = [\mathbf{q} \quad \mathbf{q}\lambda]^T$, and λ is the complex eigenfrequency.

By writing the system in state space form, the size of the problem doubles. The eigenmodes and eigenvalues are complex and because the number of unknowns doubles, the eigenvalues and eigenmodes have conjugate counterparts. The eigenmodes \mathbf{z} are orthogonal with respect to the A and B matrix which can be described as follows

$$\mathbf{z}^T A \mathbf{z} = I \quad (1.7)$$

$$\mathbf{z}^T B \mathbf{z} = \Lambda. \quad (1.8)$$

A single response parameter resulting from a single force can now be extracted and the response function becomes

$$H_{ij}(\omega) = \sum_{k=1}^N \left(\frac{z_i^T z_j}{i\omega - \lambda_k} + \frac{z_i^H \bar{z}_j}{i\omega - \bar{\lambda}_k} \right). \quad (1.9)$$

This can also be written as:

$$H_{ij}(\omega) = \sum_{k=1}^N \frac{A + i(\omega/\omega_k)B}{\omega_k^2 - \omega^2 + 2i\omega\omega_k\zeta_k}, \quad (1.10)$$

where ζ is the modal damping constant, and A and B are modal constants. The FRF can also be written as a ratio of two polynomials. This is the ratio fraction polynomial description:

$$H(\omega) = \frac{\sum_{k=0}^{2N-1} a_k (i\omega)^k}{\sum_{k=0}^{2N} b_k (i\omega)^k} \quad (1.11)$$

The system description (1.9), (1.10) and (1.11) are all identical and are used in modal analysis methods, which will be discussed in the next chapter.

1.1.2 First order perturbation method

The state space method is exact in nature, but due to the fact that the size of the problem doubles, it requires significant effort to obtain the solution. The method also lacks some of the intuitives of the traditional methods.

Using a first order perturbation method, the problem can be solved in a much simpler way [4], [26]. A harmonic solution for Equation (1.2) of the form $q(t) = xe^{i\lambda t}$ is sought. This results in the free vibration equation:

$$-\lambda_j^2 \mathbf{M} \mathbf{x}_j + i\lambda_j \mathbf{C} \mathbf{x}_j + \mathbf{K} \mathbf{x}_j = 0. \quad (1.12)$$

The undamped modeshapes belonging to the undamped system are orthogonal with respect to the \mathbf{K} and \mathbf{M} matrices. These modeshapes are described by \mathbf{y} , the modeshapes belonging to the damped system are called \mathbf{x} . Since \mathbf{y} forms a complete set of eigenvectors, \mathbf{x} can be expanded as a linear combination of \mathbf{y} . When the damping is small, the roots and the eigenvectors of both the damped and the undamped system are nearly the same. Therefore a solution can be tried in the form of

$$\mathbf{x}_j = \sum_{l=1}^N \alpha_{l(j)} \mathbf{y}_l \quad \text{where } \alpha_{j(j)} = 1 \quad \text{and} \quad |\alpha_{l(j)}| \ll 1 \quad \forall l \neq j. \quad (1.13)$$

This \mathbf{x} can now be substituted in Equation (1.12). After premultiplying this equation by \mathbf{y}_k^T , and using orthogonality properties of the undamped modeshapes, we get

$$-\lambda_j^2 \alpha_{k(j)} + i\lambda_j \sum_{l=1}^N \alpha_{l(j)} C'_{kl} + \omega_k^2 \alpha_{k(j)} = 0, \quad (1.14)$$

in which C'_{kl} is the damping matrix projected on the modes. In the case that $k = j$, and neglecting second order terms this can be written as

$$-\lambda_j^2 + i\lambda_j C'_{jj} + \omega_j^2 \approx 0, \quad (1.15)$$

from which λ_j can be calculated

$$\lambda_j \approx \pm\omega_j + iC'_{jj}/2. \quad (1.16)$$

For the case $k \neq j$, neglecting the second order terms, we get:

$$\alpha_{k(j)} \approx \frac{i\omega_j C'_{kj}}{(\omega_j^2 - \omega_k^2)}. \quad (1.17)$$

If we assume that C'_{kj} are negligible, and substitute (1.17) in (1.14), a set of totally uncoupled normal equations is obtained. This small damping assumption is the modal damping assumption proposed by Rayleigh. This assumption is only valid if the eigenfrequencies are not closely spaced, and the damping is low. The condition

$$2\zeta_j \omega_j / |\omega_j \omega_k| \ll 1, \quad (1.18)$$

proposed by Hasselman [14] gives a good indication of when modal coupling will not occur [8].

Instead of neglecting C'_{kj} they can also be used to obtain a full damping matrix of the system. α is then substituted in (1.13), and the complex modeshapes becomes:

$$\mathbf{x}_j \approx \mathbf{y}_j + i \sum_{\substack{k=1 \\ k \neq j}} \frac{i\omega_j C'_{kj}}{(\omega_j^2 - \omega_k^2)} \mathbf{y}_k. \quad (1.19)$$

These modeshapes will be used for building the damping matrix, which will be explained in Section 1.3.

1.1.3 Proportional damping

In the beginning of this section it was said that Rayleigh introduced the viscous damping model. A further idealization of reality also proposed by Rayleigh is to assume proportional damping. This can be done by building the damping matrix as a combination of the mass and stiffness matrix:

$$\mathbf{C} = a\mathbf{K} + b\mathbf{M}. \quad (1.20)$$

This idealization is proposed for mathematical convenience only, and has no physical background. The main advantage of using this method is that the system can be solved exactly like an undamped system because the eigenvectors are the same. Proportional damping is also known as 'Rayleigh Damping' or 'Classical Damping'. The damped eigenfrequency of a proportional damped system is given by

$$\lambda_r = \omega_r \sqrt{1 - \zeta_r^2}. \quad (1.21)$$

This method can only be used if there is no coupling between modes, because the damping matrix is diagonal. Because there are only two variables to tune the damping matrix, a and b , only two damping values can be fitted exactly, and that causes the damping to be overestimated in low and high frequent regions [27].

1.2 Non-viscously damped systems

In this section systems are described that have no viscous damping. In the first paragraph, a special type known as hysteretic, structural or material damping is explained. In the second paragraph, general non-viscous damped systems are described.

1.2.1 Hysteretic damping

Hysteretic damping or structural damping is a damping model that relates the amplitude of the damping force to displacement and the phase to the velocity [27]. With this model, the damping is assumed to be independent of the frequency, but proportional to the motion amplitude and in phase with velocity. Hysteretic damping violates the requirement of causality since it responds before exciting. The general equation of motion for a MDoF system with hysteretic damping is:

$$\mathbf{M}\ddot{\mathbf{q}} + (\mathbf{K} + i\mathbf{D})\mathbf{q} = \mathbf{f}. \quad (1.22)$$

Assuming that the response is limited to the forcing term $\mathbf{x} = \mathbf{z}e^{i\lambda t}$, Equation (1.22) results in a complex eigenproblem, which means that both the eigenfrequencies and the eigenmodes are complex. The eigenvalue will be chosen as

$$\lambda_r^2 = \omega_r^2 (1 + i\eta_r) \quad (1.23)$$

where η_r is the damping loss factor. The eigenvalue problem becomes

$$(\mathbf{K}' - \omega^2\mathbf{M})\mathbf{y} = \mathbf{0}, \quad (1.24)$$

where $\mathbf{K}' = \mathbf{K} + i\mathbf{D}$. The eigenmodes of this system are orthogonal with respect to \mathbf{K}' and \mathbf{M} . The system can now be solved like an undamped system. The response function can be written as [19]

$$\mathbf{H}_{jk}(\omega) = \sum_{r=1}^N \frac{{}_r A_{jk}}{\omega_r^2 - \omega^2 + i\eta_r \omega_r^2} \quad (1.25)$$

where ${}_r A_{jk}$ are complex modeshapes. This equation is also used in modal analysis, mainly with the circle fit procedure. The main difference with viscous damping is that the damping contribution of the numerator is not dependent on ω in case of hysteretic damping.

1.2.2 General non-viscous damping

Now, a more general form of equation (1.2) is used, where the damping force is written as a convolution integral over appropriate kernel functions [5]:

$$\mathbf{M}\ddot{\mathbf{q}}(t) + \int_{-\infty}^t \mathcal{G}(t-\tau)\dot{\mathbf{q}}(\tau)d\tau + \mathbf{K}\mathbf{q}(t) = \mathbf{0}. \quad (1.26)$$

In fact, $\mathcal{G}(t)$ is an $N \times N$ matrix of kernel functions describing the damping mechanisms. If just one relaxation function is taken into account, the function $\mathcal{G}(t)$ reduces to

$$\mathcal{G}(t) = \mathbf{C}g(t), \quad (1.27)$$

where \mathbf{C} is a positive definite coefficient matrix, and $g(t)$ is a damping function. The convolution integral must be non-negative in order to have a semi-positive damping matrix in the frequency domain. This can be written as the rate of energy dissipation, which must be non-negative:

$$\mathcal{D}(t) = \frac{1}{2} \dot{\mathbf{q}}^T(t) \int_{-\infty}^t \mathcal{G}(t - \tau) \dot{\mathbf{q}}(\tau) d\tau. \quad (1.28)$$

A lot of damping functions $g(t)$ are described in literature. Below, four functions are shown from Adhikari and Woodhouse [5].

- Viscous model,

$$g^{(1)}(t) = \delta \quad (1.29)$$

- Exponential model

$$g^{(2)}(t) = \mu_1 e^{-\mu_1 t}, \quad t \leq 0 \quad (1.30)$$

- Gaussian model

$$g^{(3)}(t) = 2\sqrt{\frac{\mu_2}{\pi}} e^{-\mu_2 t^2}, \quad t \leq 0 \quad (1.31)$$

- Double exponential model

$$g^{(4)}(t) = \frac{\beta_1 \mu_3 e^{-\mu_3 t} + \beta_2 \mu_4 e^{-\mu_4 t}}{(\beta_1 + \beta_2)}, \quad t \leq 0. \quad (1.32)$$

The first model is simply the viscous model. No time histories are taken into account. The other functions are all exponential decaying functions, and can be used to describe visco-elastic material. The choice for a model is dependent on material behaviour. The dynamic system of equation (1.26) can be written in the frequency domain:

$$-\lambda_j^2 \mathbf{M} \mathbf{q}_j + i \lambda_j \mathbf{G}(\lambda_j) \mathbf{q}_j + \mathbf{K} \mathbf{q}_j = \mathbf{0}, \quad (1.33)$$

where \mathbf{G} is the Fourier Transform of $\mathcal{G}(t)$. The total number of eigenvalues can be larger than $2N$, because additional eigenvalues may be formed by the damping functions. The problem is a non-linear eigenvalue problem. The most dynamic analysis methods of such 'viscoelastic systems' are state space based. There are reasons to use other, iterative methods for finding a solution. The main reason is that the state space approach is computationally very intensive, due to a large number of internal variables. Adhikari and Pascual recently proposed a new iterative method for solving viscoelastic damped systems [3]. These solution methods will not be described here.

1.3 Damping matrices

Building the damping matrix belonging to a finite element model can be done in different ways. In this section four methods will be described.

1. A common way to build one, is to assume that the system is proportionally damped. Because there are only two variables to tune, a maximum of two modal damping values can be fit to the measured data. The other modal damping values are over- or underestimated.

$$\mathbf{C} = a\mathbf{K} + b\mathbf{M} \quad (1.34)$$

2. The damping matrix can also be built on the basis of measured modal damping values. Building the damping matrix by modal expansion can be done as follows [26]:

$$\mathbf{C} = \sum_{s=1}^N \mathbf{M} \mathbf{x}_{(s)} \frac{2\epsilon_s \omega_s}{\mu_s} \mathbf{x}_{(s)}^T \mathbf{M}, \quad (1.35)$$

where μ is the modal mass and ϵ_s is the modal damping ratio. This inherently assumes that the damping matrix is diagonalizable or that the damping is small.

When only a small number of modes is included in the expansion, the matrix cannot be related to the physical topology. The theory is based on a full set of modes, but usually it is not possible to measure all eigenproperties of a system.

3. It is also possible to build a damping matrix using frequency dependent material properties [27]. This is in fact hysteretic damping as is described in Section 1.2.1, and it is related to material properties that can be tested on for instance a Dynamic Mechanical Analyzer (DMA). The matrix $(\mathbf{K} + i\mathbf{D})$ is then obtained by assuming that the structure has a complex Young's modulus

$$E_{\text{hyst}} = E' + iE'' = E'(1 + i\gamma) \quad (1.36)$$

where E' is called the storage modulus and E'' is called the loss modulus. γ is called the loss factor.

4. Another way to build a damping matrix is proposed by Adhikari and Woodhouse [4]. The method will be explained below. The method continues on the first order perturbation method of the viscously damped systems. It is possible to extract the off-diagonal terms of the damping matrix with the aid of complex modeshapes. The diagonal terms, C'_{jj} have already been found as the imaginary part of the complex eigenfrequency

$$C'_{jj} = 2\Im(\hat{\lambda}_j) \quad (1.37)$$

As stated in Section 1.1.2, the complex eigenfrequency is written as

$$\lambda_j \approx \pm\omega_j + iC'_{jj}/2. \quad (1.38)$$

It can be seen that the real part of the complex eigenfrequency is the undamped natural frequency

$$\hat{\omega}_j = \Re(\hat{\lambda}_j) \quad (1.39)$$

Similarly, the complex mode shapes can be written as:

$$\hat{\mathbf{x}}_j = \hat{\mathbf{u}}_j + i\hat{\mathbf{v}}_j, \quad (1.40)$$

where $\hat{\mathbf{u}}_j$ is the j^{th} mode, associated with the undamped system, and $\hat{\mathbf{v}}_j$ is a linear combination of the other undamped mode shapes. The imaginary part of $\hat{\mathbf{x}}_j$ can be written as a linear combination of $\hat{\mathbf{u}}_i$ as is shown in (1.19)

$$\hat{\mathbf{v}}_j = \sum_{k=1}^m B_{kj} \hat{\mathbf{u}}_k \quad \text{where} \quad B_{kj}(\hat{\omega}_j^2 - \hat{\omega}_k^2) = \hat{\omega}_j C'_{kj}. \quad (1.41)$$

Usually the number of modes considered in the study (m) is smaller than (N). Therefore this relation cannot be satisfied exactly. An error can be defined that must be minimized to find B_{kj} :

$$\varepsilon_j = \hat{\mathbf{v}}_j - \sum_{k=1}^m B_{kj} \hat{\mathbf{u}}_j \quad (1.42)$$

This error should be in the nullspace of $\hat{\mathbf{u}}_l^T$, as follows:

$$\hat{\mathbf{u}}_l^T \varepsilon_j = 0, \quad l = 1, \dots, m. \quad (1.43)$$

The error can be substituted in this equation:

$$\hat{\mathbf{u}}_l^T \left(\hat{\mathbf{v}}_j - \sum_{k=1}^m B_{kj} \hat{\mathbf{u}}_j \right) = 0 \quad \text{or} \quad \sum_{k=1}^m W_{lk} B_{kj} = S_{lj}, \quad l = 1, \dots, m, \quad (1.44)$$

with $W_{lk} = \hat{\mathbf{u}}_l^T \hat{\mathbf{u}}_k$ and $S_{lj} = \hat{\mathbf{u}}_l^T \hat{\mathbf{v}}_j$. This summation can be written as a matrix multiplication:

$$\mathbf{W}\mathbf{B} = \mathbf{S} \quad (1.45)$$

\mathbf{B} can be obtained as follows:

$$\mathbf{B} = \mathbf{W}^+ \mathbf{S} = [\hat{\mathbf{U}}^T \hat{\mathbf{U}}]^{-1} \hat{\mathbf{U}}^T \mathbf{V}, \quad (1.46)$$

where:

$$\hat{\mathbf{U}} = [\hat{\mathbf{u}}_1, \hat{\mathbf{u}}_2, \dots, \hat{\mathbf{u}}_m] \in \mathbb{R}^{N \times m}, \quad \hat{\mathbf{V}} = [\hat{\mathbf{v}}_1, \hat{\mathbf{v}}_2, \dots, \hat{\mathbf{v}}_m] \in \mathbb{R}^{N \times m}, \quad (1.47)$$

and with the B_{jk} coefficients the C'_{kj} can be calculated with the formula deduced from Equation (1.41):

$$C'_{kj} = \frac{(\hat{\omega}_j^2 - \hat{\omega}_k^2) B_{kj}}{\hat{\omega}_j}, \quad k \neq j. \quad (1.48)$$

Eventually the \mathbf{C} matrix in the physical domain becomes

$$\mathbf{C} = [(\hat{\mathbf{U}}^T \hat{\mathbf{U}})^{-1} \hat{\mathbf{U}}^T]^T \mathbf{C}' [(\hat{\mathbf{U}}^T \hat{\mathbf{U}})^{-1} \hat{\mathbf{U}}^T] \quad (1.49)$$

It can be seen that to obtain \mathbf{C} only the complex eigenfrequencies and modeshapes are needed. This method is very simple and does not require much computational time.

Four different methods have been discussed. The choice for a method will depend on what kind of measurement data is available.

Chapter 2

Modal parameter identification

In the previous chapter it has been discussed how damped linear systems can be solved, and how a damping matrix can be constructed. These solutions are based on a description of system matrices, K , C and M . In the case of real life problems such matrices are not always easy to construct. If they have been constructed, for example by using a Finite Element program, they need to be checked for accuracy. This can be done by comparing dynamic test data with model data.

From a dynamic test, Frequency Response Functions (FRF's) can be obtained. By using a curve fitting process modal parameters can be estimated, namely the eigenfrequencies, eigenmodes, and the modal damping. With these modal parameters, a modal model of a structure can be built, and from this modal model a spatial (for instance an FE model) model can be constructed. This spatial or modal model can then be used to check the correctness of the theoretical model. They can also be used to predict dynamic responses on certain (harmonic) loadcases. The objective of using curve fitting is to find the coefficients for the theoretical expressions which have been discussed in Section 1.1. These theoretical expressions should match the measured data as close as possible.

Curve fitting can be done either in the time domain or in the frequency domain. In the frequency domain the FRF's are used, and in the time domain the Impulse Response Functions (IRF's) are used, which are normally obtained by taking the Inverse Fourier Transform of the FRE. Modal analysis methods can be divided in SDoF (Single Degree of Freedom) and MDoF (Multiple Degree of Freedom) methods. SDoF methods can be used when the systems eigenmodes are not coupled and when the eigenfrequencies are well separated. MDoF methods can be used to analyse multiple DOF at once. SISO methods (Single Input Single Output) are used to analyse one FRF. There are also modal analysis algorithms that can handle multiple FRF's at once (SIMO - Single Input Multiple Output). MIMO (Multiple Input Multiple Output) methods can be used to analyse multiple references in order to extract double modes.

This chapter is divided in three parts. The first part deals with mode indicator functions, the second part describes the circle fit method. This method will be used throughout this research to obtain modal parameters, and to check them for accuracy. The third part describes MDoF modal analysis methods these methods will be used to check the validity of the results obtained with the circle fit method.

2.1 Mode indicator functions

To identify the number of eigenfrequencies that exist in a frequency band of interest, Mode Indicator Functions (MIF's) can be used. The easiest way to count the amount of poles is to look to a single FRF and count the peaks. The two main disadvantages of this method are

1. Modes may not be active in a single measurement
2. Double modes cannot be indicated because only one peak can be seen
3. Peaks cannot be seen due to high damping or coupling

For these reasons different functions have been proposed to make it possible to find all modes of interest in a given frequency band. An overview of such methods can be found for instance in [11] or [20]. From all these methods the complex mode indicator function (CMIF), and the summation function are used the most in practise. For that reason these two will be described below. Also an explanation of the stability diagram will be given.

2.1.1 Summation function

The summation function is simply a summation of all- or a subset of- selected FRF's. It is clear that with this method most peaks will be visible. However, with this method it is impossible to identify double modes. Another disadvantage of this method is that most peaks widen, which will lead to difficulties in identifying closely spaced and highly damped modes.

2.1.2 Complex mode indicator function

Mode indicator functions are meant to indicate modes in multiple reference data sets [11]. Multiple reference data sets can be obtained by using multiple sensors during a roving hammer impact test or by using multiple excitations at once during a test. This data set consists of an $n \times p$ matrix, with n the number of reference DoF and p the excitation DoF. The complex mode indicator function is a function that can handle multiple reference data sets in order to extract double or repeated modes. This mode indicator function is defined by the singular value decomposition (SVD) of the FRF submatrix ($n \times p$). The singular value decomposition is defined as:

$$\mathbf{H}(\omega)_{n \times p} = \mathbf{U}(\omega)_{n \times n} \mathbf{\Sigma}(\omega)_{n \times p} \mathbf{V}(\omega)_{p \times p}^H \quad (2.1)$$

$$\mathbf{CMIF}(\omega)_{p \times p} = \mathbf{\Sigma}(\omega)_{p \times n}^T \mathbf{\Sigma}(\omega)_{n \times p} \quad (2.2)$$

These equations imply that at each frequency point an SVD is performed. This means that at each frequency point, p singular values are calculated. These singular values can be plotted against frequency. This results in p curves in the CMIF plot. Natural frequencies can be identified by large values of the CMIF. Because of the fact that there are multiple lines, double or repeated modes will result in multiple peaks at the same frequency at different CMIF curves. The \mathbf{U} and \mathbf{V} matrices contain the left and right singular vector. The left singular vector is related to the mode shape belonging to that eigenfrequency and the right singular vector represents the force pattern which is needed to excite that mode only. Thus, this pattern is orthogonal to all the other mode shapes. If two mode shapes that belong to the same frequency are orthogonal, then they are called 'double' or 'repeated' modes. The force pattern \mathbf{V} can be used to obtain a FRF for each mode individually. This is done by

$$\mathbf{EFRF}(\omega)_{n \times p} = \mathbf{H}(\omega)_{n \times p} \mathbf{V}(\omega)_{p \times p}, \quad (2.3)$$

and this results in FRF's which consist of single peaks that can be used to obtain eigenvalue properties in SDoF modal analysis. This results in global properties, as damping and eigenfrequency, and because all FRFs are handled at once, no modeshape information can be obtained. An example of a CMIF can be seen in Figure 2.1. The three lines mean that there are three reference sensors used. The data set is measured data of the square plate that will be used later on in the research. It can be seen that near 280 Hz two lines show a resonance peak, which means that a double mode is indicated at that frequency. The same can be seen at 500 Hz and 850 Hz.

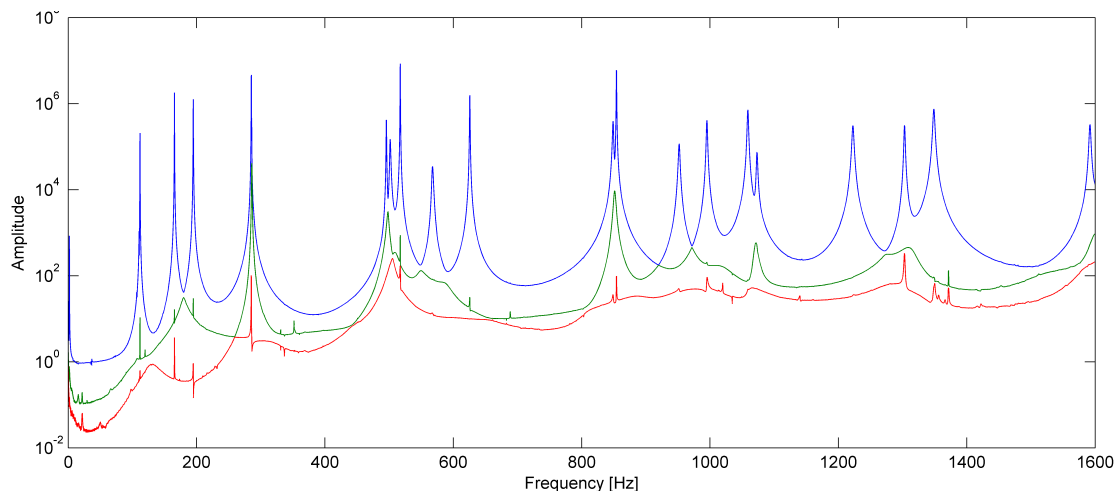


Figure 2.1: Complex Mode Indicator Function of measured data set. Three lines show squared singular values of the total receptance matrix which has dimensions [3,169].

2.1.3 Stability diagram

The basis of the stability diagram is that a certain model in the frequency or time domain will be fitted with models of different orders. The poles which are found for all the different model orders are plotted in a diagram called the stability diagram. If the model is fitted with more poles than physically exist, computational poles are calculated. An example of a stability diagram can be seen in Figure 2.2.

2.2 SDoF Circle fit method

The description of this method is based on the book Modal Testing by Ewins [11]. SDoF methods imply that the (MDoF) system can be analyzed per individual frequency. However, they do not imply that the system is reduced to an SDoF system. The basis for SDoF methods is the SDoF assumption: At the vicinity of a resonance, the FRF is dominated by the contribution of that mode and the contributions of other modes are negligible. The total system as is deduced in Chapter 1 can be described by

$$\alpha_{jk}(\omega) = \sum_{s=1}^N \frac{sA_{jk}}{\omega_s^2 - \omega^2 + i\eta_s\omega_s^2}, \quad (2.4)$$

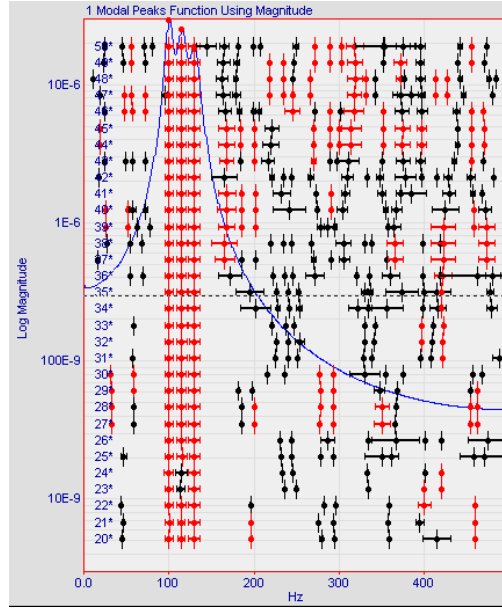


Figure 2.2: Stability Diagram in ME'Scope. The red dots are stable poles, the black dots are unstable poles. The damping of a pole is indicated by the length of the bar across the poles. the blue line on the background is a summation function [29].

This can be written as

$$\alpha_{jk}(\omega) = \frac{rA_{jk}}{\omega_r^2 - \omega^2 + i\eta_r\omega_r^2} + \sum_{\substack{s=1 \\ s \neq r}}^N \frac{sA_{jk}}{\omega_s^2 - \omega^2 + i\eta_s\omega_s^2}, \quad (2.5)$$

The SDoF assumption is that in a small frequency range around a resonance, the second term is almost independent of the frequency ω , and may be written as

$$\alpha_{jk}(\omega)_{\omega \cong \omega_r} \cong \frac{rA_{jk}}{\omega_r^2 - \omega^2 + i\eta_r\omega_r^2} + {}_rB_{jk} \quad (2.6)$$

This means that near a resonance the combined effect of all the other resonances can be described by an (imaginary) constant ${}_rB_{jk}$.

2.2.1 Theory

The circle fit method is based on the fact that the Nyquist plot of an SDoF system describes a circle in the complex plane. For a viscously damped system, the mobility (velocity over force) draws a circle, and for a hysteretically damped system the receptance (displacement over force). In this section the method will be worked out for a hysteretically damped system, because for these systems the modal identification can be explained more easily than for the viscously damped case. However, the same procedure can be written for a viscously damped system.

The receptance of a hysteretically damped system is written as

$$\alpha(\omega) = \frac{1}{k - \omega^2 m + id} = \frac{(k - \omega^2 m) - id}{(k - \omega^2 m)^2 + d^2}. \quad (2.7)$$

In the complex plane, a circle with radius r and center $y = -\frac{1}{2d}$ is written as

$$x^2 + y^2 = r, \quad (2.8)$$

where

$$x = \text{Re}(\alpha) \quad \text{and} \quad y = \text{Im}(\alpha) + \frac{1}{2d} \quad (2.9)$$

The real and imaginary part of the receptance are:

$$\text{Re}(Y) = \frac{(k - \omega^2 m)}{(k - \omega^2 m)^2 + d^2} \quad \text{and} \quad \text{Im}(Y) = \frac{-d}{(k - \omega^2 m)^2 + d^2} \quad (2.10)$$

These can be substituted in the equation for the circle, and we obtain

$$\begin{aligned} x^2 + y^2 &= \left(\frac{(k - \omega^2 m)}{(k - \omega^2 m)^2 + d^2} \right)^2 + \left(\frac{-d}{(k - \omega^2 m)^2 + d^2} + \frac{1}{2d} \right)^2 \\ &= \frac{(k - \omega^2 m)^2}{\left((k - \omega^2 m)^2 + d^2 \right)^2} + \frac{d^2}{\left((k - \omega^2 m)^2 + d^2 \right)^2} - \frac{1}{(k - \omega^2 m)^2 + d^2} + \frac{1}{4d^2} \\ &= \frac{(k - \omega^2 m)^2 + d^2 - (k - \omega^2 m)^2 - d^2}{\left((k - \omega^2 m)^2 + d^2 \right)^2} + \frac{1}{4d^2} \\ &= \frac{1}{4d^2} \end{aligned}$$

The radius of the circle is thus $\frac{1}{2d}$. And for an SDoF system this means that the damping can be deduced from the radius of the circle.

2.2.2 Fit Procedure

In this section the properties of the modal circle will be described and it will be explained how the modal properties can be deduced. The geometrical relations of the modal circle can be seen in Figure 2.3

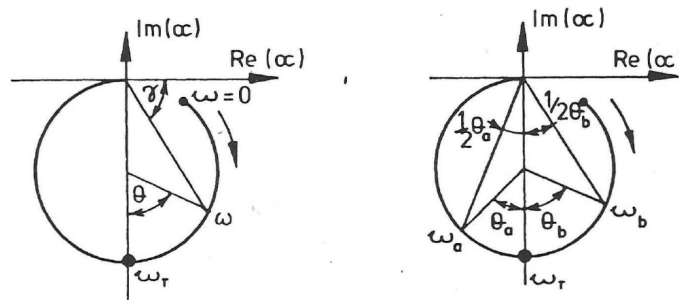


Figure 2.3: Properties of modal circle. [11]

The receptance which describes the modal circle as mentioned in the previous section is

$$\alpha_{jk}(\omega) = \frac{r A_{jk}}{\omega_r^2 - \omega^2 + i \eta_r \omega \omega_r^2}. \quad (2.11)$$

The modal constant ${}_rA_{jk}$ scales the circle, and rotates it, and will be left out of the equation.

$$\alpha_{jk}(\omega) = \frac{1}{\omega_r^2 - \omega^2 + i\eta_r\omega_r^2}. \quad (2.12)$$

A point on the circle has an angle (phase) of

$$\tan \gamma = \frac{\eta_r}{1 - (\omega/\omega_r)^2} \quad (2.13)$$

And this angle can be related to the angle between a line through the circle center and a point on the circle and the imaginary axis

$$\tan(90 - \gamma) = \tan\left(\frac{\theta}{2}\right) = \frac{1 - (\omega/\omega_r)^2}{\eta_r}. \quad (2.14)$$

The frequency can now be written as a function of the eigenfrequency, the damping and the angle θ

$$\omega^2 = \omega_r^2 \left(1 - \eta_r \tan\left(\frac{\theta}{2}\right)\right) \quad (2.15)$$

If (2.15) is differentiated with respect to the angle θ we obtain

$$\frac{d\omega^2}{d\theta} = \frac{-\omega_r^2\eta_r (1 - (\omega/\omega_r)^2)^2}{\eta_r^2} \quad (2.16)$$

The reciprocal of this function describes the rate at which the locus sweeps around the circular arc. This function reaches a minimum when $\omega = \omega_r$ as can be seen by further differentiation with respect to ω

$$\frac{d}{d\omega} \left(\frac{d\omega^2}{d\theta} \right)_{\omega^2=\omega_r^2} = 0 \quad (2.17)$$

This minimum can be found by using finite differences of the measured values, and will give an accurate estimate for the natural frequency ω_r . The damping can also be estimated by using this sweep parameter:

$$\left(\frac{d\theta}{d\omega^2} \right)_{\omega=\omega_r} = -\frac{2}{\omega_r^2\eta_r} \quad (2.18)$$

The damping can also be estimated by using equation (2.14), and two measured data points a and b . With this a set of three equations and three unknowns can be obtained:

$$\begin{aligned} \tan\left(\frac{\theta_b}{2}\right) &= \frac{1 - (\omega_b/\omega_r)^2}{\eta_r} \\ \tan\left(\frac{\theta_a}{2}\right) &= \frac{(\omega_a/\omega_r)^2 - 1}{\eta_r} \\ \theta_t &= \theta_a + \theta_b \end{aligned} \quad (2.19)$$

where θ_t can be calculated. From these equations a function for the modal damping can be written

$$\eta_r = \frac{\omega_a^2 - \omega_b^2}{\omega_r^2 (\tan(\theta_a/2) + \tan(\theta_b/2))}. \quad (2.20)$$

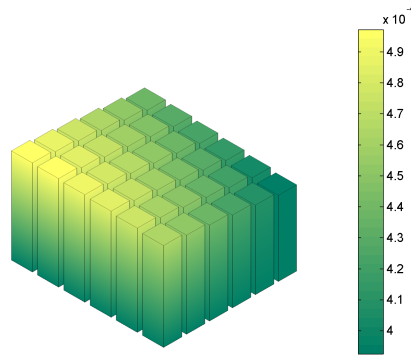


Figure 2.4: Damping plot of theoretical model

Different damping estimates can be calculated by taking different measurement positions on the modal circle. From such a set of damping estimates a damping plot can be made. An example of a damping plot can be seen in Figure 2.4. In theory, a linear SDOF system with viscous damping has a smooth and levelled damping plot. If the damping plot is not flat and levelled, this can have different reasons, for example:

- Cubic stiffness effect will lead to systematic distortion of the damping plot, it is not levelled or flat.
- A non linear damping will lead to a damping plot that is not levelled or flat.
- Closely spaced modes can lead to systematic distortion of the damping plot.

The last modal property, the complex modal constant, can be deduced from the diameter of the modal circle and the phase at which the circle is rotated.

$$D = \frac{|_r A_{jk}|}{\omega_r^2 \eta_r} \quad (2.21)$$

The phase can be deduced from the angle between the line through the circle centre and the origin of the complex plane, and the y axis. In case of viscous damping, the mobility of the system needs to be used, and the expression for the damping becomes

$$\eta_r = \frac{\omega_a^2 - \omega_b^2}{2\omega_r (\tan(\theta_a/2) + \tan(\theta_b/2))} \quad (2.22)$$

And the modal constant can be calculated by

$$D = \frac{|_r A_{jk}|}{2\omega_r \zeta_r} \quad (2.23)$$

2.3 MDoF modal analysis methods

SDoF methods are not always appropriate to use. MDoF methods are needed when modes are closely spaced in the frequency domain, or when the damping is high, and modes are coupled by the damping matrix. In those cases, the SDoF assumption is not valid anymore. In this chapter two different MDoF analysis methods, one in the frequency domain and one in the time domain will be discussed.

2.3.1 Rational fraction polynomial method

The Rational Fraction Polynomial method was presented by Richardson and Formenti [25] in 1982. It is one of the most used methods nowadays. [20]. The method is based on a viscously damped system of which the FRF is expressed as a ratio of two polynomials. This notation is called the rational fraction polynomial:

$$H_{jk}(\omega) = \frac{\sum_{k=0}^{2N-1} a_k(i\omega)^k}{\sum_{k=0}^{2N} b_k(i\omega)^k} \quad (2.24)$$

The method is based on an error between the model and the measured values, which needs to be minimized. This error is thus described as:

$$e_i = \frac{\sum_{k=0}^{2N-1} a_k(i\omega)^k}{\sum_{k=0}^{2N} b_k(i\omega)^k} - H_i^m \quad \rightarrow \quad e'_i = \sum_{k=0}^{2N-1} a_k(i\omega)^k - H_i^m \sum_{k=0}^{2N} b_k(i\omega)^k \quad (2.25)$$

This error can be written as a vector equation as follows:

$$e'_i = \begin{bmatrix} 1 & (i\omega_k) & \cdots & (i\omega_k)^{2N-1} \end{bmatrix} \begin{bmatrix} a_0 \\ a_1 \\ \vdots \\ a_{2N-1} \end{bmatrix} - H_k^m \begin{bmatrix} 1 & (i\omega_k) & \cdots & (i\omega_k)^{2N-1} \end{bmatrix} \begin{bmatrix} b_0 \\ b_1 \\ \vdots \\ b_{2N-1} \end{bmatrix} - H_k^m (i\omega_k)^{2N} b_{2N} \quad (2.26)$$

Until now the error was defined for one frequency point. If the measured FRF is defined by a set of L frequency points, then a set of L linear equations can be written in a matrix form:

$$\mathbf{E}' = \mathbf{P}\mathbf{a} - \mathbf{T}\mathbf{b} - \mathbf{w} \quad (2.27)$$

The error will now be defined as:

$$\mathbf{J} = \mathbf{E}^H \mathbf{E} \quad (2.28)$$

The error is a function of the coefficients \mathbf{a} and \mathbf{b} and results after the multiplication:

$$\begin{aligned} \mathbf{J}(\mathbf{a}, \mathbf{b}) = & \mathbf{a}^T \mathbf{P}^H \mathbf{P} \mathbf{a} + \mathbf{b}^T \mathbf{T}^H \mathbf{T} \mathbf{b} + \mathbf{w}^H \mathbf{w} - 2 \operatorname{Re}(\mathbf{a}^T \mathbf{T}^H \mathbf{P} \mathbf{b}) \\ & - 2 \operatorname{Re}(\mathbf{a}^T \bar{\mathbf{P}} \mathbf{w}) - 2 \operatorname{Re}(\mathbf{b}^T \mathbf{T}^H \mathbf{w}) \end{aligned} \quad (2.29)$$

The necessary conditions at a minimum of $\mathbf{J}(\mathbf{a}, \mathbf{b})$ are:

$$\begin{aligned} \frac{\partial \mathbf{J}}{\partial \mathbf{a}} = & 2\mathbf{P}^H \mathbf{P} \mathbf{a} - 2 \operatorname{Re}(\bar{\mathbf{P}} \mathbf{T} \mathbf{b}) - 2 \operatorname{Re}(\mathbf{P}^H \mathbf{w}) = 0 \\ \frac{\partial \mathbf{J}}{\partial \mathbf{b}} = & 2\mathbf{T}^H \mathbf{T} \mathbf{b} - 2 \operatorname{Re}(\bar{\mathbf{T}} \mathbf{P} \mathbf{a}) - 2 \operatorname{Re}(\mathbf{T}^H \mathbf{w}) = 0 \end{aligned} \quad (2.30)$$

These two equations can be written as a matrix equation:

$$\begin{bmatrix} \mathbf{Y} & \mathbf{X} \\ \mathbf{X}^T & \mathbf{Z} \end{bmatrix} \begin{bmatrix} \mathbf{a} \\ \mathbf{b} \end{bmatrix} = \begin{bmatrix} \mathbf{g} \\ \mathbf{f} \end{bmatrix} \quad (2.31)$$

where:

$$\begin{aligned}
X &= -\operatorname{Re}(\mathbf{P}^H \mathbf{T}) \\
Y &= \mathbf{P}^H \mathbf{P} \\
Z &= \mathbf{T}^H \mathbf{T} \\
\mathbf{g} &= \operatorname{Re}(\mathbf{P}^H \mathbf{w}) \\
\mathbf{f} &= \operatorname{Re}(\mathbf{T}^H \mathbf{w})
\end{aligned} \tag{2.32}$$

It is now possible to obtain a solution for \mathbf{a} and \mathbf{b} . However, the matrices seem to be ill-conditioned in most cases. For that reason, a set of orthogonal polynomials is mostly used instead of the polynomials that have been defined in Equation (2.24). Once the system has been solved, the b values can be used to obtain the eigenfrequencies and the damping, and the a values can be used to obtain the modeshapes. There is also a global method named the Global Rational Fraction Polynomial (GRFP) where multiple FRF's are taken into account simultaneously [24].

2.3.2 Complex exponential method

Modal analysis in the time domain is based on the impulse response function (IRF). This function can be obtained by the inverse fourier transformation of the FRF. The IRF is given by

$$h_{jk} = \sum_{r=1}^{2N} r A_{jk} e^{\lambda_r t}. \tag{2.33}$$

In this section two time domain methods are discussed. Use is made of Ewins [11], Maia and Silva [20] and He and Fu [15]. The complex exponential method is a frequently used modal analysis method that appeared in 1970 [28]. The advantage of this method is that it does not rely on initial estimates of modal parameters. L equally spaced time intervals are taken of the response function; this leads to the following equations:

$$\begin{aligned}
h_0 &= h(0) = \sum_{r=1}^{2N} A_r \\
h_1 &= h(\Delta t) = \sum_{r=1}^{2N} A_r V_r \\
h_2 &= h(2\Delta t) = \sum_{r=1}^{2N} A_r V_r^2 \\
&\vdots \quad \quad \quad \vdots \\
h_L &= h(L\Delta t) = \sum_{r=1}^{2N} A_r V_r^L,
\end{aligned} \tag{2.34}$$

with $V_r = e^{\lambda_r \Delta t}$. Due to the fact that the roots s_r come in conjugate pairs, and therefore also V_r , a polynomial exists with real coefficients β so that

$$\beta_0 + \beta_1 V_r + \beta_2 V_r^2 + \cdots + \beta_L V_r^L = 0. \tag{2.35}$$

This equation is known as the Prony equation. Taking (2.34) and multiplying each row by a coefficient β_k , and summing all the rows, we get

$$\sum_{i=0}^L \beta_i h_i = \sum_{j=1}^{2N} \left(A_r \sum_{i=0}^L \beta_i V_j^i \right). \tag{2.36}$$

It can be seen that the rightmost summation is in fact the polynomial written down in Equation 2.35. This means that the right hand side of the equation is always zero. If the number of time intervals is taken $2N$, and β_{2N} is set to 1, Equation (2.36) becomes

$$\sum_{i=0}^{2N} \beta_i h_i = 0 \quad \rightarrow \quad \sum_{i=0}^{2N-1} \beta_i h_i = -h_{2N}. \quad (2.37)$$

This equation can be written as a vector multiplication

$$\begin{bmatrix} h_0 & h_1 & h_2 & \cdots & h_{2N-1} \end{bmatrix} \begin{bmatrix} \beta_0 \\ \beta_1 \\ \vdots \end{bmatrix} = -h_{2N}. \quad (2.38)$$

If we now shift the time one instant, the same equation can be build

$$\begin{bmatrix} h_1 & h_2 & h_3 & \cdots & h_{2N} \end{bmatrix} \begin{bmatrix} \beta_0 \\ \beta_1 \\ \vdots \end{bmatrix} = -h_{2N+1}. \quad (2.39)$$

Taking $2N$ of this equations, a complete matrix equation can be build

$$\begin{bmatrix} h_0 & h_1 & h_2 & \cdots & h_{2N-1} \\ h_1 & h_2 & h_3 & \cdots & h_{2N} \\ \vdots & \vdots & \vdots & \ddots & \vdots \\ h_{2N-1} & h_{2N} & h_{2N+1} & \cdots & h_{4N-2} \end{bmatrix} \begin{bmatrix} \beta_0 \\ \beta_1 \\ \vdots \\ \beta_{2N-1} \end{bmatrix} = - \begin{bmatrix} h_{2N} \\ h_{2N+1} \\ \vdots \\ h_{4N-1} \end{bmatrix} \quad (2.40)$$

This can be written as

$$\mathbf{h}_{2N \times 2N} \boldsymbol{\beta}_{2N \times 1} = -\tilde{\mathbf{h}}_{2N \times 1} \quad (2.41)$$

from this equation the β coefficients can be obtained. These values can be used in the Prony equation (2.35) to solve for the V 's. The eigenfrequencies and damping values can then be obtained from these values. The modeshapes can be obtained by solving the A values in Equation 2.34. This leads to a set of equations as:

$$\begin{bmatrix} 1 & 1 & \cdots & 1 \\ V_1 & V_2 & \cdots & V_{2N} \\ \vdots & \vdots & \ddots & \vdots \\ V_1^{2N-1} & V_2^{2N-1} & \cdots & V_{2N}^{2N-1} \end{bmatrix} \begin{bmatrix} A_1 \\ A_2 \\ \vdots \\ A_{2N} \end{bmatrix} = \begin{bmatrix} h_0 \\ h_1 \\ \vdots \\ h_{2N-1} \end{bmatrix}. \quad (2.42)$$

Instead of using $2N$ time intervals in equation (2.40), the total number of time intervals that exists can be taken into account, and the system can be solved in a least square sense. This method is called the Least Square Complex Exponential Method.

The complex exponential method is based on a first estimate N for the number of poles in the system. It is hard to know beforehand how many poles exist in a certain frequency range. Therefore the problem is usually solved for multiple numbers of poles, dependent on the dynamic system. The solution in terms of poles are plotted in a stability diagram, from which stable poles can be picked.

Chapter 3

Dynamic substructuring

3.1 Introduction

In the previous chapters mechanical systems with damping and parameter identification techniques have been discussed. In this chapter the focus will be on Dynamic Substructuring. With this technique, multiple subsystems can be coupled by enforcing compatibility constraints on interfacing DoF and by demanding force equilibrium on the interface. In this research, the substructuring technique will be used to couple substructures in order to identify damping in joints. Substructuring can be done based on component modes (Component Mode Synthesis) or based on FRF's (Frequency Based Substructuring). In this research, the FBS method will be used. In Section 3.2 the method will be discussed. In the particular plate problem of this research, it is not possible to measure all DoF on the coupling interface. In order to enforce compatibility on all DoF on the interface, the set of measured DoF need to be extended with unmeasured DoF. This is described in Section 3.3. In this chapter use is made of the excellent paper 'General Framework for Dynamic Substructuring: History, Review, and Classification of Techniques' [10].

3.2 Coupling in the frequency domain

The dynamic equilibrium equations of n assembled substructures in the frequency domain are

$$\mathbf{Z}^{(s)}(\omega)\mathbf{u}^{(s)}(\omega) = \mathbf{f}^{(s)}(\omega) + \mathbf{g}^{(s)}(\omega) \quad (3.1)$$

where

$$\mathbf{Z} = \begin{bmatrix} \mathbf{Z}^{(1)} & & \\ & \ddots & \\ & & \mathbf{Z}^{(n)} \end{bmatrix}, \quad \mathbf{u} = \begin{bmatrix} \mathbf{u}^{(1)} \\ \vdots \\ \mathbf{u}^{(n)} \end{bmatrix}, \quad \mathbf{f} = \begin{bmatrix} \mathbf{f}^{(1)} \\ \vdots \\ \mathbf{f}^{(n)} \end{bmatrix}, \quad \mathbf{g} = \begin{bmatrix} \mathbf{g}^{(1)} \\ \vdots \\ \mathbf{g}^{(n)} \end{bmatrix} \quad (3.2)$$

and these are the amplitude of the harmonic response, the forces and the Dynamic Stiffness matrix which is

$$\mathbf{Z}(\omega) \triangleq -\omega^2 \mathbf{M} + j\omega \mathbf{C} + \mathbf{K} \quad (3.3)$$

the compatibility condition is

$$\mathbf{B}\mathbf{u} = \mathbf{0} \quad (3.4)$$

The matrix \mathbf{B} operates on the interface DoF and is a signed Boolean matrix. This equation states that each coinciding interface DoF of all the individual substructures has the same displacement. There is another equation needed which governs force equilibrium on the interface. This equation is

$$\mathbf{L}^T \mathbf{g} = \mathbf{0}, \quad (3.5)$$

where \mathbf{L} is also a signed boolean matrix. The total system is now described by

$$\begin{cases} \mathbf{Z}\mathbf{u} = \mathbf{f} + \mathbf{g} \\ \mathbf{B}\mathbf{u} = \mathbf{0} \\ \mathbf{L}^T \mathbf{g} = \mathbf{0} \end{cases} \quad (3.6)$$

3.2.1 Primal formulation

The substructures can now be assembled in a primal or in a dual way. In a primal formulation the system is reduced to the interface DoF, and the interface forces are eliminated as unknowns. The DoF are reduced as follows

$$\mathbf{u} = \mathbf{L}\mathbf{q} \quad (3.7)$$

where \mathbf{L} is the same matrix as used for the force equilibrium condition, and \mathbf{q} is the vector of coupling DoF. This can be substituted in the compatibility condition equation, resulting in

$$\mathbf{B}\mathbf{u} = \mathbf{B}\mathbf{L}\mathbf{q} = \mathbf{0} \quad \forall \quad \mathbf{q} \quad (3.8)$$

this condition is valid for any \mathbf{q} . This equation implies that \mathbf{L} represents the nullspace of \mathbf{B} .

Because of the fact that the compatibility condition is satisfied for any \mathbf{q} , the compatibility condition is always satisfied and is no longer part of the system equations. These system equations now become

$$\begin{cases} \mathbf{Z}\mathbf{L}\mathbf{q} = \mathbf{f} + \mathbf{g} \\ \mathbf{L}^T \mathbf{g} = \mathbf{0} \end{cases} \quad (3.9)$$

After premultiplication by \mathbf{L}^T the primal assembled system reduces to

$$\tilde{\mathbf{Z}}\mathbf{q} = \tilde{\mathbf{f}} \quad (3.10)$$

with

$$\begin{cases} \mathbf{Z} \triangleq \mathbf{L}^T \mathbf{Z} \mathbf{L} \\ \tilde{\mathbf{f}} \triangleq \mathbf{L}^T \mathbf{f} \end{cases} \quad (3.11)$$

3.2.2 Dual formulation

In a dual assembly, all the DoF are retained and the system is obtained by choosing the interface forces in the form

$$\mathbf{g} = -\mathbf{B}^T \boldsymbol{\lambda}, \quad (3.12)$$

where λ are the Lagrange multipliers representing the interface forces. The expression for \mathbf{g} can be substituted in the equilibrium condition:

$$\mathbf{L}^T \mathbf{g} = -\mathbf{L}^T \mathbf{B}^T \lambda = \mathbf{0} \quad (3.13)$$

Because it was shown that \mathbf{L} represents the nullspace of \mathbf{B} , and therefore \mathbf{B}^T represents the nullspace of \mathbf{L}^T , the system is now described by

$$\begin{cases} \mathbf{Z}\mathbf{u} + \mathbf{B}^T \lambda = \mathbf{f} \\ \mathbf{B}\mathbf{u} = \mathbf{0} \end{cases} \quad (3.14)$$

This is in matrix notation:

$$\begin{bmatrix} \mathbf{Z} & \mathbf{B}^T \\ \mathbf{B} & \mathbf{0} \end{bmatrix} \begin{bmatrix} \mathbf{u} \\ \lambda \end{bmatrix} = \begin{bmatrix} \mathbf{f} \\ \mathbf{0} \end{bmatrix} \quad (3.15)$$

In order to get a receptance matrix which describes the dynamics of the coupled structure the following equation can be obtained by eliminating the Lagrange multiplier from the system.

$$\mathbf{u} = (\mathbf{Y} - \mathbf{Y}\mathbf{B}^T(\mathbf{B}\mathbf{Y}\mathbf{B}^T)^{-1}\mathbf{B}\mathbf{Y})\mathbf{f} \quad (3.16)$$

3.3 Appending non-measured DoF to a set of measured DoF

In order to couple substructures, compatibility needs to be satisfied at interface DoF. In some cases it is not possible to measure interface DoF due to packaging, or other reasons. Then the unmeasured DoF needs to be built based on the measured DoF and on other information about the interface. This can be for example modeshapes, static stiffness or dynamic stiffness.

The impedance matrix of a system (substructure) that is partially measured, can be written in terms of measured and unmeasured DoF. The dynamic equilibrium equation in the frequency domain is then written as

$$\begin{bmatrix} \mathbf{Z}_{kk} & \mathbf{Z}_{ku} \\ \mathbf{Z}_{uk} & \mathbf{Z}_{uu} \end{bmatrix} \begin{bmatrix} \mathbf{u}_k \\ \mathbf{u}_u \end{bmatrix} = \begin{bmatrix} \mathbf{f}_k \\ \mathbf{f}_u \end{bmatrix}, \quad (3.17)$$

where \mathbf{u}_k are the measured (known) DoF, and \mathbf{u}_u are the unknown DoF. Let us assume that $\mathbf{f}_u = \mathbf{0}$. The lower equation becomes

$$\mathbf{Z}_{uk}\mathbf{u}_k + \mathbf{Z}_{uu}\mathbf{u}_u = \mathbf{0}. \quad (3.18)$$

All the DoF can now be written in terms of the measured DoF:

$$\begin{bmatrix} \mathbf{u}_k \\ \mathbf{u}_u \end{bmatrix} = \begin{bmatrix} \mathbf{I} \\ -\mathbf{Z}_{uu}^{-1}\mathbf{Z}_{uk} \end{bmatrix} \mathbf{u}_k \quad (3.19)$$

If this set of DoF is substituted in (3.17), we get:

$$\begin{bmatrix} \mathbf{Z}_{kk} - \mathbf{Z}_{ku}\mathbf{Z}_{uu}^{-1}\mathbf{Z}_{uk} \\ \mathbf{0} \end{bmatrix} \mathbf{u}_k = \begin{bmatrix} \mathbf{f}_k \\ \mathbf{f}_u \end{bmatrix} + \begin{bmatrix} \text{error}_k \\ \text{error}_u \end{bmatrix}, \quad (3.20)$$

where $\mathbf{Z}_{kk} - \mathbf{Z}_{ku}\mathbf{Z}_{uu}^{-1}\mathbf{Z}_{uk} = \mathbf{Y}_{kk}^{-1}$, which is the inverse of the admittance matrix of the known DoF, when the unknown ones have been condensed out. If the error vector is outside the space of the DoF, we can write

$$\begin{bmatrix} \mathbf{I} \\ -\mathbf{Z}_{uu}^{-1}\mathbf{Z}_{uk} \end{bmatrix}^T \begin{bmatrix} \text{error}_k \\ \text{error}_u \end{bmatrix} = \mathbf{0} \quad (3.21)$$

The error $_k$ can now be calculated:

$$\text{error}_k = (\mathbf{Z}_{uu}^{-1} \mathbf{Z}_{uk})^T \text{error}_u \quad (3.22)$$

From (3.20) it is known that $\text{error}_u = -\mathbf{f}_u$. (3.21) can now be substituted in (3.20) and we get

$$(\mathbf{Z}_{kk} - \mathbf{Z}_{ku} \mathbf{Z}_{uu}^{-1} \mathbf{Z}_{uk}) \mathbf{u}_k = \mathbf{f}_k - \mathbf{Z}_{ku} \mathbf{Z}_{uu}^{-1} \mathbf{f}_u. \quad (3.23)$$

Inverting this form, a description for the unknown DoF is obtained

$$\mathbf{u}_k = \mathbf{Y}_{kk} (\mathbf{f}_k - \mathbf{Z}_{ku} \mathbf{Z}_{uu}^{-1} \mathbf{f}_u). \quad (3.24)$$

The dynamics of the substructure can now be represented by using the following relations

$$\begin{aligned} \mathbf{u}_k &= \mathbf{Y}_{kk} (\mathbf{f}_k - \mathbf{Z}_{ku} \mathbf{Z}_{uu}^{-1} \mathbf{f}_u) \\ \mathbf{u}_u &= (-\mathbf{Z}_{uu}^{-1} \mathbf{Z}_{uk}) \mathbf{u}_k \end{aligned} \quad (3.25)$$

If $(-\mathbf{Z}_{uu}^{-1} \mathbf{Z}_{uk}) = \mathbf{C}$, the relations can be written as:

$$\boxed{\begin{aligned} \mathbf{u}_k &= \mathbf{Y}_{kk} (\mathbf{f}_k + \mathbf{C}^T \mathbf{f}_u) \\ \mathbf{u}_u &= \mathbf{C} \mathbf{u}_k \end{aligned}} \quad (3.26)$$

These relations are only exact if no forces are applied to the unknown DoF. This is not the case when using these relations to enforce compatibility on unmeasured DoF.

In order to describe the substructure, the \mathbf{C} matrix needs to be obtained. \mathbf{Z}_{uu} and \mathbf{Z}_{uk} are not measured, and the matrix \mathbf{C} can be built in different ways. The first methods that will be described are based on the existence of a FEM model. If there is no FEM model, the \mathbf{C} matrix can be built based on modes in a general sense, or based on geometrical relations between known and unknown DoF. Below, four methods to build the \mathbf{C} matrix are described

1. A Finite Element model of the substructure can be used to build the matrices \mathbf{Z}_{uu} and \mathbf{Z}_{uk} . This method is straight forward, and it will give accurate results, if the FEM model describes the substructure accurately.
2. One can also use the stiffness matrix describing the stiffness of the interface. This matrix can be built based on a static condensation of the full stiffness matrix or based on a SEREP approach.
3. The \mathbf{C} matrix can also be constructed by using interface modes. These modes have not been measured, but they can be predicted. Assuming that a set of modes can be predicted which describe the behaviour of the interface DoF accurately, the DoF can be represented like

$$\begin{bmatrix} \mathbf{u}_k \\ \mathbf{u}_u \end{bmatrix} = \Phi \boldsymbol{\gamma} = \begin{bmatrix} \Phi_k \\ \Phi_u \end{bmatrix} \boldsymbol{\gamma}, \quad (3.27)$$

where $\boldsymbol{\gamma}$ are the amplitudes of the modes. These amplitudes can be calculated using known DoF and measured modes.

$$\mathbf{u}_k = \Phi_k \boldsymbol{\gamma} \quad (3.28)$$

When the number of modes is smaller than the number of known DoF ($n_\Phi < n_k$), then the amplitudes can be calculated in a least square sense.

$$\boldsymbol{\gamma} = \left(\boldsymbol{\Phi}_k^T \boldsymbol{\Phi}_k \right)^{-1} \boldsymbol{\Phi}_k^T \mathbf{u}_k = \boldsymbol{\Phi}_k^+ \mathbf{u}_k. \quad (3.29)$$

The unknown DoF can now be expressed as follows:

$$\mathbf{u}_u = \boldsymbol{\Phi}_u \boldsymbol{\Phi}_k^+ \mathbf{u}_k \quad (3.30)$$

where $\boldsymbol{\Phi}_k^+$ scales the modeshapes which are used to find \mathbf{u}_u

4. The matrix \mathbf{C} can also be built using geometrical relations between known and unknown DoF. This method is a special case of the previous point. For instance, rotations can be related to displacements by using finite differences.

Part II

Measurements, Modelling and Validation

Chapter 4

Measurement

4.1 Introduction

As is explained in the introduction of the research, four different test structures need to be measured. In this chapter it is explained how this is done, and how the test results are processed. The test set up is described in Section 4.4. A FEM model of the structure will be made. This is explained in Section 4.3. The modal analysis methods that will be used to analyse the FRF's are described in Section 4.5. In this section is also explained how the circle fit method has been improved in order to identify closely spaced modes. In Section 4.6 different sources of damping that will influence the measurement will be discussed. A suspension test has been done to investigate the influence of damping from the suspension on the damping measured in the plate.

4.2 Test object

The test objects that have been tested are a base and an upright construction in four different configurations. The base and upright both have a hole pattern that can be used to bolt both plates together. To couple the base and upright, two steel angles and 18 bolts will be used. The plates are made of steel. A picture of the structure and the individual parts can be seen in Figure 4.1. The properties of the plates can be seen in Table 5.4. The rubber that is used to mount to the base has unknown material properties, but the dimensions can also be found in the table.

Table 4.1: Properties of test object

	Dimensions [m]	Material	Amount	Weight [kg]
Base	0.6x0.6x0.012	Steel	1	33.9
Upright	0.9x0.6x0.012	Steel	1	50.9
Angles	0.05x0.05x0.005	Steel	2	4.6
Bolts and nuts	M10x0.03	Steel	18	0.5
Rubber mountings	∅0.033 x 0.043	Rubber	4	0.2

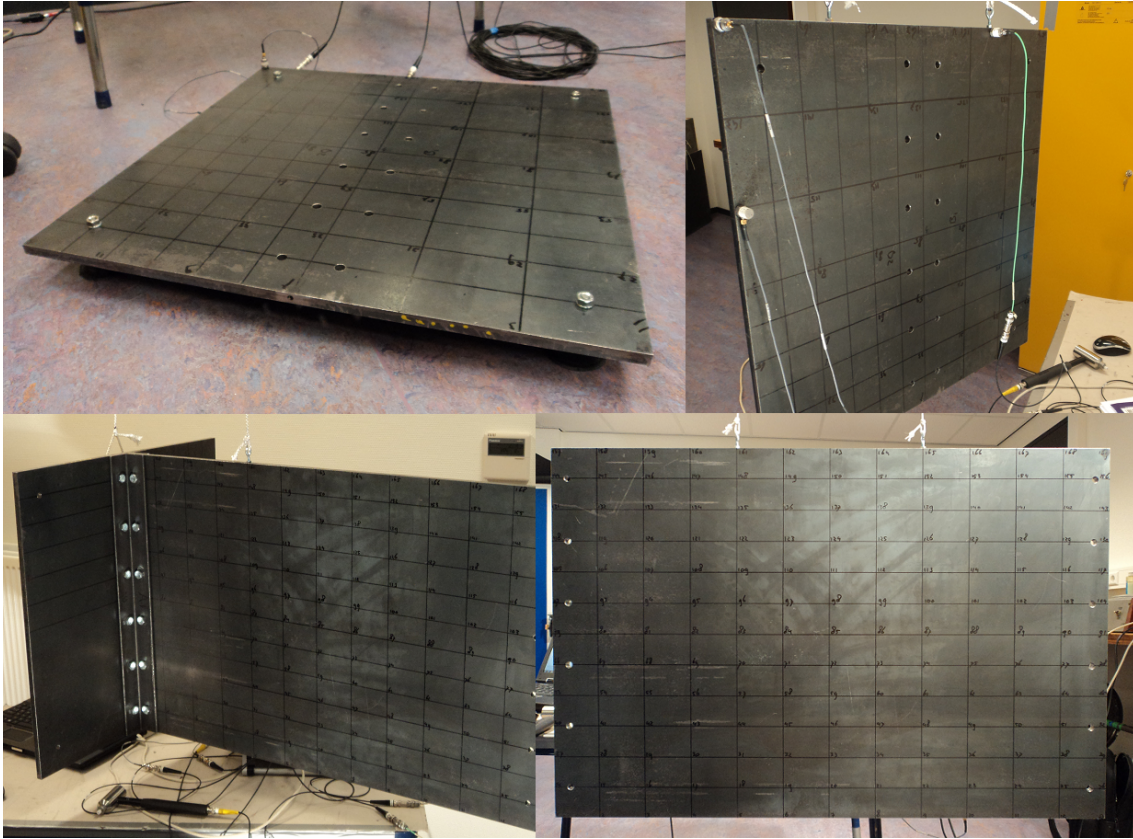


Figure 4.1: The test structures that have been measured. From top left clockwise, the base with rubbers, the suspended base, the suspended upright and the suspended base upright structure.

4.3 FEM Analysis

A FEM analysis will be made in order to predict the eigenfrequencies and the eigenmodes. A indication of the eigenfrequencies is needed to know the frequency band that will be used for the measurement. The eigenmodes can be used to define the impact and sensor positions. The eigenvectors will be compared later on with the measured eigenvectors in order to assess the quality of the measurement. The model is made in Matlab, using the Structural Dynamic Toolbox. Shell elements can be used, because the third dimension is significantly smaller than the other two. Based on these models the \mathbf{K} and \mathbf{M} matrices can be constructed. These matrices will be used to solve the dynamic eigenvalue problem:

$$\left(\mathbf{K} - \omega^2 \mathbf{M} \right) \mathbf{x} = 0, \quad (4.1)$$

where \mathbf{x} are the eigenvectors and ω are the eigenfrequencies. No boundary conditions need to be defined because the system is freely suspended. This will result in 6 low eigenfrequencies close to 0 Hz.

4.4 Test set up

The test set up consists of the suspension of the test structure, the actuator and sensor types and positions, the data acquisition system that will be used, and the settings of it. These topics will be discussed below.

4.4.1 Suspension

In modal testing it is preferred to test the object without any contact or links with any surrounding objects. This situation is called freely supported. By doing so, each of the 6 rigid body modes can be measured, and the surroundings will have no effect on the measurement. As one can imagine, it is not possible to suspend a test object freely, because one always has to cope with gravity forces. The best thing that can be done is to suspend the test object in such a way, that the impact forces, and the accelerations measured are orthogonal to the suspension [11]. The steel plate which will be tested will have low damping, and therefore the suspension should be such that it will not influence the damping measured in the plate. The plates will be suspended by chords from the ceiling, these chords will be attached to the upper side of the plates as can be seen in Figure 4.1. To investigate the influence of the suspension on the damping measured in the plate, different suspensions chords will be tested. The results of this test will be discussed later on.

4.4.2 Data acquisition

A PAK MKII data analyzer will be used to process the data. In order to measure 20-30 modes for both plates, the frequency spectrum needs to be at least 0-1500 Hz. The sample frequency determines this spectrum. It is preferred to use a sample frequency of 2^n . This can be analysed well with the Fast Fourier Transform (FFT). The spectrum that can be seen is the sample frequency divided by 2.56, to avoid aliasing. The sample frequency that fits best to our test is 4096 Hz (2^{12}). This leads to a visible frequency spectrum of 0-1600 Hz. The square plate has about 19-21 modes in that range, and the rectangular plate has about 30 modes. The structure, which is a combination of both plates, has an even higher amount of modes in that range. Because low damping is expected, a high frequency resolution is needed to make sharp peaks clearly visible. The frequency resolution is dependent on the duration of a measurement block. The total number of samples in one measurement block is limited by PAK to 65536 samples. A maximum frequency resolution of 1/16 Hz is possible using a duration of 16s. A block window will be used on the input. In order to prevent leakage, a window will be used on the response. An exponential window will be used with a large time constant to avoid introducing too much damping by the window.

4.4.3 Sensor and sensor positions

Three sensors will be used to measure the accelerations of the test structure. These sensors are lightweight to prevent modal distortion by mass loading. These sensors will be placed on positions where all modes can be seen.

4.4.4 Input force and input positions

An impact hammer with a nylon tip is used to excite the plate. The force that is given to the plate by using an impact hammer is a force that covers a wide frequency range. The total range that is excited depends on the kind of hammer tip that is used. A steel tip, which is very hard, has a very broad spectrum. A nylon tip has a smaller frequency spectrum, but puts more energy in lower frequencies. A nylon tip is well suited for this application, because the frequency band is wide enough, and more energy can be stored in the low frequencies.

In order to make the modeshapes visible that occur in the test range, a total of 13 x 13 impact points have been defined.

The datasheets of the hammer and accelerometers can be found in Appendix B.

4.5 Modal analysis

When the measurements are done, the interpretation of the data can be done by a modal analysis software program. A lot of different analysis methods have been discussed in Chapter 2. Because of the fact that the structures which are measured are lightly damped there is generally not much coupling between modes, however, the square plate will have double eigenmodes because of symmetry. The modal analysis will be done with the circle fit method. Reasons for using this method are:

- Gives insight into consistency and reliability of the measured FRF data
- Can estimate viscous and hysteretic damping
- The quality of the fit can be assured better.

In order to be able to compare the results with other methods, ME'scope has also been used. In the next sections is explained which methods of ME'scope are used and how, and also how the results of the circle fit method will be.

4.5.1 ME'scope

The circle fit method will be compared with a time domain method and with a frequency domain method. The number of eigenfrequencies will be estimated using a CMIF. Double modes are recognized in ME'scope if multiple references are used.

Ortho Polynomial Method

This method works best with a few poles at a time, so the whole frequency range will be divided in five. This method is able to handle double poles, which is needed for analysing the square plate. The process is easy, but it is recommended that the poles are known beforehand. This is the case because the plates are modelled and analysed with FEM.

Complex Exponential Method

This method works best if used with a large frequency interval. For that reason, the whole frequency interval has been chosen (0-1600 Hz). A stability diagram can be made based on a number of models with different order. The range of model orders will be chosen as 10 – 50. Stable poles can be identified by repeating poles at the same frequency with the damping in the same order of magnitude.

4.5.2 Circle fit method

The circle fit method has been discussed in Chapter 2. Some improvements on this method have been done. These will be described in this section. It is also described how the obtained modal damping values will be calculated.

The results that can be obtained by the circle fit method need to be handled with care because they are based on the SDoF assumption. Closely spaced modes can give wrong results. In this section it is described how closely spaced modes can be identified with an SDoF method. The result will be checked by means of a theoretic 2 DoF model. Beside this, the location of the determined natural frequency on the modal circle is difficult to estimate if there are few measurement points on the circle.

Determining the pole location on the circle.

The derivation of the location of the eigenfrequency on the response curve is not very accurate by using finite differences if there are few measurement points on the circle. A good estimate of this location is essential, since this will lead to an accurate estimate of the damping, and also a correct estimate of the phase at resonance. To get more accurate results a new method to locate this frequency is proposed. The method is based on the assumption that the damping plot is levelled if the eigenfrequency location on the modal circle is well estimated.

From experience it is known that the damping plot will tilt about the diagonal if the pole location is not estimated correct, see for instance Figure 2.4. The method that is proposed forces the damping plot to be levelled over de anti diagonal of the damping plot. If there are n frequency points before and after the estimated pole, the damping value of point $(1, n)$ will be set equal to the damping values of point $(n, 1)$

$$\frac{\omega_{a(1)}^2 - \omega_{b(n)}^2}{\omega_r^2 \left(\tan\left(\frac{\theta_{a(1)}}{2}\right) + \tan\left(\frac{\theta_{b(n)}}{2}\right) \right)} = \frac{\omega_{a(n)}^2 - \omega_{b(1)}^2}{\omega_r^2 \left(\tan\left(\frac{\theta_{a(n)}}{2}\right) + \tan\left(\frac{\theta_{b(1)}}{2}\right) \right)}. \quad (4.2)$$

In this equation the four angles are unknown. Four equations can be formulated that relates these unknown angles to known quantities:

$$\begin{aligned} \theta_{a(1)} + \theta_{b(n)} &= \theta_{a(1)b(n)} \\ \theta_{a(n)} + \theta_{b(1)} &= \theta_{a(n)b(1)} \\ \theta_{a(n)} - \theta_{a(1)} &= \theta_{a(n)a(1)} \\ \theta_{b(n)} - \theta_{b(1)} &= \theta_{b(n)b(1)} \end{aligned}$$

A visualisation of these angles can be seen in Figure 4.2. The unknowns can now be written as function of the known values and one unknown $\theta_{a(1)}$:

$$\begin{aligned} \theta_{b(n)} &= \theta_{a(1)b(n)} - \theta_{a(1)} \\ \theta_{a(n)} &= \theta_{a(n)a(1)} + \theta_{a(1)} \\ \theta_{b(1)} &= \theta_{a(1)b(n)} - \theta_{a(1)} - \theta_{b(n)b(1)} \end{aligned}$$

Equation (4.2) can now be written in terms of one unknown, $\theta_{a(1)}$ This leads to the following equation

$$\frac{\omega_{a(1)}^2 - \omega_{b(n)}^2}{\omega_{a(n)}^2 - \omega_{b(1)}^2} = \frac{\tan\left(\frac{\theta_{a(1)}}{2}\right) + \tan\left(\frac{\theta_{a(1)b(n)} - \theta_{a(1)}}{2}\right)}{\tan\left(\frac{\theta_{a(n)a(1)} + \theta_{a(1)}}{2}\right) + \tan\left(\frac{\theta_{a(1)b(n)} - \theta_{a(1)} - \theta_{b(n)b(1)}}{2}\right)}. \quad (4.3)$$

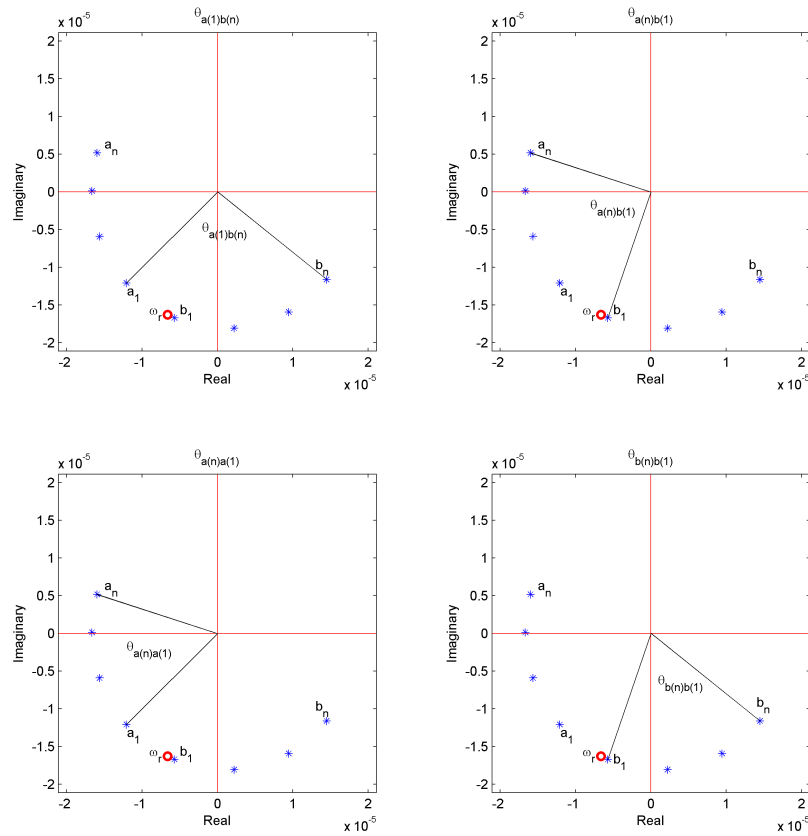


Figure 4.2: Visualisation of known angles. The blue asterisks are measured frequency points. The red circle is the estimated eigenfrequency.

This nonlinear equation can be solved for $\theta_{a(1)}$ with Matlab, and gives the $\theta_{a(1)}$ for which the damping plot is levelled over the anti diagonal.

Closely spaced modes

If there are closely spaced modes in the system, the identification by means of an SDoF method will get stuck. To see how wrong the results are, a theoretic two DoF system is built with Matlab. The modal properties for the two DoF are taken exactly the same as the two most closely spaced modes found in the measurements that will be described later. With most closely spaced we mean, the Hasselman [14] condition is the highest. This condition is as follows

$$2\zeta_j\omega_j / |\omega_j - \omega_k| \ll 1, \quad (4.4)$$

and states that for two modes which are closely spaced the condition is not much smaller than one. The condition found in the worst case in the measurement data is about 0.5. In Figure 4.3 the identification procedure can be seen of this mode, and it can be seen that the damping plot is distorted. It can be seen that due to the closely spaced modes, the damping plot can be distorted. In fact, the accuracy of the modal analysis near closely spaced modes does also depend on the sample frequency and on the amplitude of the modal factor. Near these double modes the results can be bad.

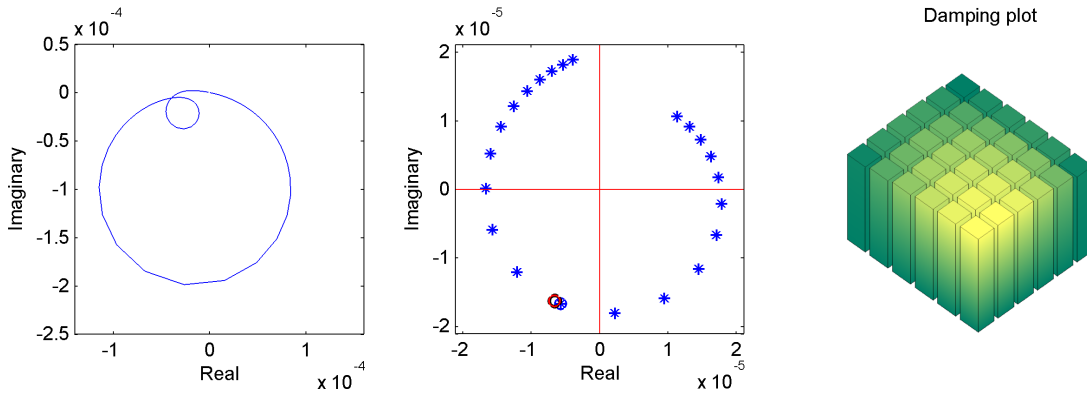


Figure 4.3: Identification of modal properties and damping plot of closely spaced mode. The first plot shows the Nyquist plot for the two closely spaced modes. The second plot shows the frequency points for the mode belonging to the smaller circle. The red circle is the estimated eigenfrequency. Due to the fact that the modes are closely spaced the identification procedure gives results that deviate from the theoretical value. The damping error is 9.5% and phase error is 10 degrees.

How the identification process of closely spaced modes can be improved will be explained now. The total system can be described by a summation of the measured modes and a residual mass and a residual stiffness as follows

$$H_{jk}(\omega) = \sum_{s=m_1}^{m_2} \frac{sA_{jk}}{\omega_s^2 - \omega^2 + i\eta_s\omega_s^2} + \frac{1}{K_{jk}^R} - \frac{1}{\omega^2 M_{jk}^R} \quad (4.5)$$

The residual mass represent the rigid body modes of a structure that are difficult to measure. The residual stiffness compensates for the modal truncation that is applied by measuring a finite set of modeshapes. The system can also be written as

$$H_{jk}(\omega) = \left(\frac{rA_{jk}}{\omega_r^2 - \omega^2 + i\eta_r\omega_r^2} \right) + \left(\sum_{\substack{s=m_1 \\ s \neq r}}^{m_2} \frac{sA_{jk}}{\omega_s^2 - \omega^2 + i\eta_s\omega_s^2} + \frac{1}{K_{jk}^R} - \frac{1}{\omega^2 M_{jk}^R} \right), \quad (4.6)$$

where one mode is set apart of which we want to optimize the identification. This mode can be identified by subtracting the second term from the measured receptance, which result in a single mode:

$$H_{jk}^m(\omega) - \left(\sum_{\substack{s=m_1 \\ s \neq r}}^{m_2} \frac{sA_{jk}}{\omega_s^2 - \omega^2 + i\eta_s\omega_s^2} + \frac{1}{K_{jk}^R} - \frac{1}{\omega^2 M_{jk}^R} \right) = \frac{rA_{jk}}{\omega_r^2 - \omega^2 + i\eta_r\omega_r^2} \quad (4.7)$$

This process can be repeated iteratively. The optimized results by using this method can be seen in Figure 4.4 An overview of the optimisation procedure can be seen in Figure 4.5.

Calculating modal damping In all the tests, multiple FRF will be measured, which means that multiple estimates for the eigenfrequencies and damping are obtained. It is needed to reduce

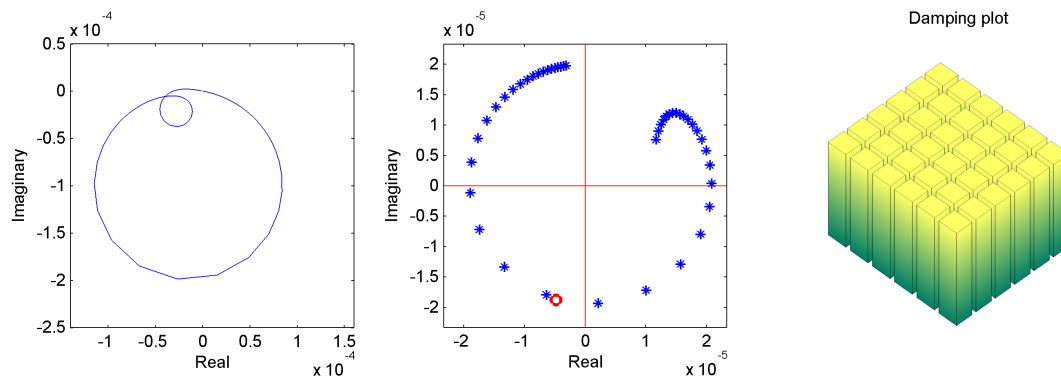


Figure 4.4: Optimized identification of closely spaced mode. Damping error is 1.7% and phase error is 2 degrees.

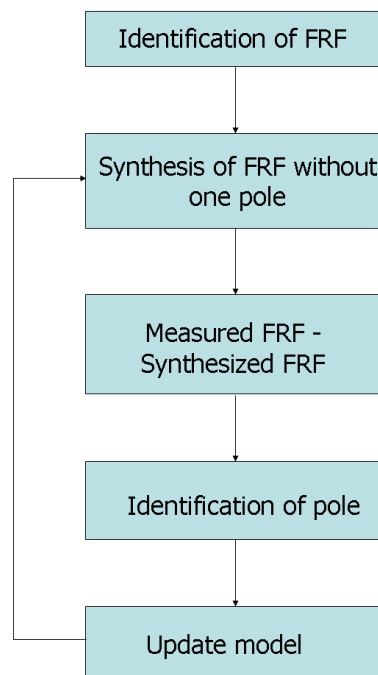


Figure 4.5: Flow chart of optimization procedure.

those values to one single value in order to be able to make a modal model. For each circle fit a fit error can be calculated. This error is defined as the average distance of the measurement points to the fitted circle, divided by the circle radius. When this error is above 0.5, the circle can not be fitted correctly, and hence no damping estimate can be made. Therefore values with a fit error of 0.5 or higher will be discarded in order to make the damping estimates reliable.

From the values that remain a 95% confidence interval will be calculated. A confidence interval

can be applied if the population distribution is normal and is approximately correct for large n . A confidence interval is defined as

$$\bar{x} \pm z^* \frac{\sigma}{\sqrt{n}}, \quad (4.8)$$

and it means that there is a probability C that the interval $\bar{x} \pm z^* \sigma / \sqrt{n}$ contains μ [21], where \bar{x} is the sample mean, μ is the unknown population mean, σ is the standard deviation divided by the mean and n is the number of samples. z^* is the value on the standard normal curve with area C between $-z^*$ and z^* . C will be taken as 0.95. From the size of this interval it can be seen how large the spread is on the damping values that are obtained. The eigenfrequencies will only be displayed by a mean value, because the deviations of this mean are very low.

4.6 Damping sources

The damping that we want to measure is the material damping in the steel plates and the damping caused by the joints. Due to measurement conditions and signal processing different damping sources will be added up to the damping that is eventually analysed during modal analysis.

Material damping Material damping is damping at molecular scale, due to molecule friction. It is expected that this type of damping is hysteretic and non-viscous. However, the damping will be low, and it is maybe impossible to identify a damping model.

Damping in Joints Due to microslip between two adjacent surfaces, energy dissipation will occur. This damping type is dry friction, and is also non-viscous. This damping will also be low because of the relative low microslip. The damping in rubber joints will be hysteretic as well, but will be higher.

Suspension The plates should be tested in free free conditions in order to have no influence from surroundings. This is not possible, and therefore, the construction will be suspended by chords. These suspension chords will have some damping, and will influence the damping. It is expected that the suspension will have influence on the measured damping. In order to estimate this amount of influence, a test is done with different suspensions. The damping in the plate is measured with different suspension cases. The different cases that will be tested can be seen in Figure 4.6. The tests have been performed with 6 sensors and 6 impacts. This results in a total of 36 FRF per test. The mean damping value of these FRF's can be found in Table 4.2. From the table it can be concluded that the damping values do depend on the way the plate is suspended. The steel wounded thread shows more damping than the nylon thread, this can be due to the friction between the steel strands. It can also be concluded that a longer cable will have less influence on the damping measured in the plate. There is no significant difference between the mid or corner configuration. For the plate measurements a 2 meter nylon chord is used.

Air damping Due to the moving plates in air, air damping may have significant influence. It is assumed that this damping is negligible

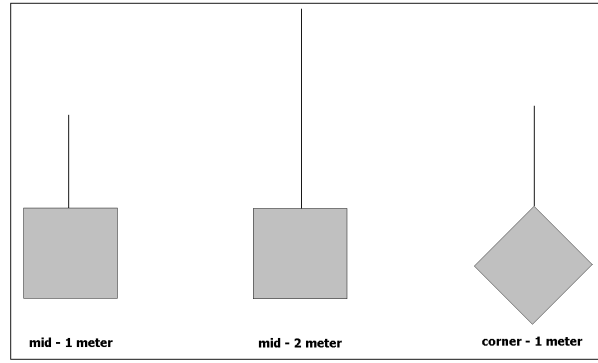


Figure 4.6: Different suspension configurations.

Table 4.2: Identified damping values of different suspension configurations.

Pole	Nylon thread		Steel cable		
	Mid - 1m	Corner - 1m	Mid - 1m	Corner - 1m	Mid - 2m
1	0.0397	0.0333	0.0609	0.0398	0.0347
2	0.0262	0.0328	0.0741	0.0218	0.0412
3	0.0421	0.0396	0.1527	0.3284	0.0322
4	0.0268	0.0391	0.0466	0.0447	0.0290
5	0.0270	0.1215	0.0748	0.0395	0.0203
6	0.0511	0.0554	0.0855	0.2650	0.0539
7	0.0583	0.0454	0.2963	0.1387	0.0536
8	0.0232	0.0281	0.2392	0.1880	0.0230
9	0.0391	0.0436	0.0503	0.0317	0.0488

Windowing Windowing is a kind of signal processing that forces the measured signal to be periodic. This is needed when performing a Fourier Transform on a signal, otherwise leakage will occur. The window that will be chosen is an exponential window in the form of e^{-at} , where a is a constant. This exponential function will be multiplied by the impulse function. This impulse function has been mentioned in Chapter 1, and is

$$h_{jk} = \sum_{r=1}^{2N} r A_{jk} e^{i\omega_r at}. \quad (4.9)$$

If this function is multiplied by e^{-at} , one obtains:

$$h_{jk} = \sum_{r=1}^{2N} r A_{jk} e^{i\omega_r at} e^{-at} \rightarrow h_{jk} = \sum_{r=1}^{2N} r A_{jk} e^{i\omega_r - (\alpha+a)t}. \quad (4.10)$$

It can be seen that windowing will have influence on the damping. The lower the damping in the structure, the more influence windowing will have.

4.7 Conclusions

It is clear that the investigation of damping will be influenced by a lot of environmental conditions. However, the goal of this research will be to be able to investigate the damping in joints. It

is therefore of minor importance to know the exact level of damping in the plate, but the relative amounts between the tests will be of major importance. For these reasons it is important to have the same boundary conditions for separate tests.

Chapter 5

Results

In the previous chapter has been discussed how the measurements should be performed and analysed. In this chapter the results will be presented. The chapter is divided in three different sections. In the first section the eigenfrequencies will be presented that are obtained by the measurements and by a FEM analysis. In Section 5.3 the modeshapes will be presented that have been obtained with the circle fit method and those will be compared to the eigenmodes of the FEM analysis using MAC tables. In the last section the damping values are shown. The damping values are obtained in three different ways. A circle fit method is used which is programmed in Matlab. Also two MDOF analysis are used namely the Complex Exponential Method and the Rational Fraction Polynomial Method. The accuracy of the damping estimates will also be discussed in the third section.

5.1 Damped base rigid motions

The base that is mounted with rubbers on the floor will have rigid body modes that are not close to 0 Hz because it is not freely supported. Two eigenfrequencies are measured below the first flexible mode. The damping of these modes is relatively high with respect to the flexible modes. The values can be seen in Table 5.1. This results are presented separately of the other results,

Table 5.1: Eigenfrequencies [Hz] and damping confidence interval of damped base

Pole	Eigenfrequencies	Damping (% of critical damping) confidence interval
1	23.78	$3.12 \pm 0.9\%$
2	35.17	$3.72 \pm 3.2\%$

because these frequencies are the rigid body frequencies, and cannot be compared to flexible modes of the suspended base.

5.2 Eigenfrequencies

The eigenfrequencies of a system can be obtained relatively easy . In the previous chapter, the method has been discussed that will be used in this research to determine the eigenfrequencies. A finite difference method will be used to estimate the eigenfrequency on the circle in the complex plane. From all the different estimates from the total amount of FRF, a mean value will be

Table 5.2: Eigenfrequencies [Hz] obtained from measurement and FEM analysis of Base Plate, Upright and Base Upright Structure

Pole	Base Damped		Base Suspended		Upright		BU-Structure	
	Measured	FEM	Measured	FEM	Measured	FEM	Measured	
1	120.9	109.6	111.8	72.68	74.57	37.33	36.78	
2	165.8	159.2	165.5	77.03	78.97	47.96	48.27	
3	197.6	195.0	194.9	167.3	170.1	89.62	86.25	
4	285.2	282.4	285.2	178.9	184.5	117.5	123.6	
5	286.5	282.4	285.9	208.0	213.4	129.8	137.5	
6	494.1	492.7	495.7	240.2	242.8	152.4	150.7	
7	501.2	492.7	501.6	309.3	312.6	179.4	188.8	
8	514.0	516.4	517.3	356.2	360.7	192.6	196.5	
9	569.2	562.1	567.5	430.2	434.3	218.1	214.4	
10	619.8	622.4	625.6	485.4	496.5	284.7	281.5	
11	846.9	854.2	848.9	524.1	529.5	289.0	299.5	
12	850.7	854.2	854.1	532.7	534.4	312.3	313.5	
13	954.2	945.7	951.8	538.9	549.0	330.2	340.6	
14	994.7	986.1	995.1	674.6	681.2	405.5	400.9	
15	1059	1062	1059	709.0	714.2	474.1	470.0	
16	1073	1062	1073	759.2	759.6	474.9	474.3	
17	1224	1237	1223	793.6	797.6	511.7	520.5	
18	1303	1307	1304	873.0	873.2	548.9	529.3	
19	1348	1361	1349	967.0	986.2	586.0	596.5	
20	1591	1599	1592	1002	1015	614.9	616.2	

taken. The standard deviation of all the samples is very small, and will not be displayed. In order to see if the measurements are performed correctly, a FEM analysis has been done. The results of this analysis, and the results of the measurements can be found in Table 5.2. In this table the first 20 poles are shown for the three different test cases. It can be observed that the measured eigenfrequencies show good resemblance with the eigenfrequencies that are calculated with FEM.

5.3 Modeshapes

The modeshapes that are measured are complex valued. This is because the motion has an amplitude and a phase. The modeshapes that have been found using the circle fit analysis will be checked for orthogonality. In theory, all the eigenmodes of an undamped system are orthogonal to each other with respect to the Mass and Stiffness matrix. An orthogonality test can be done by using a MAC table[6]. The MAC value between two modes can be defined as

$$\text{MAC}_{cdr} = \frac{|\psi_{dr}^H \psi_{cr}|^2}{\psi_{dr}^H \psi_{dr} \psi_{cr}^H \psi_{cr}} \quad (5.1)$$

where ψ is the unnormalised modeshape. A value of one means that two modes have a consistent correspondence, and a value of zero means that two modes are not correlated. The modes that are measured should be all orthogonal with respect to the mass and stiffness matrix. The mass and stiffness matrix of the plates will be homogeneous over the plate, and therefore we

can assume that the modes should also be close to orthogonal without weighting them over the mass or stiffness matrix. This will result in a diagonal MAC table. If there are not enough geometric points to display a modeshape, the higher modes can not be orthogonal, because the modeshape cannot be visualized correct. The measured modeshapes can also be compared to the modeshapes found by FEM. This can be done by using the same formula. The MAC tables of the Base, Upright and BU-structure can be seen in the Figures 5.1, 5.2 and 5.3.

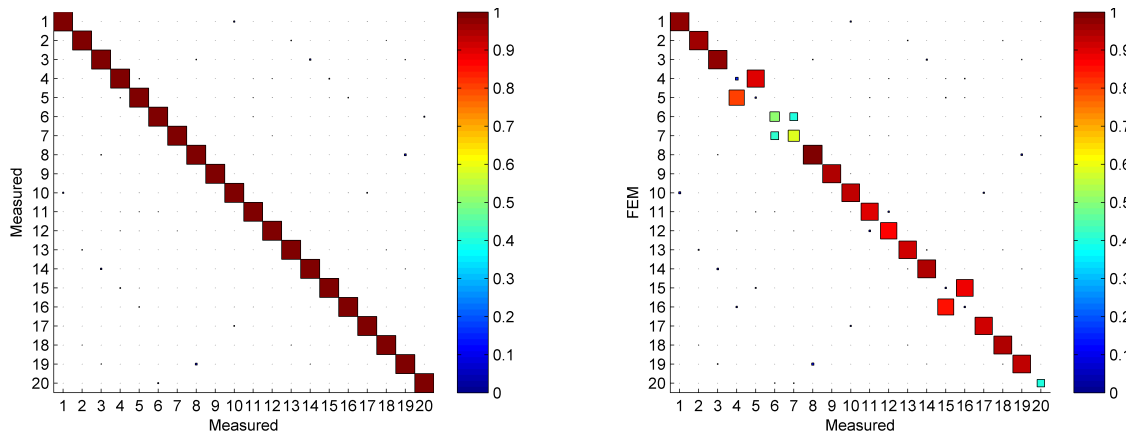


Figure 5.1: MAC plots of Base.

The left MAC table of the base shows that the modeshapes of the base structure are orthogonal with respect to each other. This means that the double modes are identified correct. It also indicates that enough measurement points are used to measure the modeshapes. In the right MAC table the modeshapes are compared with modeshapes from FEM. It can be seen that there are double modes which is visible in switching of modes, what already was known from the FEM model. The correspondence to the FEM model is good.

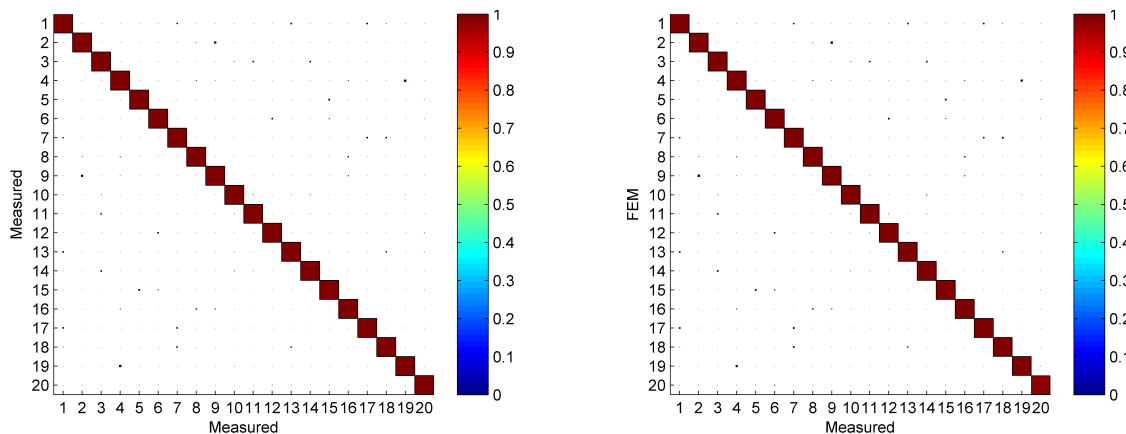


Figure 5.2: MAC plots of Upright.

The left MAC table of the upright shows that the modeshapes of the upright structure are orthogonal with respect to each other. For this structure there are also enough measurement points used. The right MAC table shows that there is a very good correspondence with the FEM model.

The left MAC table of the assembly shows that the modeshapes of the base upright structure are orthogonal with respect to each other. The right MAC table shows that a mode switching occurs

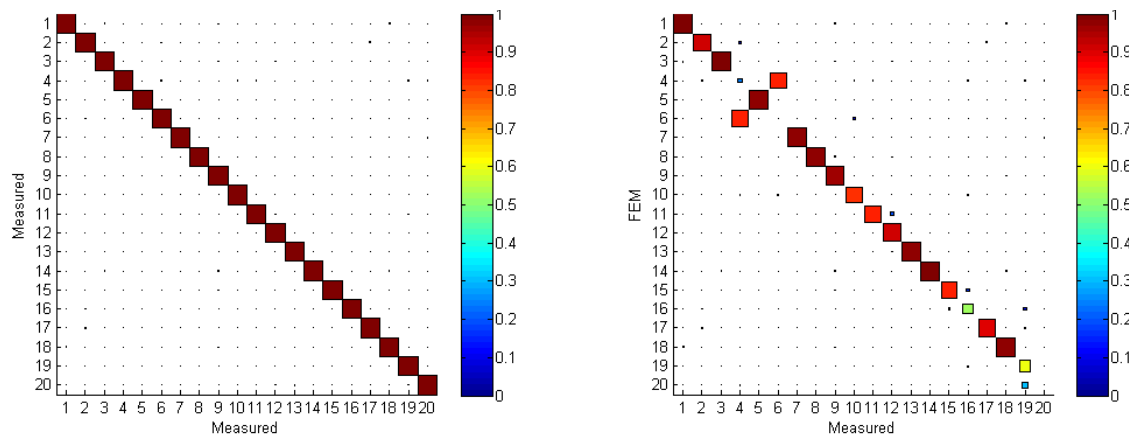


Figure 5.3: MAC plots of Base Upright structure

between the fourth and the sixth mode. Mode 16, 19 and 20 show no good correspondence with FEM. This can be due to the fact that the modeshapes can not be seen by the sensors very good.

The visualisation of the modeshapes can be found in Appendix C

5.4 Damping

The damping is estimates with three method. The Complex Exponential Method has been used to analyse the system in the time domain using the impulse response function. The Rational Fraction Polynomial Method has been used to analyse the system in the frequency domain. These two methods have been performed using ME'scope as is discussed in the previous chapter. Beside these two methods, a circle fit method is used. The damping values obtained by using the different methods can be seen in Table 5.3. The damping values obtained by the circle fit can be used to assess the values on its accuracy. In Table 5.4 the mean values can be seen, and also the standard deviation over the total number of damping estimates, divided by the mean (the coefficient of variation) is shown.

Table 5.3: Damping values in % of critical damping for the flexible modes obtained with three different modal analysis methods. CF is the circle fit method. CE means complex exponential method, RFPM means rational fraction polynomial method.

Pole	Base Suspended			Upright			BU Structure		
	CF	CE	RFPM	CF	CE	RFPM	CF	CE	RFPM
1	0.049	0.051	0.050	0.052	0.0085	0.054	0.15	0.15	0.15
2	0.032	0.034	0.032	0.055	0.013	0.051	0.095	0.098	0.098
3	0.044	0.046	0.032	0.029	0.0098	0.026	0.14	0.14	0.15
4	0.033	0.036	0.033	0.036	0.018	0.023	0.069	0.072	0.082
5	0.050	0.051	0.048	0.030	0.015	0.019	0.11	0.12	0.14
6	0.054	0.051	0.052	0.028	0.014	0.018	0.088	0.091	0.10
7	0.14	0.086	0.14	0.024	0.014	0.016	0.087	0.090	0.12
8	0.022	0.022	0.023	0.021	0.012	0.012	0.054	0.055	0.057
9	0.21	0.13	0.20	0.025	0.018	0.019	0.083	0.082	0.089
10	0.039	0.039	0.039	0.028	0.022	0.020	0.059	0.059	0.058
11	0.090	0.092	0.093	0.032	0.026	0.025	0.073	0.078	0.075
12	0.025	0.026	0.026	0.026	0.021	0.021	0.076	0.074	0.086
13	0.12	0.19	0.12	0.029	0.023	0.019	0.064	0.069	0.082
14	0.080	0.12	0.080	0.030	0.025	0.025	0.055	0.055	0.058
15	0.083	0.10	0.083	0.052	0.045	0.049	0.055	0.054	0.055
16	0.088	0.21	0.088	0.027	0.023	0.023	0.052	0.053	0.057
17	0.11	0.25	0.11	0.028	0.024	0.024	0.066	0.045	0.044
18	0.065	0.28	0.066	0.052	0.048	0.047	0.14	0.13	0.14
19	0.10	0.12	0.10	0.060	0.053	0.051	0.054	0.18	0.064
20	0.080	0.21	0.079	0.038	0.035	0.035	0.051	0.047	0.048

Table 5.4: 95 % Confidence intervals for damping values

	Base Damped	Based Suspended	Upright	BU
1	0.87 ± 0.8 %	0.049 ± 0.2%	0.052 ± 0.3%	0.15 ± 0.5%
2	0.027 ± 1.0 %	0.032 ± 0.2%	0.055 ± 0.1%	0.095 ± 0.8%
3	0.32 ± 0.1 %	0.044 ± 0.4%	0.029 ± 0.2%	0.14 ± 0.6%
4	0.18 ± 2.2 %	0.033 ± 1.0%	0.036 ± 0.1%	0.069 ± 0.7%
5	0.17 ± 3.1 %	0.050 ± 1.2%	0.030 ± 0.4%	0.11 ± 0.9%
6	0.080 ± 1.6 %	0.055 ± 2.8%	0.028 ± 0.5%	0.088 ± 0.5%
7	0.069 ± 0.9 %	0.14 ± 0.8%	0.024 ± 0.5%	0.087 ± 1.0%
8	0.081 ± 0.2 %	0.022 ± 0.1%	0.021 ± 0.3%	0.054 ± 0.7%
9	0.12 ± 2.2 %	0.21 ± 1.7%	0.025 ± 0.2%	0.083 ± 0.4%
10	0.18 ± 1.6 %	0.039 ± 0.2%	0.028 ± 0.3%	0.059 ± 0.6%
11	0.075 ± 1.0 %	0.090 ± 0.8%	0.032 ± 2.5%	0.073 ± 0.7%
12	0.073 ± 3.0 %	0.025 ± 0.2%	0.026 ± 0.3%	0.076 ± 0.6%
13	0.074 ± 0.7 %	0.12 ± 0.3%	0.029 ± 0.3%	0.064 ± 0.8%
14	0.093 ± 0.6 %	0.080 ± 0.3%	0.030 ± 0.4%	0.055 ± 0.4%
15	0.15 ± 1.1 %	0.083 ± 0.7%	0.052 ± 0.7%	0.055 ± 2.5%
16	0.14 ± 1.7 %	0.088 ± 0.7%	0.027 ± 0.2%	0.052 ± 0.6%
17	0.16 ± 0.8 %	0.11 ± 0.3%	0.028 ± 0.4%	0.066 ± 9.9%
18	0.078 ± 0.8 %	0.066 ± 0.2%	0.052 ± 0.4%	0.14 ± 0.9%
19	0.17 ± 0.8 %	0.10 ± 0.3%	0.060 ± 0.6%	0.054 ± 0.7%
20	0.18 ± 1.2 %	0.080 ± 0.9%	0.038 ± 0.3%	0.051 ± 6.3%

5.5 Discussion

The damping values that have been found are very low. This was expected. It can be seen that the damping found in the bu structure are higher than those in the separate structures. The damping values of the damped base are a lot higher than those of the suspended base. The mechanism of this damping will be discussed in Chapter 10 The modal model that is obtained with the modeshapes, dampingfactors and eigenfrequencies will be a good base for further research.

Chapter 6

Modelling

In this chapter the modal parameters that have been extracted will be used to build a response model. When having a modal model, it is easy to get a response model, but the demands of the response model are more stringent than those of the modal model.

6.1 Modal Model

A modal model contains one matrix with eigenfrequencies and damping and one with the eigenvectors. At first instance, a hysteretically damped model is assumed. The eigenfrequencies and the damping factors have already been found in Chapter 5. Also modal constant have been calculated. From this modal constant the modeshapes can be calculated. The formula which describes the system which has been discussed earlier is

$$\alpha(\omega) = \frac{{}_r A_{jk}}{\omega_r^2 - \omega^2 + i\omega_r^2 \eta_r} \quad (6.1)$$

This is the hysteretically damped system. The complex parameter ${}_r A_{jk}$ is in fact a multiplication of the two modeshape parameters ϕ_{jr} and ϕ_{kr} . Where the index j is the impact position, k is the sensor position and r denotes the modenummer. To be able to calculate these ϕ at least one driving point needs to be known. With this, the first ϕ can be calculated:

$${}_r A_{kk} = \phi_{kr} \phi_{kr} \quad \rightarrow \quad \sqrt{{}_r A_{kk}} = \phi_{kr} \quad (6.2)$$

Because it is known that

$$\phi_{jr} \phi_{kr} = {}_r A_{jk} \quad (6.3)$$

the other modeshape vector elements can be calculated now. The modal model in matrix form is

$$[\omega_r^2(1 + i\eta_r)]_{m \times m} \quad , \quad [\phi]_{n \times m} \quad (6.4)$$

6.2 Response model

The response model is the model that consist of frequency response functions. In fact that is the model where the process has been started. After measuring the structure, a response model is

obtained. From this model a modal model is made in the foregoing section. The big benefit of this modal model is that now FRF's can be resynthesized which not have been measured. As was explained earlier, only a partial H matrix has been measured of dimensions $n \times m$. With the modal model a full response model can be resynthesized with the simple formula

$$\mathbf{H}_{n \times n} = \mathbf{\Phi}_{n \times m} (\lambda_r^2 - \omega^2)^{-1}_{m \times m} \mathbf{\Phi}_{m \times n}^T \quad (6.5)$$

What will be done is rebuilding the response model on a basis of the identified modes. These FRFs can be compared with the measured FRFs to see how well the modal identification is performed. It shall be seen that the similarity at first is bad, especially visible in the anti-resonances. This is due to the absence of the rigid body modes which cannot be identified easily. Also the number of flexible modes which is identified is limited. In this section it will be explained how to cope with these problems, and results will be shown. (Out of range modes have to be included.)

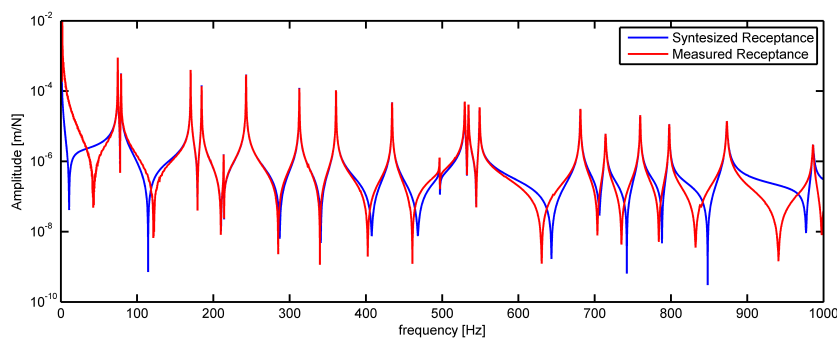


Figure 6.1: Measured and synthesized receptance

6.2.1 Rigid Body modes

As can be seen in figures 6.1 the low frequent behaviour is not optimally described by the modes that are included in the modal model. The reason for this is that the rigid body modes are not taken into account so far. The structure has been measured in free free conditions this means that there are 6 rigid body modes in which the structure can move. Three rotations and three translations. Measurements are done in only one direction, the z direction. This means that one translation and two rotations can be seen in the response functions. It is not easy to identify these modes because of the following reasons:

- The rigid body modes are near 0 Hz and therefore not easy to measure with accelerometers with a lower limit of around 0.5 Hz.
- Multiple modes are present at the same frequency.
- Due to windowing and the relative short block lengths, low eigenfrequencies will be distorted.

Another important reason is that the rigid body modes are always affected by the suspension of the test. Therefore the identification will also measure the suspension. To show this, a figure is made of the CMIF of the Upright near 0 Hz It can be clearly seen one of the rigid body modes has a frequency of 1.8 Hz. This turns out to be the swinging frequency of the plate. The properties of the plate are best described using rigid body modes at 0 Hz. The three rigid body modes which are needed, can be constructed and scaled by the modal masses and rotation inertias.

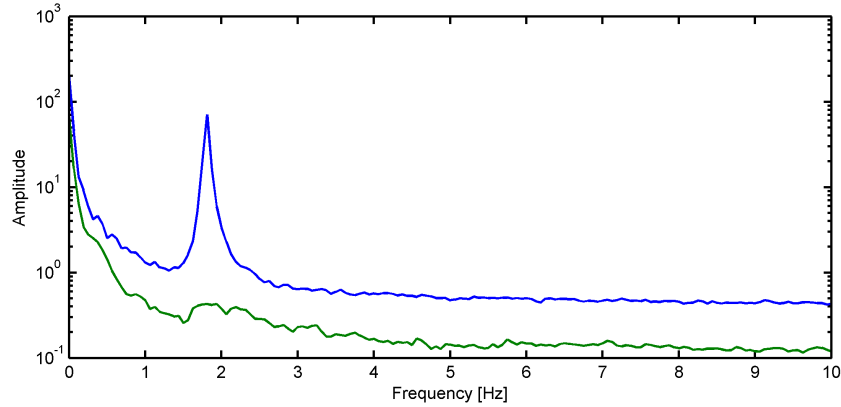


Figure 6.2: CMIF of Upright showing swinging frequency of plate. The two lines represent two sets of singular values belonging to two references (sensors).

The translational motion is described by a unit displacement on all the nodes. The modeshape amplitude will be scaled by the mass with $\frac{-1}{\sqrt{m}}$. The two other rigid body modes that can be measured are the rotational motions about the x-axis and the y-axis of the plate. These motions have to do with the inertia of the plate in those directions, and will be scaled by $\frac{-1}{\sqrt{I_x}}$ and $\frac{-1}{\sqrt{I_y}}$.

If these modeshapes are added to the modal model, and the response model is build, the low frequent behaviour is much better described as can be seen in Figure 6.3.

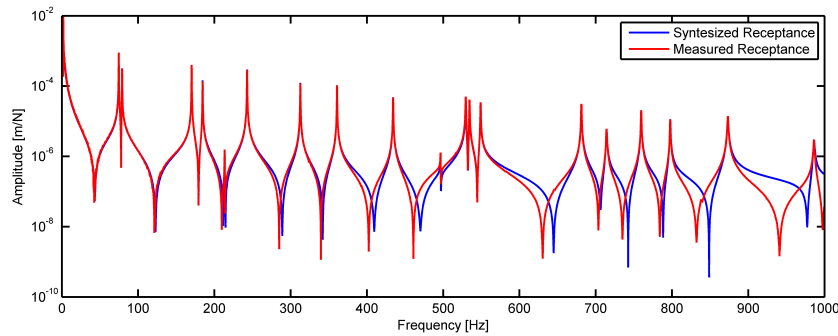


Figure 6.3: Measured and synthesized receptance with rigid body modes

6.2.2 Higher Residual modes

The high frequent behaviour does still not match the measurement FRF. This is due to the fact that high frequent modes, that not have been measured will have influence on lower frequent behaviour especially near anti resonances. In fact, the high frequent content can be build with modeshapes of a FEM model. This method gives the possibility to reconstruct responses that not have been measured. And only in this way a full \mathbf{H} matrix can be build. Another way to account for the higher residuals is to add a constant to the modal superposition. This constant can be found in a least square sense. A picture of a response constructed with an added constant can be seen in Figure 6.4.

In this research the coupled model will only be investigated in the frequency band 0-200 Hz. This means that no higher residuals are taken into account, since the synthesized model already shows very good resemblance with the measurement in this frequency band.

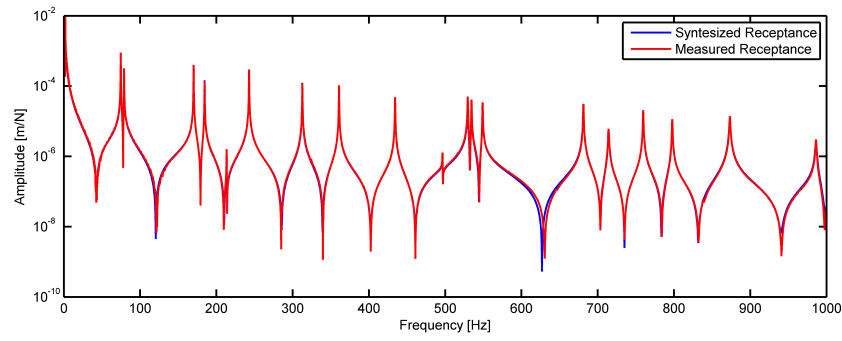


Figure 6.4: Measured and synthesized receptance with rigid body modes

6.3 Discussion

The response model has been build based on measured modes, damping and frequencies, also on calculated rigid body modes and on added modes from a FEM model. With the response models of both substructures, a basis is made for the coupling procedure.

Part III

Identification of damping in joints

Chapter 7

Coupling two plates in the frequency domain

In the final part of this thesis, the theory presented in Part I and the substructure models from Part II are combined in the experimental DS analysis of the plate problems. In this chapter it will be described how the base and upright can be coupled together. Because the interface is not measured completely, DoF on the interface need to be found in order to define compatibility on the interface. The membrane dynamics of a plate can be written as a rigid body in terms of rigid body modes and rigid body inertias this is explained in Section 7.1. When this is done, the plates can be coupled. The assembling procedure is described in Section 7.2. The compatibility on the connection points is strong, and this will cause errors due to measurement errors that will occur. A method to weaken the interface compatibility can be found in the Section 7.3.

7.1 Description of a rigid substructure

When a substructure can be assumed as rigid, all the degrees of freedom can be related to n rigid body modeshapes. This can be written as

$$\mathbf{u} \simeq \mathbf{R}\boldsymbol{\alpha} \quad (7.1)$$

where $\boldsymbol{\alpha}$ are the degrees of freedom of the structure, and \mathbf{R} is a matrix with Rigid body modes. This relation can be substituted in the dynamic equation of the substructure, $\mathbf{Z}\mathbf{u} = \mathbf{f}$, and we obtain

$$\mathbf{Z}\mathbf{R}\boldsymbol{\alpha} = \mathbf{f} \quad (7.2)$$

This equation is now multiplied by \mathbf{R}^T :

$$\mathbf{R}^T\mathbf{Z}\mathbf{R}\boldsymbol{\alpha} = \mathbf{R}^T\mathbf{f}. \quad (7.3)$$

The first part can be expanded, and due to the fact that the system is rigid we obtain:

$$\mathbf{R}^T\mathbf{Z}\mathbf{R} = \mathbf{R}^T \left(-\omega^2\mathbf{M} + i\omega\mathbf{C} + \mathbf{K} \right) \mathbf{R} = -\omega^2\mathbf{R}^T\mathbf{M}\mathbf{R} = -\omega^2\mathbf{M}_{rig} \quad (7.4)$$

The admittance of the rigid substructure can now be written:

$$\boldsymbol{\alpha} = \frac{-1}{\omega^2}\mathbf{M}_{rig}^{-1} \left(\mathbf{R}^T\mathbf{f} \right) = \mathbf{Y}_{rig} \left(\mathbf{R}^T\mathbf{f} \right). \quad (7.5)$$

When the inertia properties of the system are known, a similar set of relations of known (α) and unknowns can be written:

$$\begin{cases} \alpha = Y_{\text{rig}} (R^T f) \\ u = R\alpha \end{cases} \quad (7.6)$$

7.2 Assembling two plates based on partial measurement

In the problem treated in this research, a base and upright are measured, and will be coupled as can be seen in Figure 7.1.

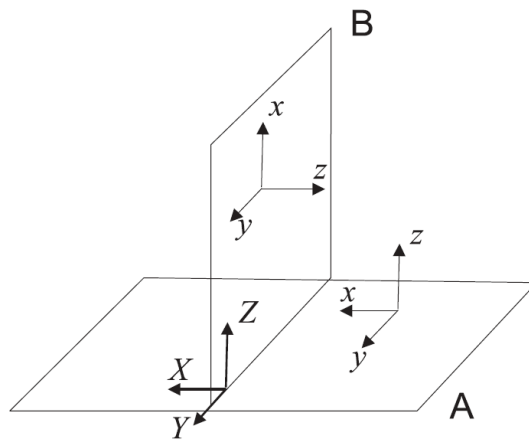


Figure 7.1: Defenition of reference axis.

The dynamics of both plates can be described as

$$\begin{bmatrix} u_{zi} \\ u_{zc} \\ \theta_{xc} \\ \theta_{yc} \\ u_{xc} \\ u_{yc} \\ \theta_{zc} \end{bmatrix} = Y^{A/B} f^{A/B}, \quad (7.7)$$

where the DoF on the interface are denoted by the subscript c and the internal DoF by the subscript i . The first four DoF describe the out of plane behaviour of the plates, and the last three DoF describe the membrane, the in-plane behaviour. It is assumed that the out of plane and membrane behaviour is fully uncoupled in a plate. The plates have been measured in out of plane direction, so there is information about displacements and forces in those directions. The dynamics of the membrane are not measured, but can be approximated by rigid body behaviour represented by u_{xc} , u_{yc} and θ_{zc} and rigid body modes R . The unknown DoF which describe out of plane behaviour will be constructed as is deduced in Section 3.3

$$\begin{bmatrix} \theta_{xc} \\ \theta_{yc} \end{bmatrix} = C \begin{bmatrix} u_{zi} \\ u_{zc} \end{bmatrix}, \quad (7.8)$$

where it is assumed that \mathbf{u}_{zi} and \mathbf{u}_{zc} are known. \mathbf{C} can be built as is explained in Section 3.3. The kinematic relations can be expanded as follows

$$\begin{bmatrix} \theta_{xc} \\ \theta_{yc} \end{bmatrix}^{A/B} = \mathbf{C} \begin{bmatrix} \mathbf{u}_{zi} \\ \mathbf{u}_{zc} \end{bmatrix}^{A/B} = \begin{bmatrix} \mathbf{C}_{\theta_{xc},zi} & \mathbf{C}_{\theta_{xc},zc} \\ \mathbf{C}_{\theta_{yc},zi} & \mathbf{C}_{\theta_{yc},zc} \end{bmatrix}^{A/B} \quad (7.9)$$

and the kinematic relations for the in-plane DoF writes:

$$\begin{bmatrix} \mathbf{u}_{xc} \\ \mathbf{u}_{yc} \\ \theta_{zc} \end{bmatrix}^{A/B} = \mathbf{R}_m^{A/B} \boldsymbol{\alpha}^{A/B} = \begin{bmatrix} \mathbf{R}_{xc} \\ \mathbf{R}_{yc} \\ \mathbf{R}_{\theta_{zc}} \end{bmatrix}^{A/B} \boldsymbol{\alpha}^{A/B} = \begin{bmatrix} \mathbf{R}_{xc}^1 & \mathbf{R}_{xc}^2 & \mathbf{R}_{xc}^3 \\ \mathbf{R}_{yc}^1 & \mathbf{R}_{yc}^2 & \mathbf{R}_{yc}^3 \\ \mathbf{R}_{\theta_{zc}}^1 & \mathbf{R}_{\theta_{zc}}^2 & \mathbf{R}_{\theta_{zc}}^3 \end{bmatrix}^{A/B} \begin{bmatrix} \alpha_1 \\ \alpha_2 \\ \alpha_3 \end{bmatrix}^{A/B} \quad (7.10)$$

\mathbf{R}_m are the rigid body modes which describe the rigid body behaviour. \mathbf{R}^1 , \mathbf{R}^2 and \mathbf{R}^3 designate respectively the translational modes along x and y , and the in plane rotational mode. The rigid body modes are constructed as follows:

$$\mathbf{R}_m^{A/B} = \begin{bmatrix} 1 & 0 & r_{1y} \\ \vdots & \vdots & \vdots \\ 1 & 0 & r_{ny} \\ 0 & 1 & 0 \\ \vdots & \vdots & \vdots \\ 0 & 1 & 0 \\ 0 & 0 & 1 \\ \vdots & \vdots & \vdots \\ 0 & 0 & 1 \end{bmatrix}^{A/B} \quad (7.11)$$

In order to couple both plates, compatibility is enforced by using compatibility equation. This equation is written as

$$\begin{array}{l} \mathbf{u}_Z \rightarrow \\ \theta_X \rightarrow \\ \theta_Y \rightarrow \\ \mathbf{u}_X \rightarrow \\ \mathbf{u}_Y \rightarrow \\ \theta_Z \rightarrow \end{array} \begin{bmatrix} \mathbf{0} & \mathbf{I} & \mathbf{0} & \mathbf{0} & \mathbf{0} & \mathbf{0} & \mathbf{0} \\ \mathbf{0} & \mathbf{0} & \mathbf{I} & \mathbf{0} & \mathbf{0} & \mathbf{0} & \mathbf{0} \\ \mathbf{0} & \mathbf{0} & \mathbf{0} & \mathbf{I} & \mathbf{0} & \mathbf{0} & \mathbf{0} \\ \mathbf{0} & \mathbf{0} & \mathbf{0} & \mathbf{0} & \mathbf{I} & \mathbf{0} & \mathbf{0} \\ \mathbf{0} & \mathbf{0} & \mathbf{0} & \mathbf{0} & \mathbf{0} & \mathbf{I} & \mathbf{0} \\ \mathbf{0} & \mathbf{0} & \mathbf{0} & \mathbf{0} & \mathbf{0} & \mathbf{0} & \mathbf{I} \end{bmatrix}^A \begin{bmatrix} \mathbf{u}_{zi} \\ \mathbf{u}_{zc} \\ \theta_{xc} \\ \theta_{yc} \\ \mathbf{u}_{xc} \\ \mathbf{u}_{yc} \\ \theta_{zc} \end{bmatrix}^A + \begin{bmatrix} \mathbf{0} & \mathbf{0} & \mathbf{0} & \mathbf{0} & -\mathbf{I} & \mathbf{0} & \mathbf{0} \\ \mathbf{0} & \mathbf{0} & \mathbf{0} & \mathbf{0} & \mathbf{0} & \mathbf{0} & \mathbf{I} \\ \mathbf{0} & \mathbf{0} & \mathbf{0} & -\mathbf{I} & \mathbf{0} & \mathbf{0} & \mathbf{0} \\ \mathbf{0} & \mathbf{I} & \mathbf{0} & \mathbf{0} & \mathbf{0} & \mathbf{0} & \mathbf{0} \\ \mathbf{0} & \mathbf{0} & \mathbf{0} & \mathbf{0} & \mathbf{0} & -\mathbf{I} & \mathbf{0} \\ \mathbf{0} & \mathbf{0} & -\mathbf{I} & \mathbf{0} & \mathbf{0} & \mathbf{0} & \mathbf{0} \end{bmatrix}^A \begin{bmatrix} \mathbf{u}_{zi} \\ \mathbf{u}_{zc} \\ \theta_{xc} \\ \theta_{yc} \\ \mathbf{u}_{xc} \\ \mathbf{u}_{yc} \\ \theta_{zc} \end{bmatrix}^B = \mathbf{0} \quad (7.12)$$

It can be seen that \mathbf{u}_y is not coupled to any out of plane DoF and thus can be left out of the equations. If the kinematic relations (7.9) and (8.11) are substituted in the compatibility equation we obtain

$$\begin{bmatrix} \mathbf{0} & \mathbf{I} & \mathbf{0} \\ \mathbf{C}_{\theta_{xc},zi} & \mathbf{C}_{\theta_{xc},zc} & \mathbf{0} \\ \mathbf{C}_{\theta_{yc},zi} & \mathbf{C}_{\theta_{yc},zc} & \mathbf{0} \\ \mathbf{0} & \mathbf{0} & \mathbf{R}_{xc} \\ \mathbf{0} & \mathbf{0} & \mathbf{R}_{yc} \\ \mathbf{0} & \mathbf{0} & \mathbf{R}_{zc} \end{bmatrix}^A \begin{bmatrix} \mathbf{u}_{zi} \\ \mathbf{u}_{zc} \\ \boldsymbol{\alpha} \end{bmatrix}^A + \begin{bmatrix} \mathbf{0} & \mathbf{0} & -\mathbf{R}_{xc} \\ \mathbf{0} & \mathbf{0} & -\mathbf{R}_{zc} \\ -\mathbf{C}_{\theta_{yc},zi} & -\mathbf{C}_{\theta_{yc},zc} & \mathbf{0} \\ \mathbf{0} & \mathbf{I} & \mathbf{0} \\ \mathbf{0} & \mathbf{0} & -\mathbf{R}_{yc} \\ -\mathbf{C}_{\theta_{xc},zi} & -\mathbf{C}_{\theta_{xc},zc} & \mathbf{0} \end{bmatrix}^B \begin{bmatrix} \mathbf{u}_{zi} \\ \mathbf{u}_{zc} \\ \boldsymbol{\alpha} \end{bmatrix}^B = \mathbf{0} \quad (7.13)$$

where $\boldsymbol{\alpha}$ are the DoF describing the membrane behaviour. This equation can be written as

$$\begin{bmatrix} \tilde{\mathbf{B}}_z^A & \mathbf{B}_{m,\text{rig}}^A \end{bmatrix} \begin{bmatrix} \mathbf{u}_z^A \\ \boldsymbol{\alpha}^A \end{bmatrix} + \begin{bmatrix} \tilde{\mathbf{B}}_z^B & \mathbf{B}_{m,\text{rig}}^B \end{bmatrix} \begin{bmatrix} \mathbf{u}_z^B \\ \boldsymbol{\alpha}^B \end{bmatrix} = \mathbf{0}. \quad (7.14)$$

It can be seen that only the known DoF are kept in the equation due to the substitution of the kinematic relations. The total dynamic equation, including the compatibility forces can be written as

$$\begin{bmatrix} \mathbf{u}_z \\ \boldsymbol{\alpha} \end{bmatrix}^{A/B} = \begin{bmatrix} \mathbf{Y}_z & \mathbf{0} \\ \mathbf{0} & \mathbf{Y}_{\text{m.rig}} \end{bmatrix}^{A/B} \left(\begin{bmatrix} \tilde{\mathbf{f}}_z \\ \mathbf{f}_{\text{m.rig}} \end{bmatrix}^{A/B} - \begin{bmatrix} \tilde{\mathbf{B}}_z^T \\ \mathbf{B}_{\text{m.rig}}^T \end{bmatrix}^{A/B} \boldsymbol{\lambda} \right) \quad (7.15)$$

The forces are defined as

$$\begin{aligned} \tilde{\mathbf{f}}_z &= \mathbf{f}_z + \mathbf{C}^T \begin{bmatrix} \mathbf{f}_{\theta_{xc}} \\ \mathbf{f}_{\theta_{yc}} \end{bmatrix} \\ \tilde{\mathbf{f}}_{\text{m.rig}} &= \mathbf{R}_m^T \mathbf{f}_m \end{aligned}$$

and $\boldsymbol{\lambda}$ can be seen as the interface forces.

$$\boldsymbol{\lambda} = [\lambda_z \quad \lambda_{\theta_x} \quad \lambda_{\theta_y} \quad \lambda_x \quad \lambda_y \quad \lambda_{\theta_z}]^T \quad (7.16)$$

The coupled problem can be summarized in a matrix equation:

$$\begin{bmatrix} \mathbf{Y}_z^{A^{-1}} & \mathbf{0} & \mathbf{0} & \mathbf{0} \\ \mathbf{0} & \mathbf{Y}_{\text{m.rig}}^{A^{-1}} & \mathbf{0} & \mathbf{0} \\ \mathbf{0} & \mathbf{0} & \mathbf{Y}_z^{B^{-1}} & \mathbf{0} \\ \mathbf{0} & \mathbf{0} & \mathbf{0} & \mathbf{Y}_{\text{m.rig}}^{B^{-1}} \\ \tilde{\mathbf{B}}_z^A & \mathbf{B}_{\text{m.rig}}^A & \tilde{\mathbf{B}}_z^B & \mathbf{B}_{\text{m.rig}}^B \end{bmatrix} \begin{bmatrix} \tilde{\mathbf{B}}_z^{A^T} \\ \mathbf{B}_{\text{m.rig}}^{A^T} \\ \tilde{\mathbf{B}}_z^{B^T} \\ \mathbf{B}_{\text{m.rig}}^{B^T} \\ \mathbf{0} \end{bmatrix} \begin{bmatrix} \mathbf{u}_z^A \\ \boldsymbol{\alpha}^A \\ \mathbf{u}_z^B \\ \boldsymbol{\alpha}^B \\ \boldsymbol{\lambda} \end{bmatrix} = \begin{bmatrix} \tilde{\mathbf{f}}_z^A \\ \mathbf{f}_{\text{m.rig}}^A \\ \tilde{\mathbf{f}}_z^B \\ \mathbf{f}_{\text{m.rig}}^B \\ \mathbf{0} \end{bmatrix} \quad (7.17)$$

7.3 Weakening of interface compatibility

In the previous section, the compatibility has been enforced on all interfacing DoF. This compatibility will be too strong when measurement data is used. This ‘strong’ compatibility might stiffen the interface connection, and measurement errors will cause wrong coupling results. In stead of using the strong compatibility as is used in Section 3.3, the compatibility can be weakened. Weakening of the compatibility means that only compatibility is enforced on rigid body modes of the interface, and simple deformation modes. The higher modes will ‘left free’. This weakening will preserve stiffening of the interface due to the bad estimation of higher modes. In first instance, only interface rigid body modes will be used and these can be written as

$$\begin{bmatrix} \mathbf{u}_z \\ \theta_x \\ \theta_y \\ \mathbf{u}_x \\ \mathbf{u}_y \\ \theta_z \end{bmatrix} = \begin{bmatrix} \mathbf{R}_z & \mathbf{0} \\ \mathbf{R}_{\theta_x} & \mathbf{0} \\ \mathbf{0} & \boldsymbol{\Psi}_{\theta_y} \\ \mathbf{R}_x & \mathbf{0} \\ \mathbf{R}_y & \mathbf{0} \\ \mathbf{R}_{\theta_z} & \mathbf{0} \end{bmatrix} \begin{bmatrix} \alpha_\Gamma \\ \mu_\Psi \end{bmatrix} = \begin{bmatrix} \mathbf{0} & \mathbf{0} & \mathbf{0} & \mathbf{R}_{xc}^{1B} & \mathbf{R}_{xc}^{2B} & \mathbf{R}_{xc}^{3B} & \mathbf{0} \\ \mathbf{0} & \mathbf{0} & \mathbf{0} & -\mathbf{R}_{\theta_{zc}}^{1B} & -\mathbf{R}_{\theta_{zc}}^{2B} & -\mathbf{R}_{\theta_{zc}}^{3B} & \mathbf{0} \\ \mathbf{0} & \mathbf{0} & \mathbf{0} & \mathbf{0} & \mathbf{0} & \mathbf{0} & \boldsymbol{\Psi}_{\theta_{yc}} \\ \mathbf{R}_{xc}^{1A} & \mathbf{R}_{xc}^{2A} & \mathbf{R}_{xc}^{3A} & \mathbf{0} & \mathbf{0} & \mathbf{0} & \mathbf{0} \\ \mathbf{R}_{yc}^{1A} & \mathbf{R}_{yc}^{2A} & \mathbf{R}_{yc}^{3A} & \mathbf{R}_{yc}^{1B} & \mathbf{R}_{yc}^{2B} & \mathbf{R}_{yc}^{3B} & \mathbf{0} \\ \mathbf{R}_{\theta_{zc}}^{1A} & \mathbf{R}_{\theta_{zc}}^{2A} & \mathbf{R}_{\theta_{zc}}^{3A} & \mathbf{0} & \mathbf{0} & \mathbf{0} & \mathbf{0} \end{bmatrix} \begin{bmatrix} \alpha_1^A \\ \alpha_2^A \\ \alpha_3^A \\ \alpha_1^B \\ \alpha_2^B \\ \alpha_3^B \\ \mu_\Psi \end{bmatrix} \quad (7.18)$$

θ_Y is not related to any membrane rigid body mode, and the modes $\Psi_{\theta_{yc}}$ represent the rigid modes for those rotations. The rigid body modes can be described by ones at the 'diagonal', which means that \mathbf{R}_x^1 , \mathbf{R}_y^2 and $\mathbf{R}_{\theta_z}^3$ contain unit displacements. \mathbf{R}_x^3 describes the translations in x direction caused by the rigid rotation θ_z (see Equation 7.11). Furthermore can be noted that $\alpha_2^A = \alpha_2^B$, and therefore one line can be eliminated from the equation. The resulting equation with non-zero entries is:

$$\begin{bmatrix} \mathbf{u}_Z \\ \theta_X \\ \theta_Y \\ \mathbf{u}_X \\ \mathbf{u}_Y \\ \theta_Z \end{bmatrix} = \begin{bmatrix} \mathbf{0} & \mathbf{0} & \mathbf{0} & \mathbf{R}_{xc}^{1B} & \mathbf{R}_{xc}^{3B} & \mathbf{0} \\ \mathbf{0} & \mathbf{0} & \mathbf{0} & \mathbf{0} & -\mathbf{R}_{\theta_z}^{3\alpha} & \mathbf{0} \\ \mathbf{0} & \mathbf{0} & \mathbf{0} & \mathbf{0} & \mathbf{0} & \Psi_{\theta_{yc}} \\ \mathbf{R}_{xc}^{1A} & \mathbf{0} & \mathbf{R}_{xc}^{3A} & \mathbf{0} & \mathbf{0} & \mathbf{0} \\ \mathbf{0} & \mathbf{R}_{yc}^{2A} & \mathbf{0} & \mathbf{0} & \mathbf{0} & \mathbf{0} \\ \mathbf{0} & \mathbf{0} & \mathbf{R}_{\theta_z}^{3A} & \mathbf{0} & \mathbf{0} & \mathbf{0} \end{bmatrix} \begin{bmatrix} \alpha_1^A \\ \alpha_2^A = \alpha_2^B \\ \alpha_3^A \\ \alpha_1^B \\ \alpha_3^B \\ \mu_\Psi \end{bmatrix} = \mathbb{G}_\Gamma \boldsymbol{\gamma} \quad (7.19)$$

The interface modes can be ortho-normalized by the following operation, which does not change the basis,

$$\mathbf{G} = \mathbb{G}_\Gamma (\mathbb{G}_\Gamma^T \mathbb{G}_\Gamma)^{-1} \quad (7.20)$$

The compatibility equation (8.13) can now be weakened by multiplying it by \mathbf{G}^T :

$$\mathbf{G}^T \begin{bmatrix} \tilde{\mathbf{B}}_z^A & \mathbf{B}_{\text{m.rig}}^A \end{bmatrix} \begin{bmatrix} \mathbf{u}_z^A \\ \boldsymbol{\alpha}^A \end{bmatrix} + \mathbf{G}^T \begin{bmatrix} \tilde{\mathbf{B}}_z^B & \mathbf{B}_{\text{m.rig}}^B \end{bmatrix} \begin{bmatrix} \mathbf{u}_z^B \\ \boldsymbol{\alpha}^B \end{bmatrix} = \mathbf{0} \quad (7.21)$$

By using the relation definitions (7.19) and (7.21) we obtain

$$\begin{bmatrix} \mathbf{G}^T \tilde{\mathbf{B}}_z^A \begin{bmatrix} 1 & 0 & 0 \\ 0 & 1 & 0 \\ 0 & 0 & 1 \\ 0 & 0 & 0 \\ 0 & 0 & 0 \\ 0 & 0 & 0 \end{bmatrix} \begin{bmatrix} \mathbf{u}_z^A \\ \boldsymbol{\alpha}^A \end{bmatrix} + \mathbf{G}^T \tilde{\mathbf{B}}_z^B \begin{bmatrix} 0 & 0 & 0 \\ 0 & -1 & 0 \\ 0 & 0 & 0 \\ -1 & 0 & 0 \\ 0 & 0 & -1 \\ 0 & 0 & 0 \end{bmatrix} \begin{bmatrix} \mathbf{u}_z^B \\ \boldsymbol{\alpha}^B \end{bmatrix} \end{bmatrix} \quad (7.22)$$

Chapter 8

Validation of methods

In Chapter 7 a method has been proposed to couple two partially measured plates. To be able to couple both plates two assumptions have been made:

- The membrane behaviour is assumed to be rigid
- The non measured interface DoF can be written in terms of modes that are related to internal measured DoF

The effects of these assumptions on the coupling results will be investigated in this chapter. The results will be compared to FRF's constructed with data from a base-upright model in FEM. The nodes that will be used as a reference can be seen in Figure 8.1. The first nine flexible modes of the FEM model can be seen in Figure 8.2. In Section 8.1 it is described what the consequences are of the rigid membrane assumption. In the Section 8.2 the results will be presented that are obtained by using rotational DoF on the interface that are based on modes, and some conclusions will be made.

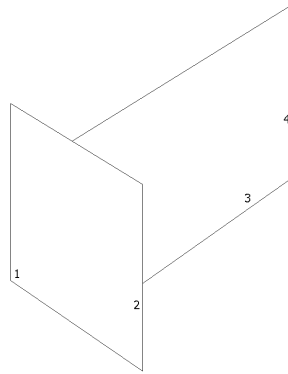


Figure 8.1: Input and response positions of FRFs.

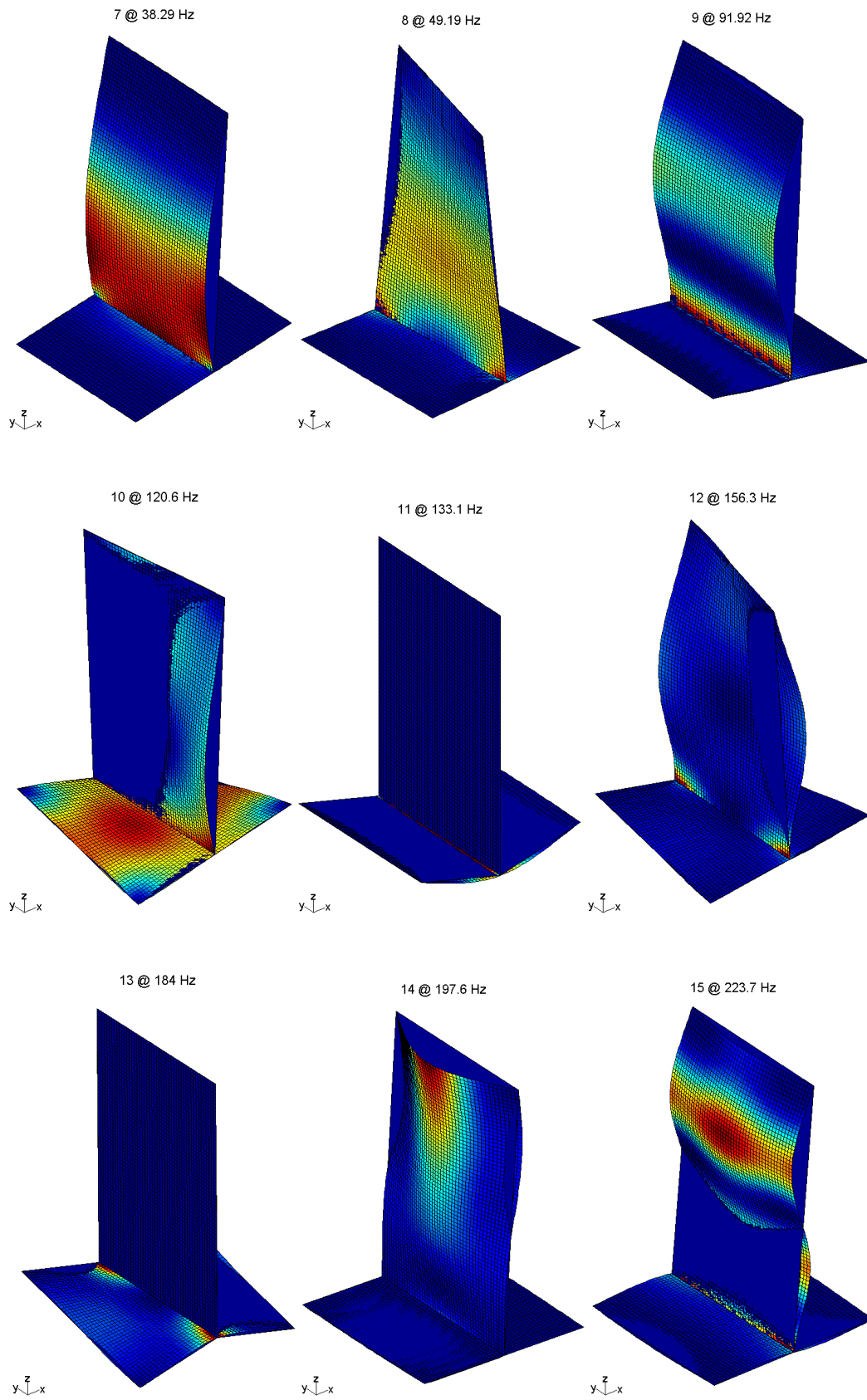


Figure 8.2: First nine flexible modeshapes of the coupled system computed with FEM. The colours show the vm stress levels in the structure.

8.1 Rigid membrane behaviour

The assumption has been done that the in-plane dynamics described by the in-plane DoF \mathbf{x} , \mathbf{y} and θ_z are totally uncoupled from the DoF that describe the out-of plane behaviour, namely the \mathbf{z} , θ_x and θ_y . In this section will be investigated of this assumption is correct. The \mathbf{y} direction will be excluded from this investigation because this direction will not be used to couple in-plane DoF of one plate to out of plane dof of the other plate. The system will be divided in a flexible part and in a rigid membrane part:

$$\begin{bmatrix} \mathbf{u}_z \\ \theta_x \\ \theta_y \\ \mathbf{u}_x \\ \theta_z \end{bmatrix} = \begin{bmatrix} \mathbf{Y}_{z,\theta_x,\theta_y} & \mathbf{0} \\ \mathbf{0} & \mathbf{Y}_{x,\theta_z} \end{bmatrix} \begin{bmatrix} \mathbf{f}_z \\ \mathbf{m}_x \\ \mathbf{m}_y \\ \mathbf{f}_x \\ \mathbf{m}_z \end{bmatrix} \quad (8.1)$$

The off-diagonal terms show that there is no coupling between in-plane and out-of-plane DoF

8.1.1 Construction of system matrices

The matrix $\mathbf{Y}_{z,\theta_x,\theta_y}$ will be built using the equation

$$\mathbf{Y}_{z,\theta_x,\theta_y} = \left(-\omega^2 \mathbf{M} + \mathbf{K} \right)^{-1}. \quad (8.2)$$

This system matrix can be constructed for a set of DoF on the interface by solving the equation

$$\left(-\omega^2 \mathbf{M} + \mathbf{K} \right) \mathbf{z} = \mathbf{f} \quad (8.3)$$

for the unknown displacements \mathbf{z} , in this case \mathbf{u}_z , θ_x and θ_y . \mathbf{f} are unit forces imposed on these degrees of freedom.

The \mathbf{Y}_{x,θ_z} will be built using rigid body modes, and the mass matrix of the structure:

$$\mathbf{Y}_{x,\theta_z} = \frac{-1}{\omega^2} \left(\mathbf{R}^T \mathbf{M} \mathbf{R} \right)^{-1} \quad (8.4)$$

These rigid body modes \mathbf{R} can be found by imposing a unit displacement in 6 DoF on the coupling node

$$\mathbf{R}_1 = \mathbf{I}_6 \quad (8.5)$$

where \mathbf{R}_1 is the part of the rigid body modes belonging to the coupling node (centre of rotation). \mathbf{R}_2 can now be calculated using the stiffness matrix. The stiffness matrix will be partitioned according to the coupling node and the remaining DoF. The forces will be set to zero because only rigid body motions are considered, which means that no internal forces are needed for equilibrium.

$$\begin{bmatrix} \mathbf{K}_{11} & \mathbf{K}_{12} \\ \mathbf{K}_{21} & \mathbf{K}_{22} \end{bmatrix} \begin{bmatrix} \mathbf{R}_1 \\ \mathbf{R}_2 = \mathbf{I} \end{bmatrix} = \mathbf{0} \quad (8.6)$$

From the first line, the rigid body motions can be obtained:

$$\mathbf{R}_1 = -\mathbf{K}_{11}^{-1} \mathbf{K}_{12} \quad (8.7)$$

The total mass matrix can now be weighted over these rigid body motions, and we obtain the mass and inertia of the plate for this centre of motion

$$\mathbf{R}^T \mathbf{M} \mathbf{R} = \mathbf{M}_\alpha. \quad (8.8)$$

The \mathbf{Y}_{x,θ_z} can now be written:

$$\mathbf{Y}_{x,\theta_z} = \frac{-1}{\omega^2} \mathbf{M}_\alpha^{-1} \quad (8.9)$$

The matrix that is obtained is a 6 by 6 matrix. In our case only the x and θ_z entries will be used.

8.1.2 Construction of Boolean matrices

The compatibility equations that enforce compatibility on all the interface DoF can be written as follows

$$\begin{aligned} u_Z &\rightarrow \begin{bmatrix} \mathbf{0} & \mathbf{I} & \mathbf{0} & \mathbf{0} & \mathbf{0} & \mathbf{0} \end{bmatrix}^A \begin{bmatrix} \mathbf{u}_{zi} \\ \mathbf{u}_{zc} \\ \boldsymbol{\theta}_{xc} \\ \boldsymbol{\theta}_{yc} \\ \mathbf{u}_{xc} \\ \boldsymbol{\theta}_{zc} \end{bmatrix}^A + \begin{bmatrix} \mathbf{0} & \mathbf{0} & \mathbf{0} & \mathbf{0} & -\mathbf{I} & \mathbf{0} \\ \mathbf{0} & \mathbf{0} & \mathbf{0} & \mathbf{0} & \mathbf{0} & \mathbf{I} \\ \mathbf{0} & \mathbf{0} & \mathbf{0} & -\mathbf{I} & \mathbf{0} & \mathbf{0} \\ \mathbf{0} & \mathbf{I} & \mathbf{0} & \mathbf{0} & \mathbf{0} & \mathbf{0} \\ \mathbf{0} & \mathbf{0} & -\mathbf{I} & \mathbf{0} & \mathbf{0} & \mathbf{0} \end{bmatrix}^A \begin{bmatrix} \mathbf{u}_{zi} \\ \mathbf{u}_{zc} \\ \boldsymbol{\theta}_{xc} \\ \boldsymbol{\theta}_{yc} \\ \mathbf{u}_{xc} \\ \boldsymbol{\theta}_{zc} \end{bmatrix}^B = \mathbf{0} \quad (8.10) \end{aligned}$$

where the DoF in front of the compatibility equation are defined in Figure 7.1. The in-plane DoF are related to two rigid motions α :

$$\begin{bmatrix} \mathbf{u}_{xc} \\ \boldsymbol{\theta}_{zc} \end{bmatrix}^{A/B} = \begin{bmatrix} \mathbf{R}_{xc}^1 & \mathbf{R}_{\theta_{zc}}^2 \\ \mathbf{R}_{\theta_{zc}}^1 & \mathbf{R}_{\theta_{zc}}^2 \end{bmatrix}^{A/B} \begin{bmatrix} \alpha_1 \\ \alpha_2 \end{bmatrix}^{A/B} \quad (8.11)$$

\mathbf{R}_m are the rigid body modes which describe the rigid body behaviour. \mathbf{R}^1 and \mathbf{R}^2 designate respectively the translational modes along x and the in plane rotational mode θ_z .

If these relations are substituted in the compatibility equation (8.10) we obtain

$$\begin{aligned} u_Z &\rightarrow \begin{bmatrix} \mathbf{0} & \mathbf{I} & \mathbf{0} & \mathbf{0} & \mathbf{0} \\ \mathbf{0} & \mathbf{0} & \mathbf{I} & \mathbf{0} & \mathbf{0} \\ \mathbf{0} & \mathbf{0} & \mathbf{0} & \mathbf{I} & \mathbf{0} \\ \mathbf{0} & \mathbf{0} & \mathbf{0} & \mathbf{0} & \mathbf{R}_{xc} \\ \mathbf{0} & \mathbf{0} & \mathbf{0} & \mathbf{0} & \mathbf{R}_{\theta_{zc}} \end{bmatrix}^A \begin{bmatrix} \mathbf{u}_{zi} \\ \mathbf{u}_{zc} \\ \boldsymbol{\theta}_{xc} \\ \boldsymbol{\theta}_{yc} \\ \alpha_1 \\ \alpha_2 \end{bmatrix}^A + \begin{bmatrix} \mathbf{0} & \mathbf{0} & \mathbf{0} & \mathbf{0} & -\mathbf{R}_{xc} \\ \mathbf{0} & \mathbf{0} & \mathbf{0} & \mathbf{0} & \mathbf{R}_{\theta_{zc}} \\ \mathbf{0} & \mathbf{0} & \mathbf{0} & -\mathbf{I} & \mathbf{0} \\ \mathbf{0} & \mathbf{I} & \mathbf{0} & \mathbf{0} & \mathbf{0} \\ \mathbf{0} & \mathbf{0} & -\mathbf{I} & \mathbf{0} & \mathbf{0} \end{bmatrix}^A \begin{bmatrix} \mathbf{u}_{zi} \\ \mathbf{u}_{zc} \\ \boldsymbol{\theta}_{xc} \\ \boldsymbol{\theta}_{yc} \\ \alpha_1 \\ \alpha_2 \end{bmatrix}^B = \mathbf{0}. \quad (8.12) \end{aligned}$$

The compatibility equations can be written in short notation:

$$\begin{bmatrix} \mathbf{B}_{z,\theta_x,\theta_y}^A & \mathbf{B}_{m.rig}^A \end{bmatrix} \begin{bmatrix} \mathbf{u}_{z,\theta_x,\theta_y}^A \\ \boldsymbol{\alpha}^A \end{bmatrix} + \begin{bmatrix} \mathbf{B}_{z,\theta_x,\theta_y}^B & \mathbf{B}_{m.rig}^B \end{bmatrix} \begin{bmatrix} \mathbf{u}_{z,\theta_x,\theta_y}^B \\ \boldsymbol{\alpha}^B \end{bmatrix} = \mathbf{0}. \quad (8.13)$$

The total dynamic equation, including the compatibility forces can be written as

$$\begin{bmatrix} \mathbf{u}_{z,\theta_x,\theta_y} \\ \boldsymbol{\alpha} \end{bmatrix}^{A/B} = \begin{bmatrix} \mathbf{Y}_{z,\theta_x,\theta_y} & \mathbf{0} \\ \mathbf{0} & \mathbf{Y}_{m.rig} \end{bmatrix}^{A/B} \left(\begin{bmatrix} \mathbf{f}_{z,\theta_x,\theta_y} \\ \mathbf{f}_{m.rig} \end{bmatrix}^{A/B} - \begin{bmatrix} \mathbf{B}_{z,\theta_x,\theta_y}^T \\ \mathbf{B}_{m.rig}^T \end{bmatrix}^{A/B} \boldsymbol{\lambda} \right), \quad (8.14)$$

where λ are the interface forces. The coupled problem can be summarized in a matrix equation:

$$\begin{bmatrix} \mathbf{Y}_{z,\theta_x,\theta_y}^{A^{-1}} & \mathbf{0} & \mathbf{0} & \mathbf{0} \\ \mathbf{0} & \mathbf{Y}_{m.rig}^{A^{-1}} & \mathbf{0} & \mathbf{0} \\ \mathbf{0} & \mathbf{0} & \mathbf{Y}_{z,\theta_x,\theta_y}^{B^{-1}} & \mathbf{0} \\ \mathbf{0} & \mathbf{0} & \mathbf{0} & \mathbf{Y}_{m.rig}^{B^{-1}} \\ \mathbf{B}_{z,\theta_x,\theta_y}^A & \mathbf{B}_{m.rig}^A & \mathbf{B}_{z,\theta_x,\theta_y}^B & \mathbf{B}_{m.rig}^B \end{bmatrix} \begin{bmatrix} \mathbf{B}_{z,\theta_x,\theta_y}^{A^T} \\ \mathbf{B}_{m.rig}^{A^T} \\ \mathbf{B}_{z,\theta_x,\theta_y}^{B^T} \\ \mathbf{B}_{m.rig}^{B^T} \\ \mathbf{0} \end{bmatrix} \begin{bmatrix} \mathbf{u}_{z,\theta_x,\theta_y}^A \\ \boldsymbol{\alpha}^A \\ \mathbf{u}_{z,\theta_x,\theta_y}^B \\ \boldsymbol{\alpha}^B \\ \boldsymbol{\lambda} \end{bmatrix} = \begin{bmatrix} \mathbf{f}_{z,\theta_x,\theta_y}^A \\ \mathbf{f}_{m.rig}^A \\ \mathbf{f}_{z,\theta_x,\theta_y}^B \\ \mathbf{f}_{m.rig}^B \\ \mathbf{0} \end{bmatrix}, \quad (8.15)$$

This equation can be solved by eliminating the interface forces, and the final equation that will be used to obtain the coupled system writes

$$\mathbf{u} = (\mathbf{Y} - \mathbf{Y}\mathbf{B}^T(\mathbf{B}\mathbf{Y}\mathbf{B}^T)^{-1}\mathbf{B}\mathbf{Y})\mathbf{f}. \quad (8.16)$$

8.1.3 Results

In Figure 8.3 the results of the coupling procedure can be seen.

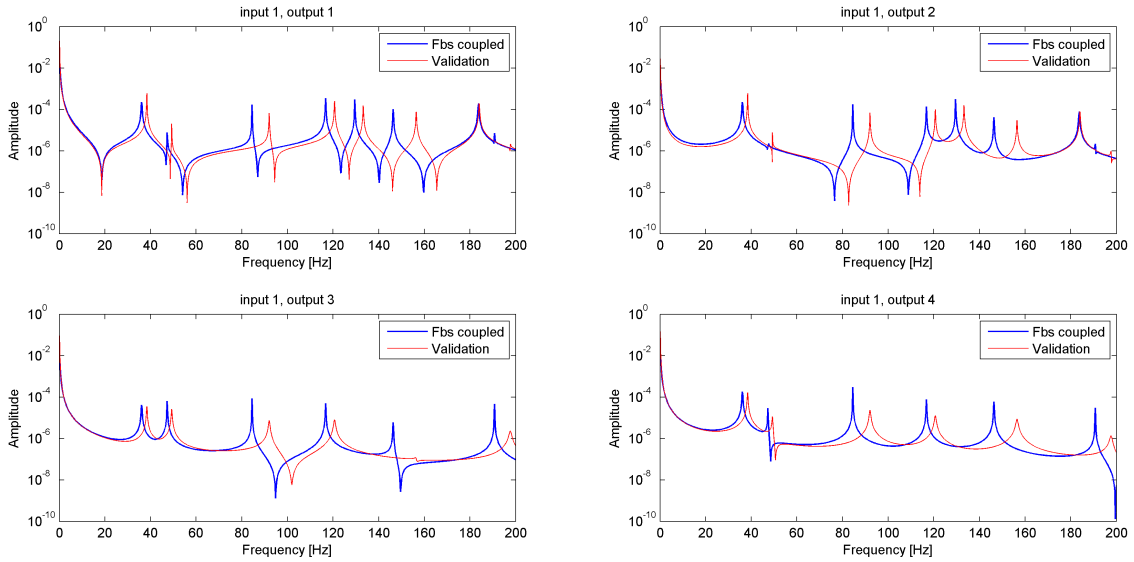


Figure 8.3: FRFs of the coupled model FEM (red line, validation) and the coupled model by assuming that the membrane behaviour of the plates are rigid.

The following observations can be made of Figure 8.3:

- Over the whole frequency range the eigenfrequencies will be underestimated.
- The two lines show good resemblance although the higher poles deviate a bit.
- The rigid body modes seem to be predicted correctly.

It can be seen that the eigenfrequencies will be underestimated if the membrane is assumed to be rigid. This observation is strange since we expected that the coupled dynamics should be more stiff due to stiffening of the membrane behaviour. The overall description of the coupled dynamics is good. This will justify the assumption that the membrane behaviour can be described by rigid motions.

8.2 Describing rotational DoF on the interface with modes.

In this section will be investigated how well the unmeasured DoF on the interface, can be described with modes. This process has been described extensively in Chapter 3. The compatibility will be enforced on the same modes as that are used for building the interface basis. First only rigid body modes are used to describe the DoF on the coupling lines of the plates. This is discussed in Section 8.2.1. In Section 8.2.2 also flexible modes are included in the basis.

The kinematic relations between the known and unknown DoF is constructed as is described below

1. Choose a set of (orthogonal) modes Φ_u that can describe the plate behaviour on the interface.
2. Calculate the modes Φ_k on the known DoF that are geometric consistent with the unknown modes.
3. Calculate the modal participation factors with $\gamma = (\Phi_k^T \Phi_k)^{-1} \Phi_k^T u_k$
4. The kinematic relation between the known and unknown DoF is $u_u = \Phi_u \gamma$ which becomes $u_u = \Phi_u \Phi_k^+ u_k$

The DoF u_k and u_u are chosen the same as in the real experiment.

8.2.1 Rigid body modes

First the unknown DoF θ_x and θ_y are only described by rigid body modes. in Figure 8.4 the results of this procedure can be seen.

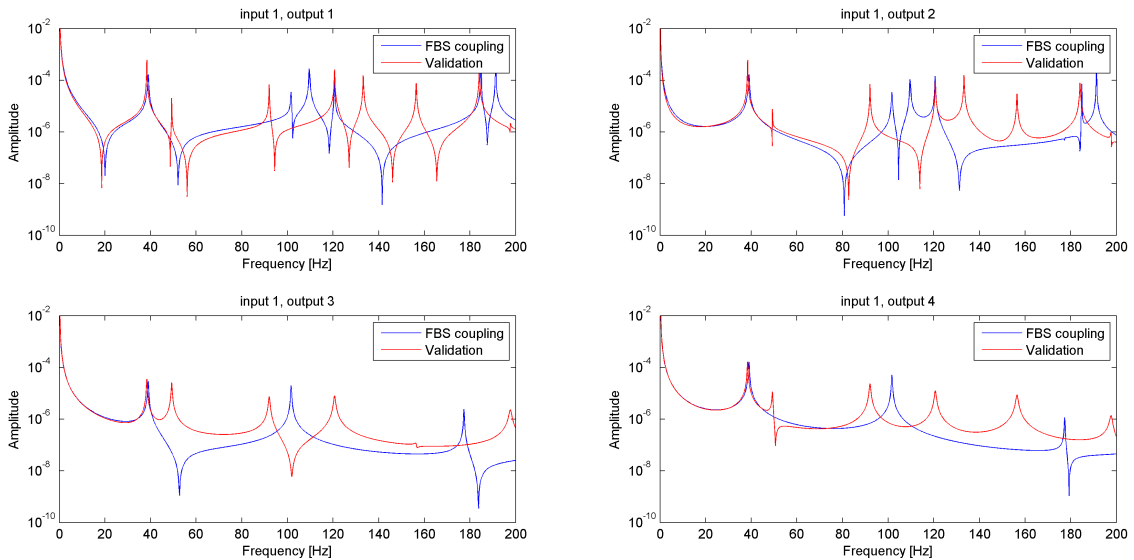


Figure 8.4: The coupled plates with interface described by rigid body modes only.

From Figure 8.4 the following can be observed:

- The first mode shows good resemblance with the validation measurement.

- Mode 5 (120 Hz) and mode 9 (190 Hz) also show good resemblance
- The other modes do not correspond to any of the other peaks.

It can be concluded that the rigid body behaviour is modelled well because the FRF's show resemblance to the validation measurement very well in the low frequent region. The modes that are not well described are probably modes that cause the interface to deform.

8.2.2 Flexible modes

To obtain better coupling results, the description of the unknown DoF need to be expanded with flexible modes. This will allow the interface to deform.

For the DoF θ_y , the same set of modes is used for each plate, because they will be coupled directly to the other plate. Some experiments have been done with different sets of expanding modes. θ_y can best be described by a half sine and a half cosine function over the interface DoF.

The DoF θ_x of both plates will be used to enforce compatibility with the membrane DoF θ_z of the other plate. A set of sine and cosine functions to describe the unknown DoF is used to obtain good results.

in Figure 8.5 the results are presented of the interface connection described by rigid body motions and flexible modes.

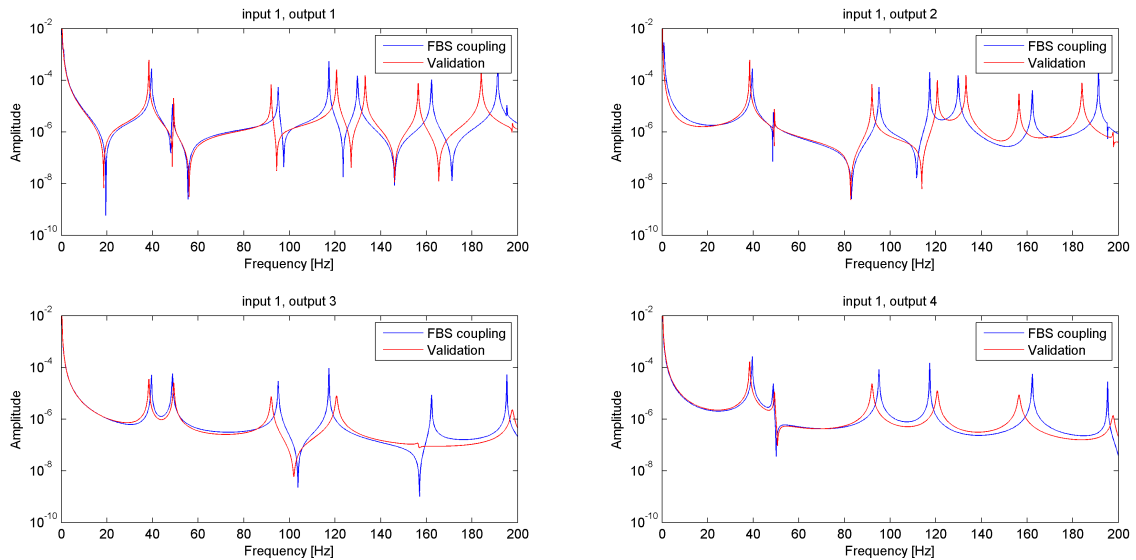


Figure 8.5: Coupled system with flexible modes and rigid body modes.

From Figure 8.5 the following observations can be done

- The FRFs of the coupled system show very good resemblance with the validation measurement
- From the third mode onwards little deviations in the eigenfrequencies are visible.

It can be concluded that the interface is accurately described by the set of modes that is used. From this we can conclude that it should be possible to couple partially measured plate models. The true experimental models will be coupled in the next chapter.

Chapter 9

Coupling measured plates

In this chapter the method that is validated will be used to couple the plate models. These plate models are the resynthesized FRF models which were built and described in Chapter 6. The same modes for building the unknown DoF will be used in this section as is described in the validation chapter. The compatibility is also enforced on the same modes as are used to describe the unknown DoF.

9.1 Rigid body modes

In Figure 9.1 the results of the coupled plate models with the interface described only by rigid body motions can be seen, compared to the validation measurement. This validation measurement is the base and upright physically coupled with bolted joints.

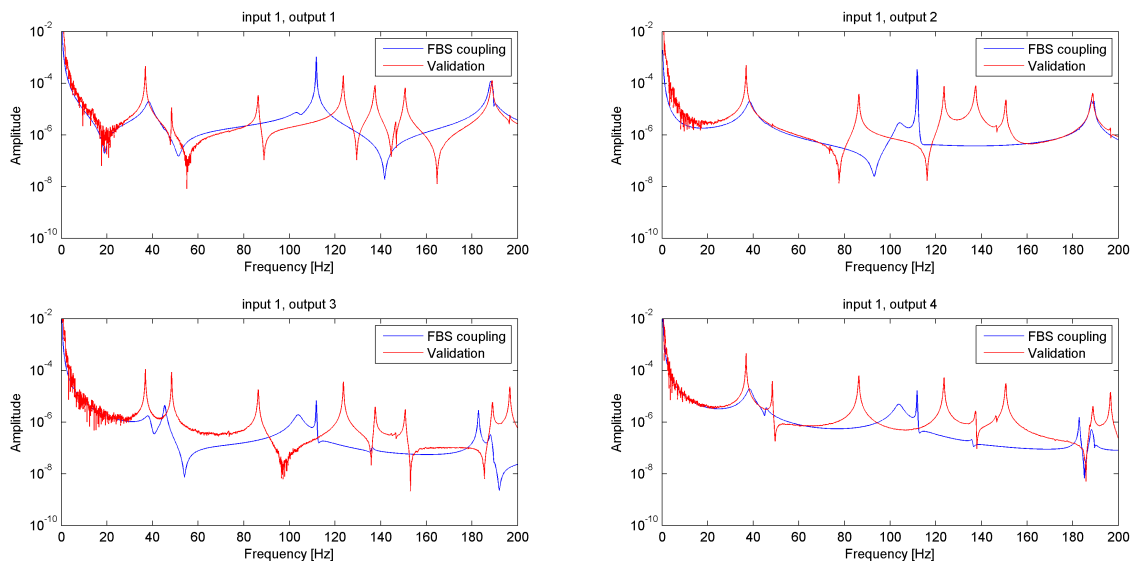


Figure 9.1: Coupled plate models with the interface described by rigid body motions only, compared to the validation measurement

From Figure 9.1 it can be observed that:

- The first mode, and the mode near 190 Hz show resemblance. The other frequencies are badly estimated.
- The peaks are much more damped than the peaks in the FRFs of the validation measurement.

The modes that show resemblance can be described with rigid motions on the interface. The other modes probably not. This will lead to different eigenfrequencies.

9.2 Flexible modes

In Figure 9.2 the results of the plate coupling for the unknown DoF described with flexible modes can be seen.

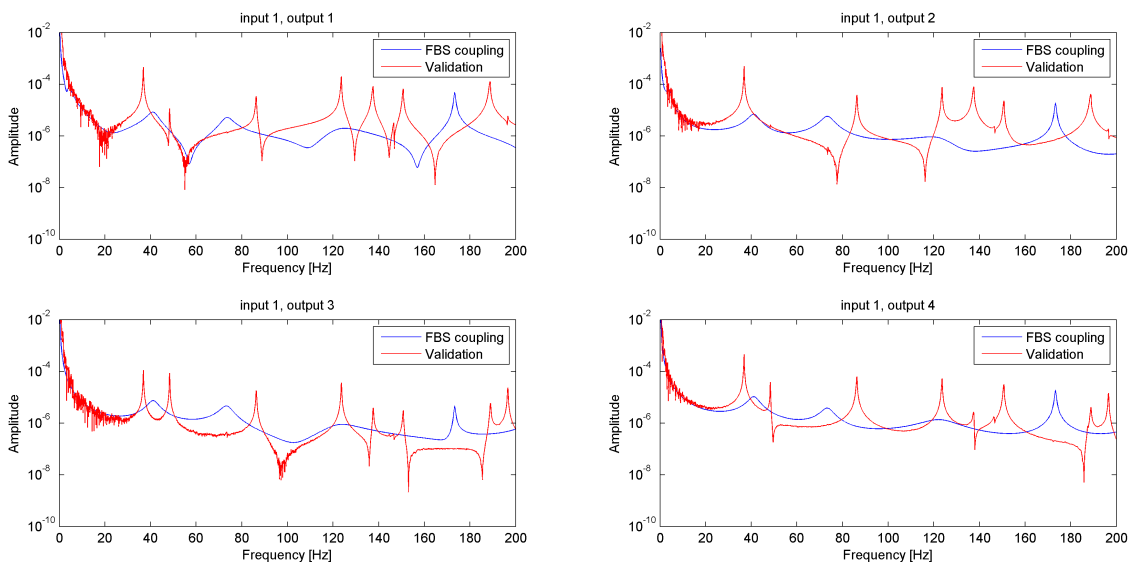


Figure 9.2: Coupled plate models with the interface described by rigid body motions and flexible modes, compared to the validation measurement

It can be seen that the lines show bad resemblance and that the coupled system has a lot of damping. A possible explanation could be that the modes Φ_k that are used for expanding the set of DoF cannot be represented by the modes that are used in the modal superposition to build the plate models.

In Figure 9.3 the results of the coupling procedure with fewer flexible modes incorporated can be seen.

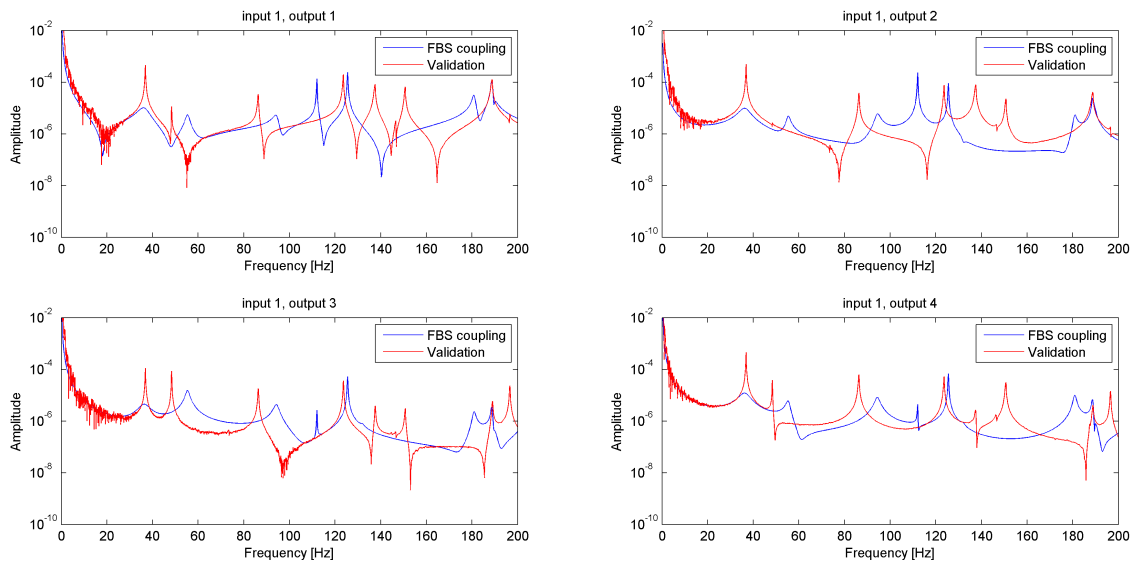


Figure 9.3: Coupled plate models with the interface described by rigid body motions and few flexible modes compared to the validation measurement

From Figure 9.3 it can be observed that the results improve. The first, the fifth (125 Hz) and the ninth (190 Hz) mode show good resemblance. The second and third mode are shifted upwards. It can also be observed that especially the low frequent peaks contain more damping than expected. A possible explanation is that the damping in the plates is overestimated by the experiment setup or the windowing. This will lead to more damping in the coupled model.

Another explanation for the bad results can be that an incorrect set of modes for describing the unknown DoF is used.

As can be concluded, the damping in the computationally coupled structure is higher than the physically coupled structure, and the coupling results are not accurate enough. This means that for now no joint identification can be performed on this system.

Chapter 10

Identification of damping in rubber mountings

The second part of the research is about identification of joints of rubber mountings. The same base as is used in the previous part is used as a test object. This baseplate is supported on the floor with rubber mountings. The rubber mountings that are used are mountings that are used in industry to damp the vibration of small machines. In Chapter 4 and 5 the measurement of the base plate with rubber mountings and the results have been presented. In Section 10.1, the rubber mounting is described, and a prediction of the identification result is given based on literature values for rubber. In Section 10.2 two models for a rubber mounting are proposed that will be used as substructure in the identification procedure. This procedure is described in Section 10.3. In Section 10.4 the identification procedure is described and the results are presented.

10.1 Rubber mounting properties

The properties of the rubber that is used are not known exactly. The test object and the mounting can be seen in Figure 10.1

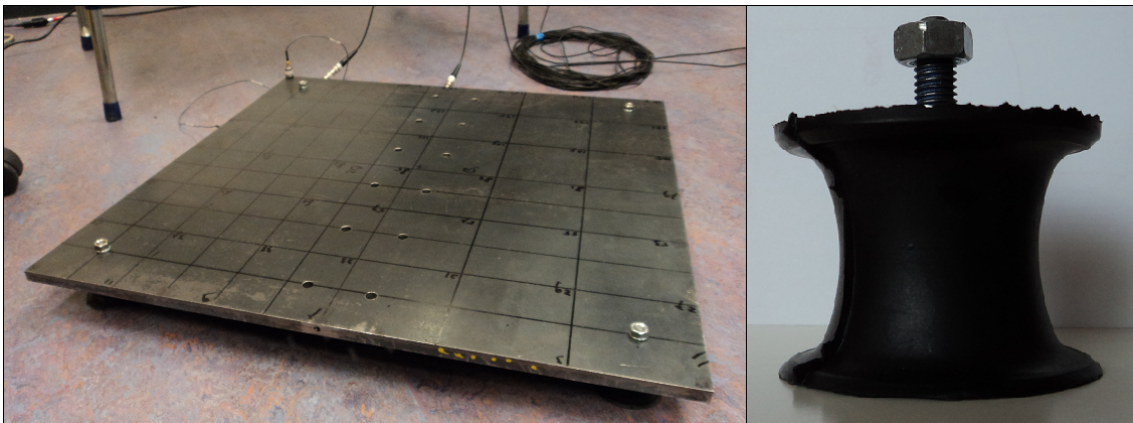


Figure 10.1: Base supported on the floor with rubber mountings and the rubber mounting.

Although the properties of the rubber are not known exactly, an estimation of the stiffness and damping factor can be made based on literature values. The Youngs modulus of rubber is 0.01 –

0.1 GPa [1]. With this modulus an estimation of the stiffness can be made. The equation $k = EA/l$ expresses the stiffness as a function of the Young's modulus E , the area A and the length l . If the dimensions of the rubber mounting are substituted in this equation, we get an estimate for the stiffness of 0.2 kN/mm - 2 kN/mm. The rubber that is used is relatively soft, so the stiffness is assumed to be low. The damping of rubber is often expressed as a loss factor, which means that an hysteretic damping model is assumed. Loss factors for different types of rubber are: for natural rubber 0.05, for neoprene rubber 0.1 and for butyl rubber 0.4. [2].

10.2 Model descriptions

To investigate the damping, two different models will be used in the identification namely a viscous model and a hysteretic damping model. The joint model will consist of two DoF that are connected by a spring and a damper. Rubber is often described with a visco-elastic model, and a hysteric model can be seen as the most simple visco-elastic model. In this study will be examined if this model is able to describe the damping mechanism sufficient. The results found with this model will be compared to a system that is damped by a viscous damping model.

Hysteretic damping It is predicted that the rubber has a hysteretic damping type. Hysteretic damping is not frequency dependent, but it is in phase with the velocity. Hysteretic damping will be described by the following equation (see Chapter 1)

$$z = k(1 + \gamma i) \quad (10.1)$$

where k is the stiffness and γ is the loss factor. In this investigation both variables will be determined.

Viscous damping Another damping model which is often used for describing damping in systems is the viscous damping model. This damping model is frequency dependent, and is also in phase with velocity. The dynamic stiffness of a viscous damped joint is described as

$$z = i\omega c + k, \quad (10.2)$$

where k is the stiffness and c is the viscous damping factor. This factor c is not often used to express the damping value. In stead the fraction of the critical damping ratio is used, namely ζ . The relation between ζ and the damping factor c is $\zeta = c/(2\sqrt{mk})$, where m and k are the modal mass and modal stiffness. In this investigation both the ζ and k will be determined.

10.3 Coupling procedure

As is discussed in the introduction, the model of the base will be coupled to a joint model of the rubber mountings in order to investigate the damping in the rubber mounting. The construction of the response model of the base is described in Chapter 3. This model will now be reconstructed with another set of nodes. At least the four nodes are needed to which the rubber dampers are coupled to the plate. Furthermore, 4 internal nodes will be used. A Figure of the locations of the nodes can be seen in Figure 10.2.

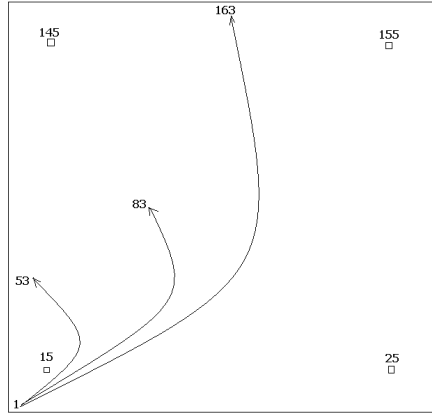


Figure 10.2: Locations of nodes on base. Nodes 15, 25, 145 and 155 are attached to the rubber mountings.

The total system of the base plate and the joints is described by the following set of equations

$$\begin{cases} \mathbf{ZLq} = \mathbf{f} + \mathbf{g} \\ \mathbf{L}^T \mathbf{g} = \mathbf{0}, \end{cases} \quad (10.3)$$

as was described in Chapter 3. $\mathbf{Lq} = \mathbf{u}$, where \mathbf{q} is the unique set of DoF, and \mathbf{u} is the set of all the DoF. And this is written as

$$\begin{bmatrix} \mathbf{u}_i^A \\ \mathbf{u}_c^A \\ \mathbf{u}_c^B \end{bmatrix} = \begin{bmatrix} \mathbf{I} & \mathbf{0} \\ \mathbf{0} & \mathbf{I} \\ \mathbf{0} & \mathbf{I} \end{bmatrix} \begin{bmatrix} \mathbf{u}_i^A \\ \mathbf{u}_c \end{bmatrix} \quad (10.4)$$

\mathbf{g} are the interface forces and these will be eliminated by premultiplying the first row of Equation (10.3) by \mathbf{L}^T , and the system becomes

$$\left(\mathbf{L}^T \begin{bmatrix} \mathbf{Z}_{\text{base}} & \mathbf{0} \\ \mathbf{0} & \mathbf{Z}_{\text{rubber}} \end{bmatrix} \mathbf{L} \right) \mathbf{q} = \mathbf{L}^T \mathbf{f} \quad (10.5)$$

The \mathbf{Z} matrix of the rubber is a diagonal matrix with as entries the dynamic stiffnesses of the joint.

10.4 Identification of damping and stiffness

The identification process of the dynamic stiffness is visualized in a flowchart that can be seen in Figure 10.3. The two parameters that describe the joint models will be iteratively modified to get convergence to the validation measurement. The stiffness of the joint will influence the eigenfrequencies of the rigid body modes, so a close correspondence to these poles need to be found. The damping factor has to be adjusted to get a good correspondence to the modal damping of the poles in the frequency spectrum of 0 – 600 Hz. The modal damping will be calculated using the circle fit routine, and the values are presented as ζ which is $\eta/2$. This is done to make comparison with the validation measurement possible.

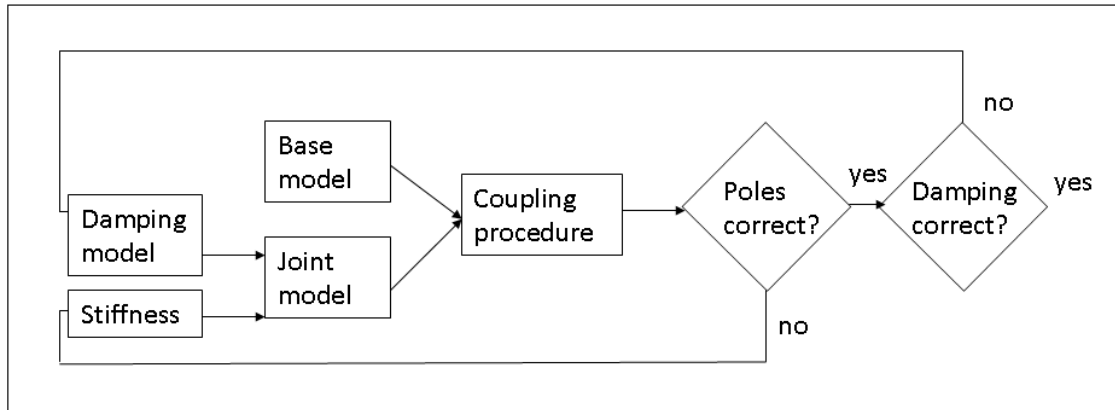


Figure 10.3: Flowchart of flexible joint identification.

Hysteretic model The hysteretic model can be identified well. The results of the coupled model can be seen in Figure 10.4. The stiffness is found to be 0.2 kN/mm for this model. This is within the interval of the predicted stiffness. The loss factor for the hysteretic model is about 0.07. This value lies between the value of the loss factor for natural rubber and the value for neoprene rubber.

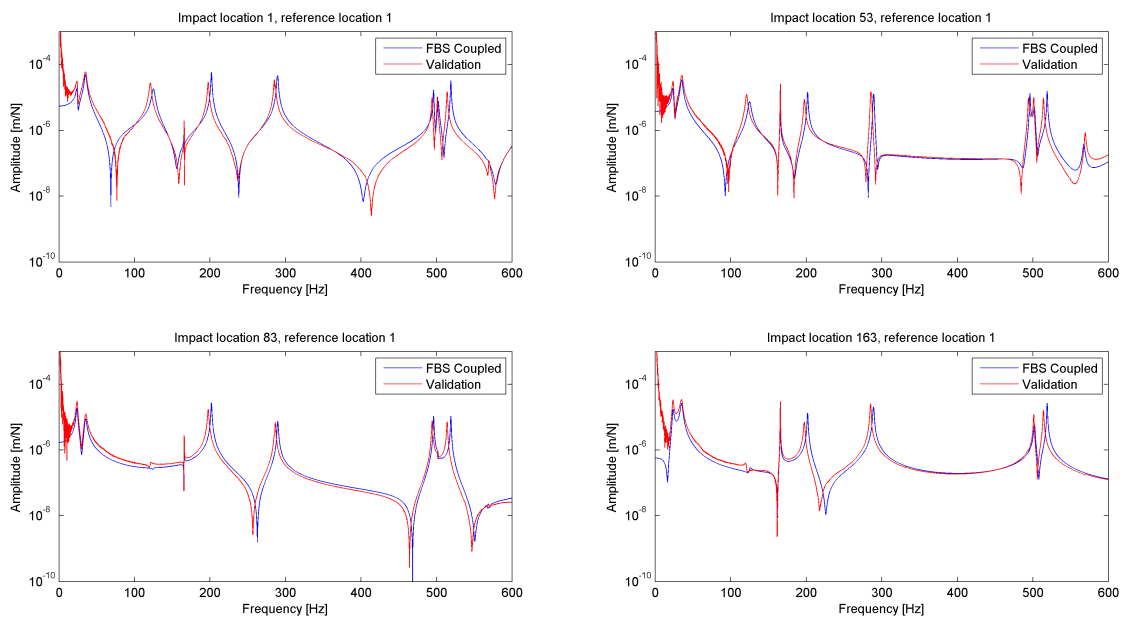


Figure 10.4: FRFs of validation measurement and hysteretic damping model coupled to base model.

The following observations can be made from inspection of Figure 10.4.

- All the FRFs show a pretty good agreement with the validation measurement. It is observed that all frequencies of the fbs coupled base are slightly higher than those of the validation measurement.
- Two rigid body frequencies are reasonably well described by the joint model.

- At low frequencies the FRFs show a stiffness line. The validation measurement not, which is strange.

The modal damping values that are found for the coupled model will be compared to the validation measurement. These results can be seen in Figure 10.5.

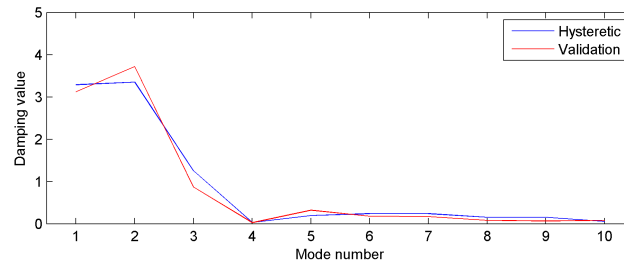


Figure 10.5: Modal damping values (% of critical damping). The first two modes are the rigid body modes of the structure.

From observation of Figure 10.5 the following observations can be made.

- There is very good agreement for the modal damping values
- The first flexible mode, mode 3, shows a high damping compared to the other flexible modes.
- The second flexible mode, mode 4, shows a low damping compared to the other flexible modes.

Viscous model The viscous model can be identified not so good as the hysteretic model. The damping value cannot be identified very well, for that reason the result of two damping values are presented. The first identification shows pretty good agreement with the rigid body modal damping values (lower frequencies). The second identification shows more or less agreement with the modal damping of the flexible modes (higher frequencies). The stiffness for both identification procedures is found to be 0.2 kN/mm, which is the same as for the hysteretic model. The results of the rubber model with a damping factor of 0.73 % can be seen in Figure 10.6.

The following observations can be made from inspection of Figure 10.4.

- The eigenfrequencies are estimated reasonably well. Most of the frequencies are estimated a little bit too high
- The damping at low frequencies shows a good correspondence to the validation measurement
- At high frequencies the damping is much higher than the damping of the validation measurement

The modal damping values belonging to these results can be seen in Figure 10.7

The same conclusions can be made as for the figure showing the FRFs. It is noted that the damping belonging to the fourth mode is very low with respect to the other modes.

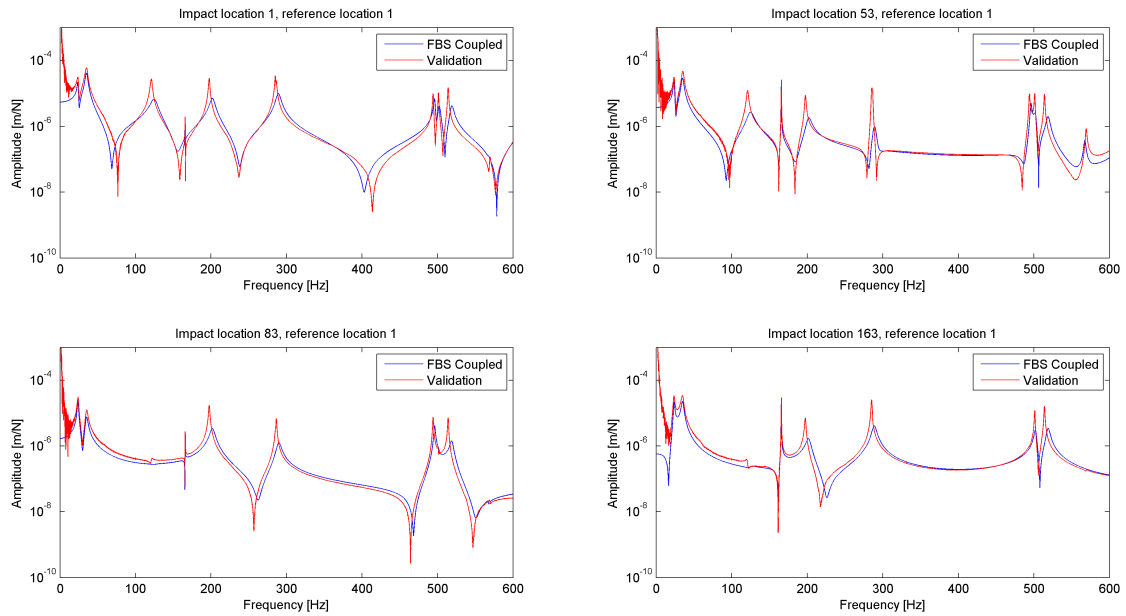


Figure 10.6: FRFs of validation measurement and viscous damping model coupled to base model.

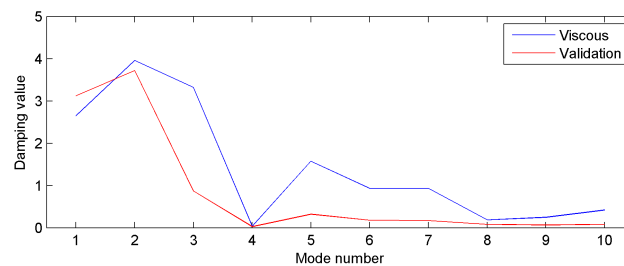


Figure 10.7: Modal damping values (% of critical damping). The first two modes are the rigid body modes of the structure.

The viscous model has also been identified with a much lower damping factor in order to have a better correspondence to the damping of the higher modes, a damping factor of 0.2 % is used. The result of the coupling procedure with this damping model can be seen in Figure 10.8

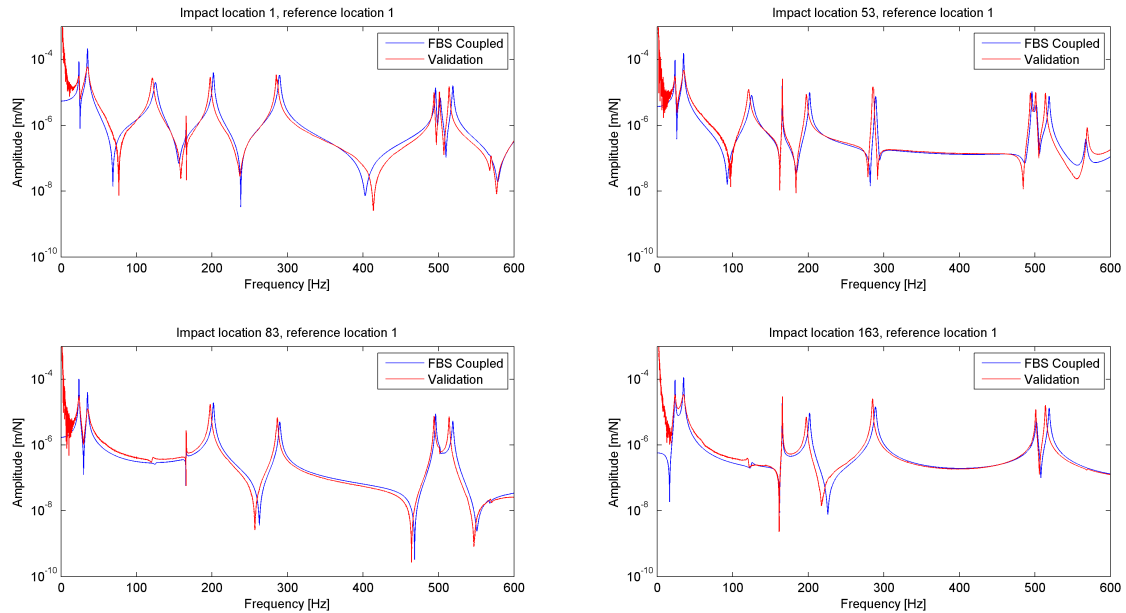


Figure 10.8: Modal damping values (% of critical damping). The first two modes are the rigid body modes of the structure.

From Figure 10.8 and Figure 10.9 the following can be observed

- The damping of the first two modes (rigid body modes) is underestimated.
- The damping of the higher modes shows good correspondence to the validation measurement, but is overestimated.

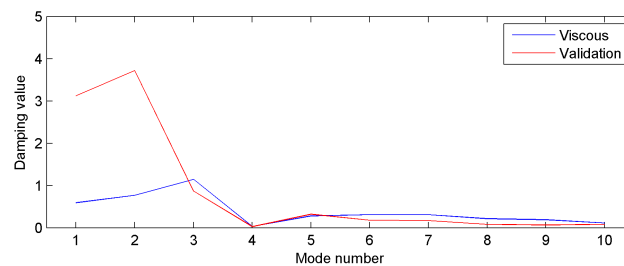


Figure 10.9: Modal damping values (% of critical damping). The first two modes are the rigid body modes of the structure.

A possible explanation for the upward frequency shift could be the stiffening of the whole plate model by adding four rubber mountings. An explanation for the fact that the viscous model cannot be well identified could be that this is not the correct damping model for a rubber mounting. It can be seen that the viscous model underestimates the damping at low frequencies, and overestimates the damping at high frequencies. This is due to the frequency dependent behaviour of the model. The hysteretic model fits the measured data more accurately.

Chapter 11

Conclusions and Recommendations

11.1 Summary

The research context which was presented in the introduction of this thesis, gave rise to the main research question: Investigation of the use of dynamic substructuring techniques to identify damping in joints. This was divided into two sub questions. One part is about the general use of substructuring techniques with a completely measured interface. The other part is to investigate the use of these techniques when the interface is only partially measured and not all important interface DoF are known. To be able to answer the two sub questions two test cases have been used: a base which was supported on the ground with rubbers with a completely measured interface and a bolted joint of a base-upright structure with a partially measured interface. In the first part of this thesis a background was given of damping models and modal identification. Also the basics of dynamic substructuring have been discussed. This knowledge has been used in this research to investigate the use of these substructuring techniques for the identification of joint models. In the second part of this research the measurements of the substructures and thus of the two test cases have been described. A simple modal analysis method has been used to identify the modal parameters of the measured test structures. This modal analysis method has been coded in Matlab and has been improved to be able to work with closely spaced modes. At the end of the second part the modelling of the different test structures is presented. The coupling procedures and coupling results were presented in the third part. In this chapter, the conclusions are given of the research in Section 11.2, and recommendations are made in Section 11.3.

11.2 Conclusions

11.2.1 Identification of rubber mounting properties

In Chapter 3 the substructuring techniques were explained which have been used to couple a test structure to rubber mountings. The results of this coupling procedure were presented in Chapter 10. It was seen that the properties of the joints could be identified correctly for this test-case. The damping model could even be identified as hysteretic, which was to be expected. A few conclusions can be drawn for this test.

- The properties of flexible joints can be identified with the use of substructuring techniques

- It is important to use a hysteretic damping model for rubber mountings because a viscous model cannot describe the damping well enough.
- The hysteretic model is sufficient to describe the dynamic behaviour of the rubber. More advanced modelling techniques for damping seem to be unnecessary for this rubber mounting.

From this identification procedure it can also be concluded that the modelling of the base was done correctly. Especially the rigid body modes were important to be correct. But also the flexible modes were identified, and modelled correctly.

11.2.2 Identification of bolted joint properties

Validation of coupling method

The second part of this research is about the identification of a joint that is only partially measured. A base upright structure is chosen as a test structure. The modelling of the both substructures has been described in Chapter 6. Two assumptions have been done to be able to couple the plate models. The first assumption is to consider the membrane behaviour as rigid. This assumption seems to be correct, although downward frequency shifts were observed.

The second assumption is to describe the unknown DoF on the interface with modes. When only rigid modes are used to describe the unknown DoF, the coupled modeshapes 1, 5 and 7 are described well. (In these modeshapes the dynamics of one plate can be described by rigid motions.) The other peaks do not correspond well to the validation measurement.

When also flexible modes are used for description of the unknown DoF, the eigenfrequencies in the range 0-200 Hz are all visible although some frequency shifts are observed. The modes that have been used for the description of the unknown DoF seems to be sufficient. It can be concluded that the method seems to work for this test structure. Further investigation has to be done about which modes can be used best for expanding the set of DoF.

Coupling plate models

In Chapter 9 the coupling method is used to couple the plate models that have been built before. The coupling results show a lot of damping and the resemblance to the validation measurement is less accurate. It has been observed that the more modes are used to describe the interface with, the more damping was perceived in the coupled model.

The plate models are built with fewer modes than that were used in the simulated experiments. This is due to the finite number of modes that can be measured. A result of this can be that the known modes Φ_k belonging to the unknown interface modes Φ_u cannot be described with the finite set of modes that is used to built the plate models. This can lead to an inaccurate description of the unknown DoF. Which can cause high interface forces f_u .

Identification of damping

In order to identify the joint properly a substructure will be placed in between the two plates which variables should be identified. Due to the fact that the coupling of the plate models could not be done very accurately and due to the fact that the damping in the computational coupled

model is already higher than the damping in the physically coupled model, no identification of the joint can be performed. However it can be seen that the physically coupled system has more damping than the separate plates, which means that the joint will add damping to the system.

Summary

To summarize these conclusions:

- Substructuring techniques can be used for joint identifications as is shown by the identification of the rubber mounting.
- The method that is proposed to couple both plates with partially measured interface DoF works well with simulated experiments. This means that it is in theory possible to couple substructures with incomplete interface measurements
- The coupling results of the measured plates did show less good resemblance to the validation measurement. Some further investigation is needed to improve the results.

11.3 Recommendations

Extend the set of measured modes with computational modes to expand the modal superposition. It was shown that in theory it is possible to couple the plate models. However, the measured plate models gave bad coupling results after the coupling procedure. The results could maybe improve by expanding the plate models with a larger number of modes than that is used now.

Further theoretical investigation on expansion of unknown DoF. In this research unknown modes (Φ_u) are used to describe the unmeasured DoF. Further research is needed to know which modes need to be used for the expansion of the DoF in order to get an accurate description of the unmeasured DoF.

Investigate the use of joint stiffness in the plate coupling. When there are correct coupling results of the measured plate models, the joint needs to be identified. This can be done by adding a third substructure between the other two substructures. This system should have rotational stiffness and damping.

Use decoupling methods for joint identification In this thesis substructuring techniques have been used for the identification of joints. It is maybe possible to use also decoupling techniques to decouple both plates from a measured and modelled BU model and to identify the remaining system as a joint with stiffness and damping.

Nomenclature

q	Generalized degree of freedom
$f(t)$	Time varying excitation force
t	Time variable
m	Number of included modes
N	Total number of degrees of freedom/coordinates
n	Number of measured DoF
r	Current mode number
j, k, l	Integers
l	Number of time intervals
f	Frequency of vibration [Hz]
ω	Frequency of vibration [$rad\ s^{-1}$]
i	$\sqrt{-1}$
τ	Dimensionless time constant
δ	Kronecker delta function
\star^T	Transpose
$\bar{\star}$	Complex conjugate
\star^H	Complex conjugate transpose (Hermitian)
\star^+	Pseudo inverse
\star^{-1}	Inverse
I	Identity matrix
Σ	Rectangular matrix of singular values
ϵ	Value of an error
M	Mass matrix
C	Viscous damping matrix
D	Hysteretic damping matrix
K	Stiffness matrix

C'_{kl}	Element of damping matrix in modal coordinates
H	Receptance
H_{ij}	Transfer function in frequency domain
h_{ij}	Impulse response function in time domain
$g(t)$	Damping function
$\mathcal{G}(t)$	Matrix containing damping functions
$G(t)$	Fourier transform of $\mathcal{G}(t)$
$\mathcal{D}(t)$	Dissipation function
x	Modeshape belonging to damped system
y	Modeshape belonging to undamped system
z	Complex mode shape obtained from state space description
ϕ	Unnormalized mode shape
Z	Dynamic stiffness matrix
Y	Receptance matrix
B	Signed Boolean matrix
L	Boolean localization matrix
λ	Vector of Lagrange multipliers
g	Vector of connecting forces
u	Vector of degrees of freedom

Bibliography

- [1] <http://www.engineeringtoolbox.com>, November 2011.
- [2] www.earsc.com/pdfs/engineering/designforquietwhthtpper.pdf, November 2011.
- [3] S. Adhikari and B. Pascual. Iterative methods for eigenvalues of viscoelastic systems. *Journal of Vibration and Acoustics*, 133:021002, 2011.
- [4] S. Adhikari and J. Woodhouse. Identification of damping: part 1, viscous damping. *Journal of Sound and Vibration*, 243:43–61, 2000.
- [5] S. Adhikari and J. Woodhouse. Identification of damping: part 2, non-viscous damping. *Journal of Sound and Vibration*, 243:63–88, 2000.
- [6] R.J. Allemang. The modal assurance criterion \bar{U} twenty years of use and abuse. *Journal of Sound and Vibration*, 37:14–21, 2003.
- [7] M. Bakker. Linear damped systems and modal identification techniques.
- [8] E. Balmes, J.P. Philipe, and J.M. Leclere. *Structural Dynamics Toolbox User's guide*. SDtools, 2008.
- [9] C.W. Bert. Material damping: an introductory review of mathematical models, measure and experimental techniques. *Journal of Sound and Vibration*, 29:129–153, 1973.
- [10] D. de Klerk, D.J. Rixen, and S.N. Voormeeren. General framework for dynamic substructuring: History, review, and classification of techniques. *AIAA Journal*, 46(5):1169–1181, May 2008.
- [11] D.J. Ewins. *Modal Testing: Theory, Practice and Application*. Research Studies Press Ltd., 2000.
- [12] Michel Geradin and Daniel Rixen. *Mechanical Vibrations*. Wiley, 1994.
- [13] D.J. Gorman. Free vibration analysis of the completely free rectangular plate by the method of superposition. *Journal of Sound and Vibration*, 57:437–447, 1978.
- [14] T. Hasselman. Modal coupling in lightly damped structures. *AIAA Journal*, 14:1627–1628, 1967.
- [15] Jimin He and Zhi-Fang Fu. *Modal Analysis*. Butterworth-Heinemann, 2001.
- [16] Shikazo Iguchi. Die eigenschwingungen und klangfiguren der vierseitig freien rechteckigen platte. pages 317–385, 1942.
- [17] B.J. Lazan. *Damping of Materials and Members in Structural Mechanics*. Oxford: Pergamon Press, 1968.
- [18] Arthur W. Leissa. *Vibration of plates*. National Aeronautic and Space Administration, 1969.

- [19] R.M Lin and J Zhu. On the relationship between viscous and hysteretic damping models and the importance of correct interpretation for system identification. *Journal of Sound and Vibration*, 325:14–33, 2009.
- [20] N. M. M. Maia and J. M. M. Silva. Modal analysis identification techniques. *Philosophical Transactions of The Royal Society London A*, 359:29–40, 2001.
- [21] David S. Moore and George P. McCabe. *Introduction to the practice of statistics*. W. H. Freeman and Company, 2003.
- [22] Z. Osiniski. *Damping of Vibrations*. A.A. Balkema Publishers, 1998.
- [23] Lord Rayleigh. *Theory of Sound*. New York: Dover Publications, 1945.
- [24] M. H. Richardson and D. L. Formenti. Global curve fitting of frequency response measurements using the rational fraction polynomial method. *Proceedings of the third international Modal Analysis Conference*, pages 390–397, 1985.
- [25] Mark H. Richardson and David L. Formenti. Parameter estimation from frequency response measurements using rational fraction polynomials. *Proceedings of the first international modal analysis conference*, 1:167–181, 1982.
- [26] D. J. Rixen. Engineering dynamics lecture notes.
- [27] D. J. Rixen. Mechanical analysis for engineering - lecture notes. Delft University of Technology, September 2009.
- [28] F.R. Spitznogle and A.H. Quazi. Representation and analysis of time-limited signals using a complex exponential algorithm. *Journal of Acoustical Society of America*, 47:1150–1155, 1970.
- [29] Technology Vibrant. Inc. mescopeves application note 19, using the z-polynomial method with the stability diagram. Technical report, 2004.
- [30] J. Woodhouse. Linear damping models for structural vibration. *Journal of Sound and Vibration*, 215:547–569, 1998.

Appendix A

Fundamentals of Plates

In this chapter a short theoretical background of dynamic analysis of rectangular plates is described. This analysis is based on the book of Leissa, *Vibration of Plates*. [18]

A.1 Homogeneous equations

The classical differential equation of motion for the transverse displacement w of a plate is given by:

$$D\nabla^4 w + \rho \frac{\partial^2 w}{\partial t^2} = 0 \quad (\text{A.1})$$

where D is the flexural rigidity and is defined by

$$D = \frac{Eh^3}{12(1-\nu^2)} \quad (\text{A.2})$$

E is Young's modulus, h is the plate thickness, ν is Poisson's ratio, ρ is mass density per unit area of the plate, t is time and $\nabla^4 = \nabla^2 \nabla^2$, where ∇^2 is the Laplacian operator. When free vibrations are assumed, the motion is expressed as

$$w = W \cos \omega t \quad (\text{A.3})$$

where ω is the circular frequency (expressed in radians/unit time) and W is a function only of the position coordinates. Substituting equation (A.3) into equation (A.1) yields

$$(\nabla^4 - k^4)W = 0 \quad (\text{A.4})$$

where k is a parameter of convenience defined as

$$k^4 = \frac{\rho\omega^2}{D} \quad (\text{A.5})$$

Equation (A.4) will usually be factorized into

$$(\nabla^2 + k^2)(\nabla^2 - k^2)W = 0 \quad (\text{A.6})$$

whence, by the theory of linear differential equations, the complete solution to equation (A.6) can be obtained by superimposing the solutions on the equations

$$\left. \begin{aligned} \nabla^2 W_1 + k^2 W_1 &= 0 \\ \nabla^2 W_2 - k^2 W_2 &= 0 \end{aligned} \right\} \quad (\text{A.7})$$

A.2 Analytical solutions

The boundary conditions which will be used in this research are free-free conditions. It turns out that the solutions to the differential equations of the completely free rectangular plate are the most difficult ones to solve. Over the years different methods have been invented to analyse the completely free rectangular plate. It remains a fact that most theoretical solutions to this classical problem are considered to be a best approximate in nature [13]. The analytical solution belonging to the free boundary conditions are Fourier series expansions that do not have an exact solution, but they can be calculated to a certain order. Leissa used the work of Iguchi [16] among others to describe the square plate in terms of eigenmodes and eigenfrequencies. Iguchi used the series method to solve the problem for the general rectangle. Nodal patterns for the first five modes can be seen in Figure A.1. The eigenfrequencies are given as a dimensionless number, and can be calculated for the plate dimensions that has been tested.

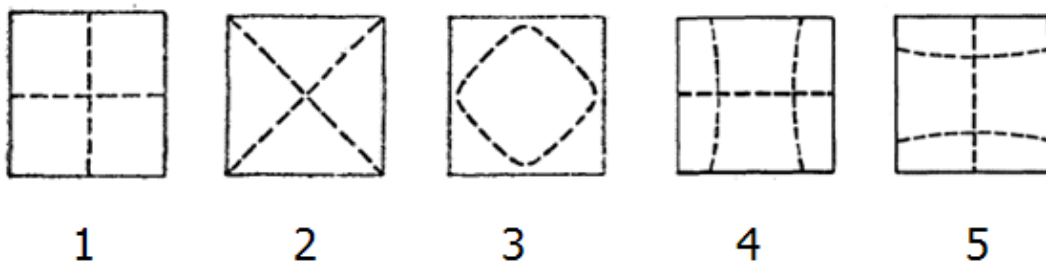


Figure A.1: Nodal patterns of first five modeshapes of a square plate.

Appendix B

Data sheets

K-Shear® Accelerometers

Type 8702B..., 8704B...

General Purpose, Voltage Mode Accelerometers

Small, relatively light weight general purpose accelerometers for vibration measurements in wide range of applications. Available in three measuring ranges 25 g, 50 g and 100 g, all range types are available in a ground isolated option. These accelerometers feature a rugged, hermetically sealed construction.

- Low impedance, voltage mode
- Quartz-shear sensing elements
- Ultra-low base strain
- Minimal thermal transient response
- Lightweight, hermetically sealed Titanium case
- Conforming to CE

Description

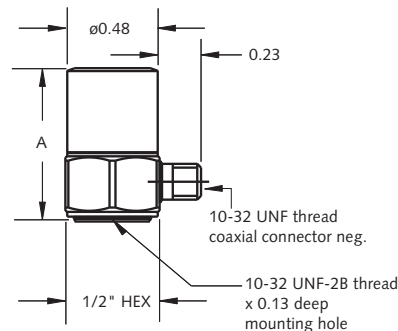
The Type 8702B... side connector and 8704B... top connector accelerometer series use a unique shear mode sensing element made of stable quartz crystals. The quartz sensing elements afford excellent long-term stability that ensure repeatable, accurate measurements for many years. Additionally the shear element design provides low transverse sensitivity along with an insensitivity to base strain and thermal transients.

All units are hermetically sealed and are constructed entirely of titanium or a combination of titanium and stainless steel. An internal circuit Piezotron® impedance converter provides a high signal level at low impedance output.

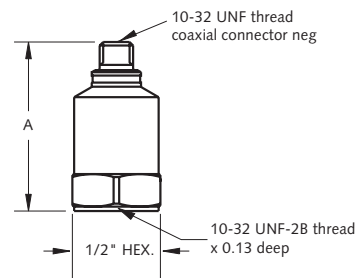
Models identified with an M1 are ground isolated versions. All units are hermetically sealed and are constructed entirely of titanium or a combination of titanium and stainless steel.

Application

All types are designed for general purpose vibration measurement in a laboratory or industrial environment. They can be used for environmental testing (with or without temperature cycling), ESS, vehicle tests, automotive NVH testing, rotating machinery vibration analysis.



Dim	Type 8702B...	Type 8702B...M1
A	0.76	0.80



Dim	Type 8704B...	Type 8704B...M1
A	0.96	0.98

Accessing TEDS Data

Accelerometers with a "T" suffix are variants of the standard version incorporating the "Smart Sensor" design. Viewing an accelerometer's data sheet requires an Interface/Coupler such as Kistler's Type 5134B... or 5000M04 with TEDS Editor software. The Interface provides negative current excitation (reverse polarity) altering the operating mode of the PiezoSmart® sensor allowing the program editor software to read or add information contained in the memory chip.

8702B_000-239a-03.08

Technical Data

Specification	Unit	Type 8702/4B25	Type 8702/4B50	Type 8702/4B100
Acceleration range	g	±25	±50	±100
Acceleration limit	gpk	±50	±100	±200
Transverse acceleration limit	gpk	±50	±100	±200
Threshold nom.	grms	0.002	0.004	0.006
Sensitivity, ±5 %	mV/g	200	100	50
Resonant frequency mounted nom.	kHz	54	54	54
Frequency response, ±5 %	Hz	1 ... 8000	0.5 ... 10000	0.5 ... 10000
Amplitude non-linearity	%FSO	±1	±1	±1
Time constant nom.	sec	1	2	1.5
Transverse sensitivity nom., (max. 3)	%	1.5	1.5	1.5
Long term stability	%	±1	±1	±1

Environmental

Base strain sensitivity @ 250 µε	g/µε	0.01	0.01	0.01
Shock limit (1 ms pulse)	gpk	2000	2000	2000
Temperature coeff. of sensitivity	%/°F	-0.03	-0.03	-0.03
Operating temperature range	°F	-65 ... 210	-65 ... 210	-65 ... 210
Storage temperature range	°F	-100 ... 250	-100 ... 250	-100 ... 250

Output

Bias nom.	VDC	11	11	11
Impedance	Ω	<100	<100	<100
Voltage full scale	V	±5	±5	±5
Current	mA	2	2	2

Source

Voltage	VDC	20 ... 30	20 ... 30	20 ... 30
Constant current	mA	4	4	4
Impedance min.	kΩ	100	100	100

Construction

Sensing element	Type	quartz-shear	quartz-shear	quartz-shear
Housing/base	material	Titanium/St. Stl.	Titanium/St. Stl.	Titanium/St. Stl.
Degree of protection case/connector	Type	hermetic	hermetic	hermetic
Connector	Type	10-32 neg.	10-32 neg.	10-32 neg.
Ground isolated		with pad/M1	with pad/M1	with pad/M1
Mass	grams	8.7/7.5	8.7/7.5	8.7/7.5
	M1 grams	9.7/8	9.7/8	9.7/8
Mounting (10-32 thd.x0.13 dp)	Type	stud	stud	stud
Mounting torque	lbf-in	18	18	18

1 g = 9.80665 m/s², 1 inch = 25.4 mm, 1 gram = 0.03527 oz, 1 lbf-in = 0.1129 N-m

Mounting

A threaded 10-32 UNF stud provides positive attachment of the accelerometer to the test structure. Reliable and accurate measurements require that the mounting surface be clean and flat.

The instruction manual for the Type 8702B... and 8704B... series accelerometers provides detailed information regarding mounting surface preparation.

Included Accessories

- | | |
|--|---------------------|
| • 10-32 mounting stud | Type
8402 |
| • Mounting stud, 10-32 to M6; shipped only outside N.A | 8411 |

Optional Accessories

- | | |
|--------------------------|----------------------|
| • Mounting magnet | Type
8452A |
| • Triaxial mounting cube | 8502 |

Ordering Key

Connector location

Side connector	2B
Top connector	4B

Range

±25 g	25
±50 g	50
±100 g	100

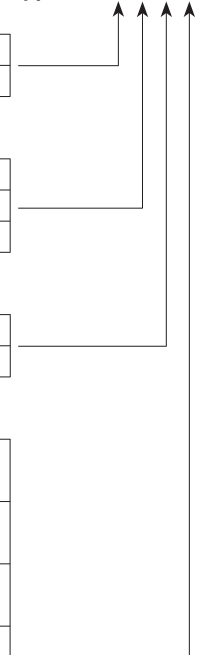
Variant

Standard	
Ground isolated	M1

TEDS Templates

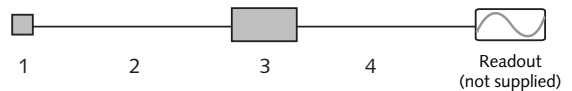
Default, IEEE 1451.4 V0.9	T
Template 0 (UTID 1)	
IEEE 1451.4 V0.9 Template 24 (UTID 116225)	T01
LMS Template 117, Free format Point ID	T02
LMS Template 118, Automotive Format (Field 14 Geometry =1)	T03
LMS Template 118, Aerospace Format (Field 14 Geometry =1)	T04
P1451.4 v1.0 template 25 – Transfer Function Disabled	T05
P1451.4 v1.0 template 25 – Transfer Function Enabled	T06

Type 870



Measuring Chain

- | | |
|--|----------------------------|
| 1 Low impedance sensor | Type
8702/04B... |
| 2 Sensor cable, 10-32 pos. to BNC pos. | 1761B... |
| 3 Power supply/signal conditioner | 51... |
| 4 Output cable, BNC pos. to BNC pos. | 1511 |



Quartz

Type 9726A...

Impulse Force Hammer; High Force Range

Dynamic quartz sensor elements contained within instrumented hammers are used to deliver a measurable force impulse (amplitude and frequency content) to excite a mechanical structure under test. A response signal measured with an accelerometer in conjunction with a FFT analyzer provides the transfer function of the structure.

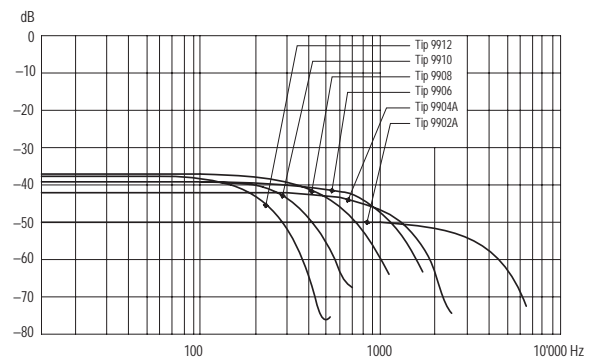
- Low impedance, voltage mode
- Quartz sensing element guarantees long-term stability
- Accessories for various applications
- Sensor cable integrated to hammer handle
- Conforming to CE

Description

The dynamic response of a mechanical structure while either in a development phase or an actual use environment can readily be determined by impulse force testing. Using a FFT analyzer, the transfer function of the structure can be determined from a force pulse generated by the impact of a hammer and the response signal measured with an accelerometer. The impulse force test method, yields extensive information about the frequency and attenuation behavior of the system under test.

The stainless steel head of an impulse force hammer, is equipped with a quartz, low impedance force sensor which accepts impact tips varying in hardness. A selection of steel, plastic, PVC and rubber tips along with an extender mass allow the hammer to be tailored to impart to the test structure, a desired spectrum of frequencies. Shear quartz accelerometers operating in a voltage mode and featuring insensitivity to base strain, thermal transients and transverse motion are available to measure the response of the test specimens ranging from thin-walled structures to steel bridge members.

The hammer incorporates a quartz measuring cell with built-in Piezotron® low impedance electronics. The cell's voltage mode operation, guarantees a stable signal transmission insensitive to ambient influences. A wide selection of single or multi-channel couplers are available to provide power and signal processing for the hammer and accelerometers.



Application

The hammer may be used for testing medium to heavy structures such as large rotating machinery and truck gear assemblies and structural members at low to medium frequencies. The impulse force hammer is used to analyze the dynamic behavior of mechanical structures. The vibrations induced by the hammer impact are measured by an accelerometer.

9726A_000-274e-05.05

Technical Data

Type	Units	9726A5000	9726A20000
Force Range	N	0 ... 5000	0 ... 20000
Maximum Force	N	10000	25000
Sensitivity nom.	mV/N	1	0,2
Resonant Frequency	kHz	27	27
Frequency range with steel impact tip (-10 dB)	Hz	5000	5400
Time Constant nom.	s	500	500
Rigidity	kN/μm	0,8	0,8
Temperature Range Operating	°C	-20 ... 70	-20 ... 70
Output:			
Voltage FSO	V	±5	±5
Bias nom.	VDC	11	11
Impedance	Ω	<100	<100
Source:			
Voltage	V	20 ... 30	20 ... 30
Constant current	mA	2 ... 20	2 ... 20
Hammer head dimensions:			
Diameter	mm	32	32
Length	mm	94	94
Weight	grams	500	500
Length of handle	mm	236	236
Connector	type	BNC neg.	BNC neg.

1 N = 0,2248lb, 1 g = 9,80665 m/s², 1 inch = 25,4 mm, 1 gram = 0,03527 oz

Accessories Included

	Type
• impact tip, steel	9902A
• impact tip, steel with Delrin cap	9904A
• impact tip, soft PVC	9906
• impact tip, rubber hard (green)	9908
• impact tip, rubber medium (red)	9910
• impact tip, rubber soft (gray)	9912
• adapter for rubber impact tips	9928
• extender mass (250 grams)	9926
• impact tip wrench	1370
• Plastic carrying case	

Ordering Key

Measuring Range

5000 N	5000
20000 N	20000

9726A

9726A_000-274e-05.05

Appendix C

Mode Shapes

The modeshapes can be plotted in the 2 dimensional surface plot, where the colour indicates the height. Below the modeshapes that have been identified can be seen in different figures.

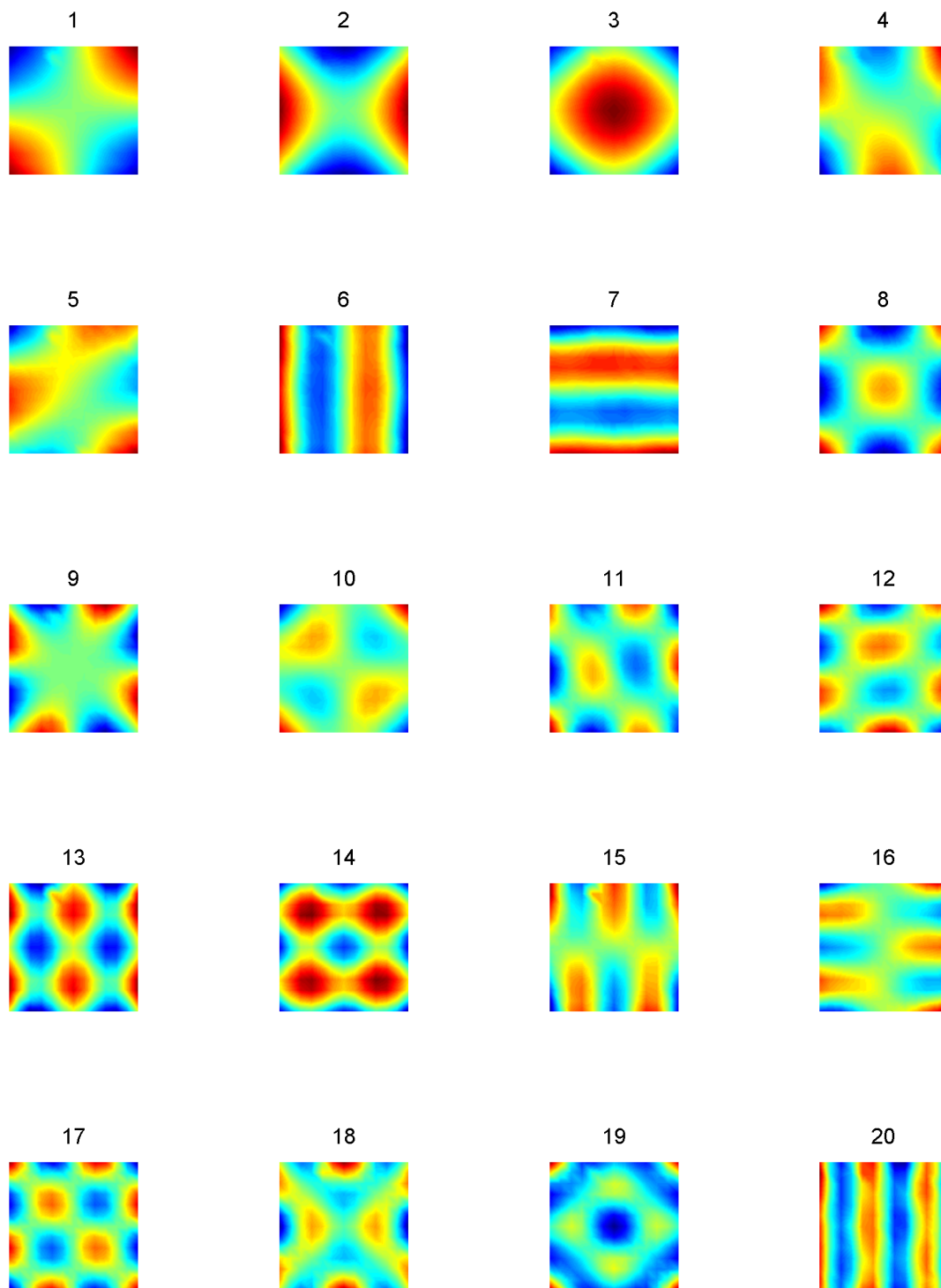


Figure C.1: Measured modeshapes of Base

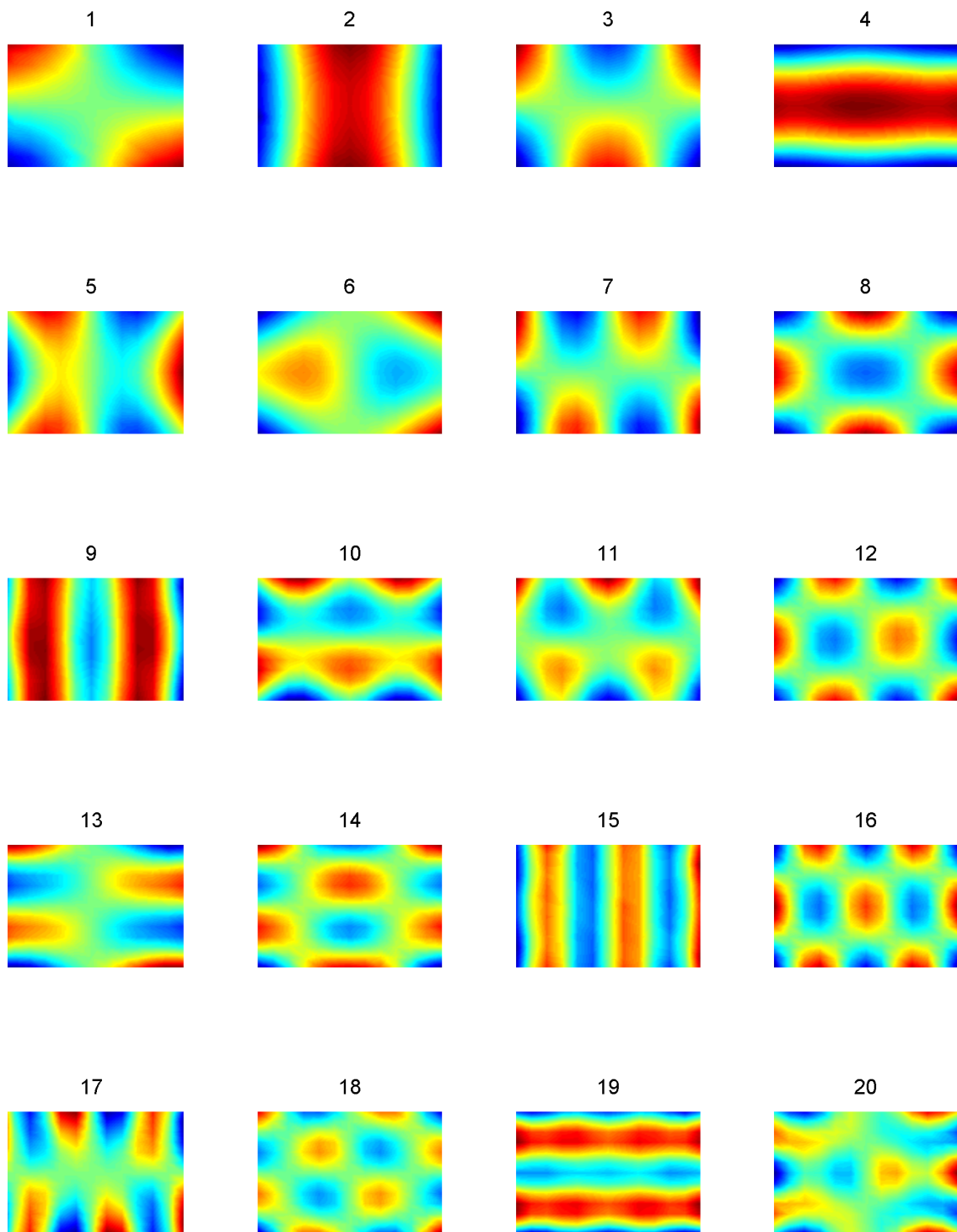


Figure C.2: Measured modeshapes of Upright

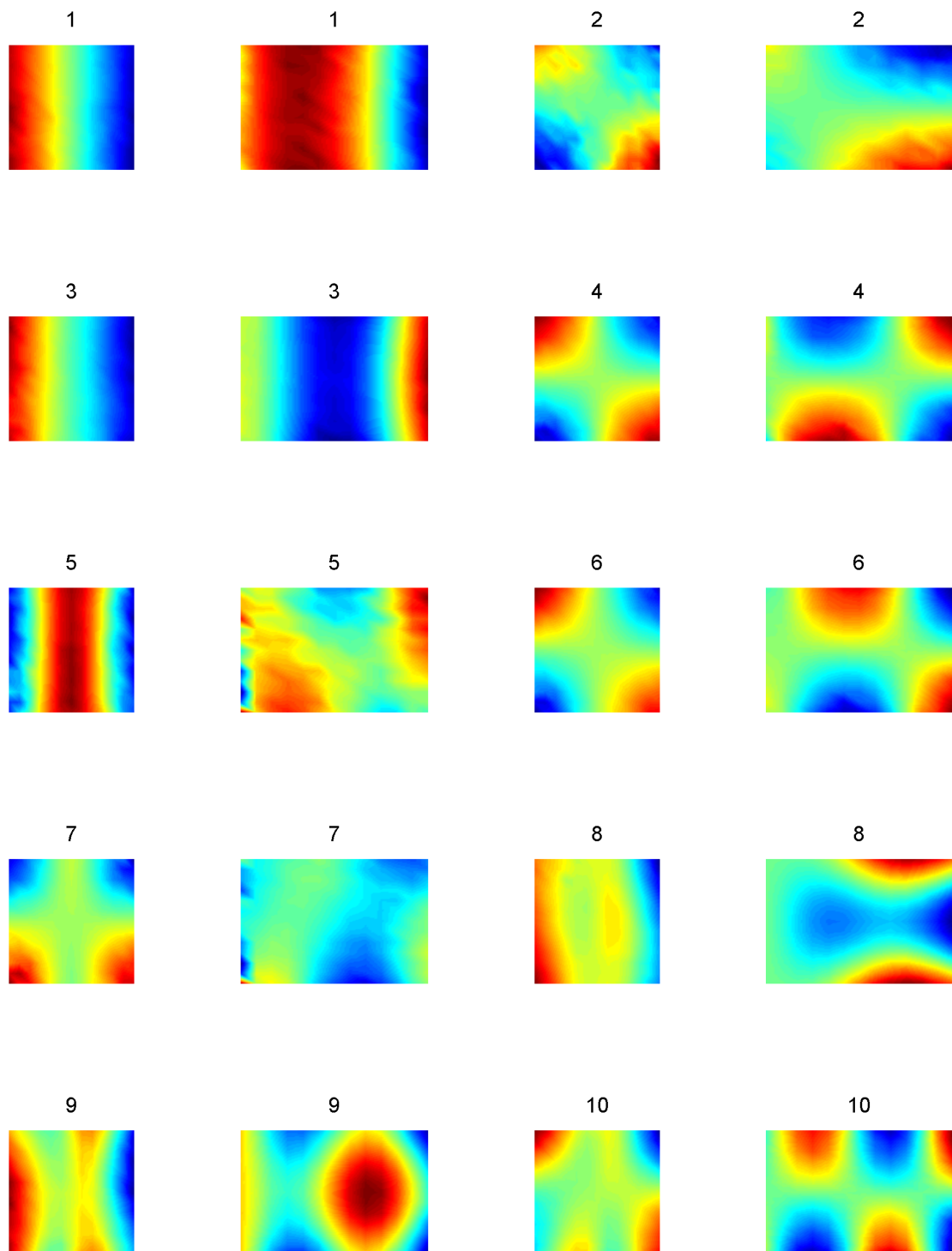


Figure C.3: Measured modeshapes of BU structure. The left side of the modeshape is the base-plate part, and the right side of the mode shape is the upright part.

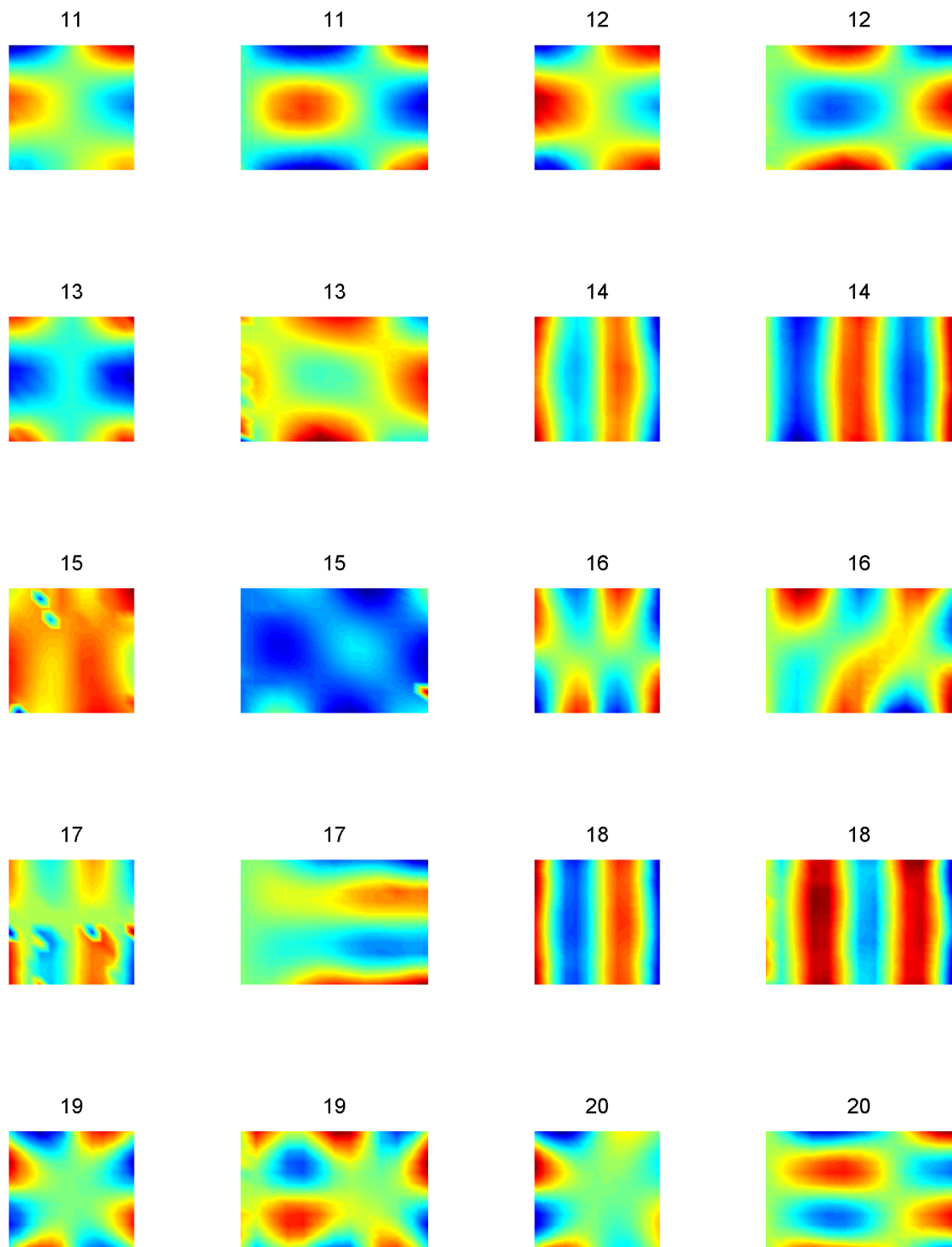


Figure C.4: Measured modeshapes of BU structure. The left side of the modeshape is the base-plate part, and the right side of the mode shape is the upright part.

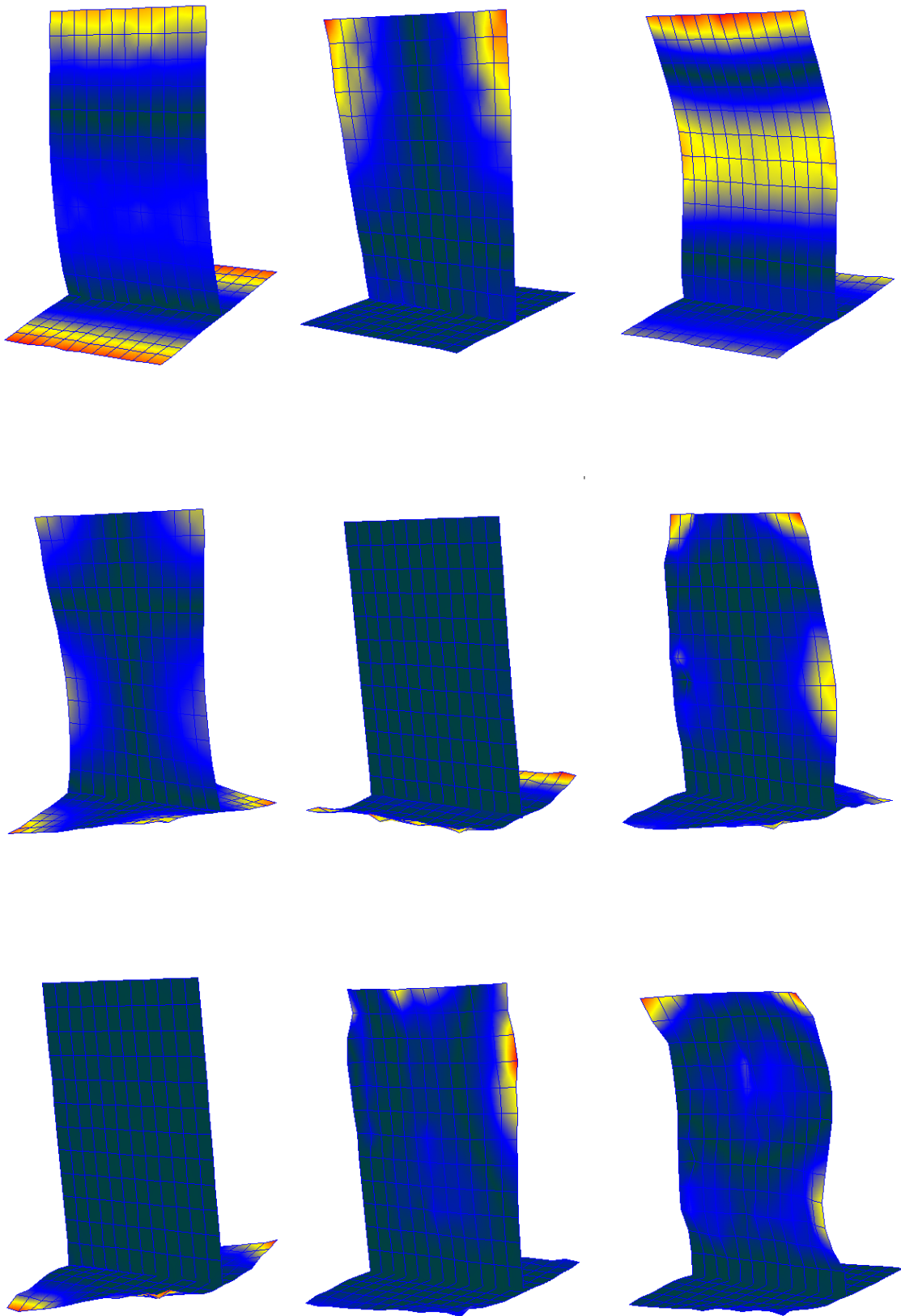


Figure C.5: Measured modeshapes of BU structure. 3d pictures build with ME'Scope.